EXPERIMENTAL AND MODELLING-BASED EVALUATION OF NOVEL CO_2 ADSORBENTS FOR DIRECT AIR CAPTURE

Lappeenranta–Lahti University of Technology LUT

Master's Programme in Bioenergy Systems, Master's Thesis

2022

Aaro Luukkonen

Examiners: Professor, Tero Tynjälä

D.Sc. (Tech.), Eero Inkeri

Supervisor: Research Scientist, Jere Elfving

ABSTRACT

Lappeenranta–Lahti University of Technology LUT

LUT School of Energy Systems

Energy Technology

Aaro Luukkonen

Experimental and modelling-based evaluation of novel CO_2 adsorbents for direct air capture

Master's thesis

2022

115 pages, 37 figures, 10 tables and 7 appendices

Examiners: Professor Tero Tynjälä and D.Sc. (Tech.) Eero Inkeri

Supervisor: Research Scientist Jere Elfving

Keywords: direct air capture, CO_2 adsorption, amine-functionalized adsorbent

Direct air capture (DAC) has shown high potential for climate change mitigation by removing CO_2 from the atmosphere and then either storing it into geological storages to generate negative emissions or utilizing it as a feedstock in various applications. The DAC technology based on amine-functionalized adsorbents has proven to be a particularly promising method for CO_2 capture. However, the costs of DAC are still too high for large-scale deployment due to the technical challenges related to adsorbents and high specific energy requirement (SER) of the process. Improving the performance of the adsorbents is the most important way to reduce the costs.

In this thesis, experiments and modelling were used to evaluate how different operating conditions and adsorbent parameters affect the performance of the amine-functionalized adsorbents. The experiments investigated the CO_2 adsorption and desorption capacities of the adsorbent, while the modelling utilized a dynamic CO_2 adsorption model to simulate CO_2 productivity and SER in a fixed adsorbent bed.

It was noticed that humidity may even double the CO_2 adsorption capacity, but the co-adsorbed H_2O increased the SER in regeneration. Increasing the regeneration temperature, on the other hand, accelerated the regeneration and thus improved CO_2 productivity. Both CO_2 productivity and SER could also be improved by optimizing the cycle duration. Among the adsorbent properties, the most significant in terms of CO_2 productivity and SER were cyclic stability, maximum capacity and kinetic parameters.

TIIVISTELMÄ

Lappeenrannan–Lahden teknillinen yliopisto LUT

LUT Energiajärjestelmät

Energiatekniikka

Aaro Luukkonen

Uudenlaisten CO_2-adsorbenttimateriaalien kokeellinen ja mallinnuspohjainen arviointi hiilidioksidin talteenottoon suoraan ilmakehästä

Energiatekniikan diplomityö

2022

115 sivua, 37 kuvaa, 10 taulukkoa ja 7 liitettä

Tarkastajat: Professori Tero Tynjälä ja TkT Eero Inkeri

Ohjaaja: Tutkija Jere Elfving

Avainsanat: hiilidioksidin talteenotto suoraan ilmakehästä, CO_2-adsorptio, amiinifunktionalisoitu adsorbentti

Hiilidioksidin talteenotto suoraan ilmakehästä (DAC) on osoittanut suurta potentiaalia ilmastonmuutoksen hillitsemisessä ja kaapattua hiilidioksidia voidaan hyödyntää joko geologiseen varastointiin negatiivisten päästöjen tuottamiseksi tai raaka-aineeksi erilaisiin prosesseihin. Amiineilla funktionalisoituihin adsorbentteihin perustuva DAC-tekniikka on osoittautunut erityisen lupaavaksi menetelmäksi CO_2:n talteenotossa. DAC:n kustannukset ovat kuitenkin edelleen liian korkeat laajamittaiseen käyttöönottoon johtuen adsorbentteihin liittyvistä teknisistä haasteista ja prosessin korkeasta ominaisenergiatarpeesta (SER). Adsorbenttien suorituskyvyn kehittäminen onkin siksi tärkein keino pienentää kustannuksia.

Tässä diplomityössä arvioitiin kokeiden ja mallinnuksen avulla, miten erilaiset käyttöolosuhteet ja adsorbentin ominaisuudet vaikuttavat amiinifunktionalisoitujen adsorbenttien suorituskykyyn. Kokeilla tutkittiin adsorbentin CO_2-adsorptio- ja desorptiokapasiteetteja, kun taas mallinnuksessa käytettiin dynaamista CO_2-adsorptiomallia simuloimaan CO_2-tuottavuutta ja SER:iä kiinteässä adsorbenttipedissä.

Työssä havaittiin, että ilmankosteus voi jopa kaksinkertaistaa CO_2-adsorptiokapasiteetin, mutta tällöin adsorboitunut vesi kasvattaa SER:iä pedin regenerointivaiheessa. Regenerointilämpötilan kohottaminen sen sijaan nopeutti regenerointia ja siten paransi CO_2-tuottavuutta. CO_2-tuottavuutta ja SER:iä voitiin parantaa myös optimoimalla syklin kestoa. Adsorbentin ominaisuuksista merkittävimmät CO_2-tuottavuuden ja SER:in kannalta olivat syklinen kestävyys, maksimikapasiteetti ja kineettiset ominaisuudet.

ACKNOWLEDGEMENTS

First of all, I would like to thank my supervisor Jere Elfving for the excellent guidance and numerous ideas related to the thesis. I am grateful to VTT for the opportunity to immerse myself in this inspiring topic that deals with meaningful issues. I also want to thank my examiners Tero Tynjälä and Eero Inkeri from LUT University for their comments and effort during the work.

Jyväskylä, August 2022
Aaro Luukkonen

SYMBOLS AND ABBREVIATIONS

Roman characters

b	adsorption affinity	[1/bar]
b_1	adsorption affinity in reaction 1	[$bar^{-1}(mol/kg)^{1-t1}$]
b_2	adsorption affinity in reaction 2	[$bar^{-2}(mol/kg)^{1-t2}$]
c	concentration	[mol/m^3]
c_p	specific heat capacity	[J/(kg K)]
C	GAB isotherm parameter	[-]
CCD	cyclic capacity drop coefficient	[%/cycle]
CRF	capital recovery factor	[-]
d	diameter	[m]
D_L	axial dispersion coefficient	[m^2/s]
E	energy	[J]
h	heat transfer coefficient	[$W/(m^2 K)$]
$-\Delta H$	isosteric heat of reaction	[J/mol]
ΔH_C	enthalpy difference between mono- and multilayer adsorption	[J/mol]
ΔH_K	enthalpy difference between H_2O condensation and multilayer adsorption	[J/mol]
i	interest rate	[-]
k	parameter in linear and Freundlich isotherm models	[-]
$k_{\mathrm{f},1}$	forward reaction kinetic constant in reaction 1	[$bar^{-1}s^{-1}(mol/kg)^{1-t1}$]
$k_{\mathrm{f},2}$	forward reaction kinetic constant in reaction 2	[$bar^{-2}s^{-1}(mol/kg)^{1-t2}$]
$k_{i,\mathrm{LDF}}$	linear driving force model kinetic constant of species i	[1/s]
K	GAB isotherm parameter	[-]
K_z	axial effective heat conductivity	[W/(m K)]
L	length	[m]
m	mass	[kg]
n	plant lifetime	[a]

$\dot{n}$	molar flow rate	[mol/s]
n_{Fr}	Freundlich isotherm exponential parameter	[-]
n_{Sips}	Sips isotherm exponential parameter	[-]
N	number of cells	[-]
p	partial pressure	[bar]
Δp	pressure drop	[Pa]
P	pressure	[bar]
q	adsorption capacity / uptake	[mol/kg]
q_{m}	maximum adsorption capacity	[mol/kg]
$q_{\mathrm{m,mono}}$	monolayer adsorption capacity of water	[mol/kg]
$\bar{q}_i$	average adsorption capacity of species i	[mol/kg]
R	radius	[m]
R_{id}	ideal gas constant	[J/(mol K)]
Re	Reynolds number	[-]
t	time	[s]
t_{Toth}	Toth isotherm exponential parameter	[-]
t_1	exponential parameter in reaction 1	[-]
t_2	exponential parameter in reaction 2	[-]
T	temperature	[K]
v	velocity	[m/s]
V	volume	[m^3]
$\dot{V}$	volume flow rate	[m^3/s]
y	volume fraction	[-]
z	axial coordinate	[m]

Greek characters

ε	adsorbent bed porosity	[-]
ν	kinematic viscosity	[m^2/s]
ρ	density	[kg/m^3]

Subscripts

a	adsorbent
b	backward
bed	adsorbent bed
B	bulk
des	desorption
exp	experimental
ext	external
eq	equilibrium
f	forward
fan	air fan
feed	feed gas
g	gas
i	interstitial
i	adsorbing gas species
j	number of the computational cell under consideration
in	inlet
out	outlet
p	particle
s	superficial
sat	saturation
sen	sensible
tot	total
vac	vacuum
w	wall
0	initial/reference/zero loading
1	reaction 1 (dry conditions)
2	reaction 2 (humid conditions)

Abbreviations

BECCS	Bioenergy carbon capture and storage
BFB	Bubbling fluidized bed

Capex	Capital expenditures
CCS	Carbon capture and storage
CCU	Carbon capture and utilization
CCUS	Carbon capture, utilization, and storage
CFB	Circulating fluidized bed
CSA	Concentration swing adsorption
DAC	Direct air capture
DACCS	Direct air carbon capture and storage
GAB	Guggenheim-Anderson de Boer isotherm
GHG	Greenhouse gas
HT DAC	High-temperature direct air capture
LCOD	Levelized cost of direct air capture
LDF	Linear driving force
LT DAC	Low-temperature direct air capture
NET	Negative emission technology
MOF	Metal-organic framework
MSA	Moisture swing adsorption
Opex	Operating expenditures
PSA	Pressure swing adsorption
PSCC	Point-source carbon capture
SER	Specific energy requirement
S-TVSA	Steam-assisted temperature-vacuum swing adsorption
TCSA	Temperature-concentration swing adsorption
TS	Temperature swing
TSA	Temperature swing adsorption
TVSA	Temperature-vacuum swing adsorption
TVCSA	Temperature-vacuum-concentration swing adsorption
VSA	Vacuum swing adsorption

Table of contents

Abstract

Acknowledgements

Symbols and abbreviations

1. Introduction 11
    1.1 Strategies for reducing CO_2 emissions 11
    1.2 Direct air capture (DAC) technologies 15
    1.3 Objectives and scope of the thesis 17
    1.4 Thesis structure 18
2. Review of adsorbent-based DAC process 19
    2.1 Adsorption process 20
        2.1.1 Adsorption equilibrium and isotherms 21
        2.1.2 Transport mechanisms and dynamics 26
    2.2 Regeneration methods 28
        2.2.1 Pressure (PSA) and vacuum swing adsorption (VSA) 29
        2.2.2 Concentration swing adsorption (CSA) 30
        2.2.3 Temperature swing adsorption (TSA) 30
        2.2.4 Temperature-concentration swing adsorption (TCSA) 31
        2.2.5 Temperature-vacuum swing adsorption (TVSA) 32
    2.3 DAC process configurations 33
    2.4 Adsorbent materials 35
        2.4.1 Desirable adsorbent properties 36
        2.4.2 Amine-functionalized adsorbents 38
        2.4.3 Other adsorbent materials 43
    2.5 Economics 44
        2.5.1 Cost estimates of DAC systems 45
        2.5.2 Cost breakdown of DAC systems 48
        2.5.3 Energy requirement 51
3. Experimental and modelling methods 54
    3.1 Experimental methods 54

3.1.1 Adsorbent sample 54
3.1.2 Fixed-bed adsorption/desorption device and experimental setup 54
3.1.3 Experiments 56
3.1.4 CO_2/H_2O capacity calculation 60
3.2 Modelling methods 62
3.2.1 Kinetic CO_2 adsorption model 63
3.2.2 Dynamic CO_2 adsorption model 65
3.2.3 Specific energy requirement modelling 71
3.2.4 Cycle time optimization 73
3.2.5 Execution of the sensitivity analysis 75
4. Results and discussion 76
4.1 Experimental results 76
4.1.1 Experimental CO_2 working capacity 76
4.2 Modelling results 79
4.2.1 Model validation 80
4.2.2 CO_2 productivity and specific energy requirement 85
4.2.3 Sensitivity analysis of adsorbent-related parameters 91
5. Conclusions 103
References 108

Appendices

Appendix 1. DAC plants in operation and under development.

Appendix 2. Model parameters used in the dynamic CO_2 adsorption model validation and experiment-based calculations of CO_2 productivity and SER.

Appendix 3. Model parameters used in the sensitivity analysis that differ from the previously presented parameters.

Appendix 4. Experimental and simulated CO_2/H_2O concentration and temperature profiles from the closed TVSA experiment and closed-inlet model.

Appendix 5. Experimental and simulated CO_2/H_2O adsorption and desorption capacity profiles from the TCSA experiment and open-inlet model.

Appendix 6. Experimental and simulated CO_2/H_2O adsorption and desorption capacity profiles from the closed TVSA experiment and closed-inlet model.

Appendix 7. The impacts of certain +/- changes in the adsorbent-related parameters on CO_2 productivity and SER.

1. Introduction

There is a large amount of scientific evidence pointing out that human-induced increases in global greenhouse gas (GHG) concentrations have led to an increase in global surface temperatures. IPCC has reported that the observed global mean surface temperature was 1.09 ℃ higher in 2011-2020 compared to 1850-1900 level (IPCC, 2021, pp. 4–5). In 2019, global annual GHG emissions reached a record of 58.1 Gt CO_2 equivalent from which the main contributor, fossil CO_2 emissions, accounted for 37.9 Gt CO_2 equivalent. The global average atmospheric CO_2 concentration has risen dramatically from around 280 ppm to 412.5 ppm by 2020 from the pre-industrial era (Lindsey, 2020). Although CO_2 is the major GHG (74%), other noteworthy GHG emissions also exist including methane CH_4 (17%), nitrous oxide N_2O (6%) and some fluorinated gases (2%) (Ritchie, Roser and Rosado, 2020). (UNEP, 2021, pp. 4–5)

Due to the severe influences of climate change, such as precipitation changes, increase in the global sea level, and increases in the frequency of many weather and climate extremes, nearly every nation on Earth has adopted the Paris Agreement that is aiming to limit the temperature increase to 1.5℃ or at least holding the temperature increase well below 2℃ above the pre-industrial levels (UNFCCC, 2015, p. 3; IPCC, 2021, pp. 5–8). Limiting the temperature increase to a certain level requires limiting the global cumulative CO_2 emissions to within a carbon budget. The remaining carbon budget to limit global warming to 1.5℃ with a likelihood of 83% is 300 Gt CO_2 equivalent, which will be exceeded in six years at the current level of GHG emissions, unless annual GHG emissions, especially CO_2 emissions, are substantially reduced. (IPCC, 2021, pp. 28–29)

1.1 Strategies for reducing CO_2 emissions

The countries adopted the Paris Agreement are obliged to advance climate-resilient development so that global GHG emissions could be peaked at latest in the second half of this century (UNFCCC, 2015, p. 4). This will require massive reductions in CO_2 emissions,

especially in the fossil-based power, heat, and industry sectors. Such reductions could be implemented by replacing fossil fuel-based energy with renewable energy, nuclear power, or less emitting fossil-based energy (e.g. switching coal to natural gas), improving the efficiency of energy transformation or transmission processes, and using conventional carbon capture, storage and utilization (CCUS) technologies. The conventional CCUS is also referred to as point-source carbon capture (PSCC) (Fasihi, Efimova and Breyer, 2019, p. 958). The PSCC technologies separate CO_2 from large point sources, such as fossil fuel-based power plants and industrial facilities by pre-combustion capture, post-combustion capture or oxyfuel combustion. (Fawzy et al., 2020, pp. 2073–2077)

As illustrated in Figure 1, most CO_2 emission reductions required by scenarios aimed at limiting the temperature increase to a certain level can be implemented using the conventional emission abatement technologies. However, there are sectors, such as air and marine transportation, agriculture, some heavy industries as well as land use, land use change and forestry, where conventional reduction of CO_2 emissions may not be technically or economically feasible (Erans et al., 2022, p. 4). Therefore, the net zero or net negative emissions cannot be reached in a sufficient time frame without supplementing the conventional abatement technologies with negative emission technologies (NETs) that can offset such remaining hard-to-abate emissions. NETs remove CO_2 from the atmosphere, and therefore they are able to capture and sequester CO_2 emissions from distributed sources, while conventional PSCC technologies are limited to large point sources with higher CO_2 concentrations in the feed. The climate change mitigation scenarios presented in the literature highlight the need for negative emissions, even with high levels of conventional abatement efforts. (EASAC, 2018, pp. 4–5; Fawzy et al., 2020, pp. 2077–2078)

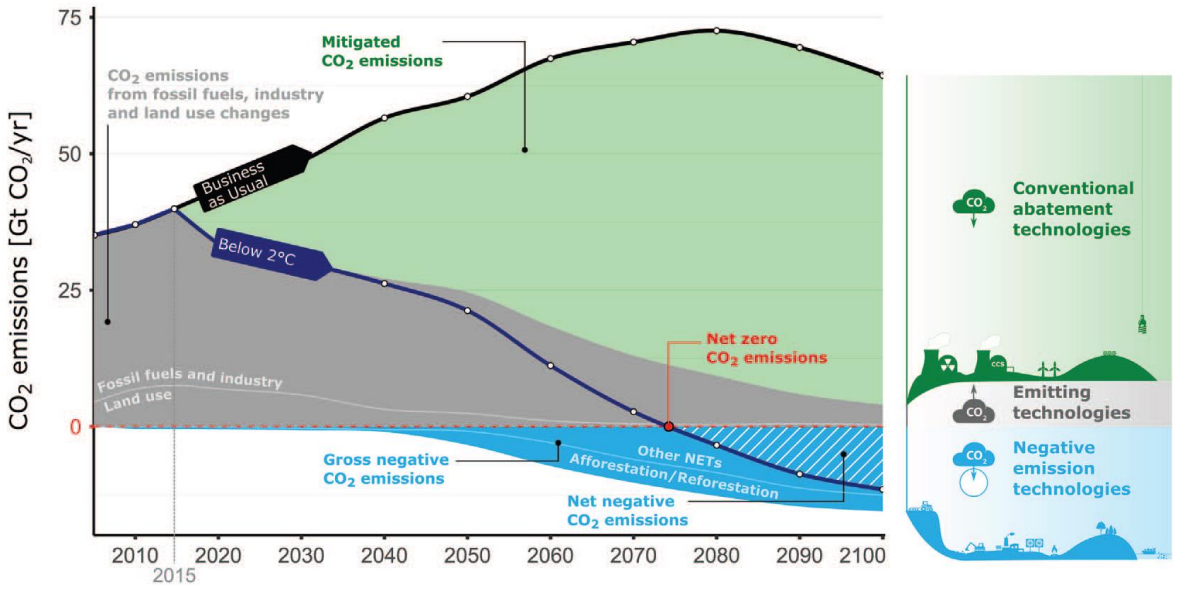

Figure 1. The role of NETs in CO_2 emissions pathways (Fuss et al., 2018, p. 5).

NETs can be classified into technology-based solutions and nature-based solutions. Technology-based NETs available today include direct air capture (DAC) combined with carbon storage (DACCS) as well as bioenergy production with carbon capture and storage (BECCS). These technologies generate negative emissions by storing the captured CO_2 similarly as conventional carbon capture and storage (CCS) technologies. The captured CO_2 is stored into products, e.g. concrete, or compressed and permanently injected into deep underground geological formations, such as depleted oil and gas reservoirs and saline formations. Kearns et al. (2017, p. 4708) have estimated that globally accessible geological CO_2 storage capacity is between 8000 and 55000 Gt with current technology. (IEA, 2020a, pp. 77–80, 109–112)

Although geological storage of captured CO_2 should be the primary option in climate change mitigation strategies, the concentrated CO_2 stream can also be utilized as a feedstock in the production of wide range of carbon-based fuels (e.g. gasoline, diesel and jet fuel) and chemicals (e.g. methanol and methane) using Power-to-X technologies. This is called carbon capture and utilization (CCU) (IEA, 2020a, pp. 108–109). By converting CO_2 to fuels and chemicals, the hard-to-abate transportation and industry sectors could be at least partly decarbonized by displacing the conventional fossil fuels. The captured CO_2 can also be

utilized in an enhanced oil recovery process to increase the yield of oil fields by injecting CO_2 into the reservoir. When a nearly pure CO_2 stream is required for geological storage, it is often possible to use lower CO_2 concentrations of 3-5% in some end-use options of CCU, such as for supply to enclosed greenhouses and algae farms, which expands the number of applicable capture technologies (Hou et al., 2017; National Academies of Sciences, 2019, p. 133). (Erans et al., 2022, p. 7)

The most promising nature-based NETs include afforestation and reforestation, enhanced weathering, ocean fertilization, biochar, and soil carbon sequestration. These methods take advantage of enhanced natural processes, land management approaches to increase the carbon content in soils, or the ability of biomass to sequester carbon during photosynthesis. (Fuss et al., 2018)

Each of these NET types has its own advantages and disadvantages. DACCS and BECCS are both currently in the small-scale demonstration phase but are still at a higher level of development compared to some nature-based NETs, such as enhanced weathering and ocean fertilization, which are only at fundamental research level. DACCS also has potential for easy scalability as well as the lowest land and water footprint among the most mature NETs. Carbon removal technologies that utilize biomass, such as BECCS and biochar, will compete for biomass resources with other end-users as well as may cause problems related to biodiversity loss and food security. In addition, the permanence of CO_2 storage is excellent with DACCS, whereas biomass-based NETs are vulnerable to weather events, pests, and fires. The problem related to ocean fertilization is that it will likely cause ocean eutrophication. With DACCS, faster CO_2 capture rate could be achieved compared to nature-based methods. The major advantage of DACCS is the flexibility of the location. It can be deployed close to renewable energy and storage facilities, minimizing transportation and grid costs. However, for a DACCS to be truly carbon negative, the electricity it consumes must come from renewable energy sources and the heat acquired from e.g. waste heat (National Academies of Sciences, 2019, p. 150). Although DACCS shows great potential and has many advantages over other NETs, its main disadvantage is the relatively high CO_2

capture costs due to high energy and material demands of the process. (EASAC, 2018, pp. 7–13; Fuss et al., 2018, pp. 1–2, 9–35)

1.2 Direct air capture (DAC) technologies

Direct air capture process extracts CO_2 directly from the ambient air using sorbent materials that bind CO_2 molecules. Numerous different sorbents have been developed and experimentally tested for both conventional carbon capture and DAC processes. The choice of sorbent depends mostly on the concentration and partial pressure of CO_2 in the gas stream (National Academies of Sciences, 2019, p. 131). Some sorbents that work well with conventional PSCC may not be suitable choices for DAC, because the concentration of CO_2 is much lower in the ambient air (approx. 400 ppm) compared to flue gas (around 5-15%), for example (Erans et al., 2022, p. 8). Most of the DAC plants in operation use solid sorbents, but also liquid sorbents (such as aqueous sodium or potassium hydroxide solutions) and non-sorbent technologies (such as electrochemical CO_2 capture and membranes) have been proposed (Sanz-Pérez et al., 2016, pp. 11843–11863). The solid sorbents can bind CO_2 from the gas stream either through an adsorption reaction onto the surface of the solid sorbent material or through an absorption reaction into the material, whereas the liquid sorbents can bind CO_2 only by dissolving it into the sorbent through absorption (Nakao et al., 2019, pp. 23–24, 46). (Shi et al., 2020, pp. 6986–6987)

The sorbent-based DAC process is reversible, and it can be cycled many times, first capturing CO_2 through adsorption or absorption, and then releasing the captured CO_2 through desorption (Gambhir and Tavoni, 2019, pp. 405–406). The desorption step is called regeneration because it returns the sorbent material to its original state.

The two main DAC technologies that are ready for commercial scale implementation are low-temperature (LT) DAC based on solid adsorbents and high-temperature (HT) DAC based on aqueous solutions. Even though HT carbon capture technology is more mature and is also used in PSCC applications, regeneration of liquid absorbents often requires

temperatures of around 900°C, which makes the regeneration costly and complex. Heating and evaporating a liquid also cause significant heat losses (Shi et al., 2020, pp. 6986–6987). Such a high temperature often requires use of fossil fuels (e.g. natural gas) thus limiting the generation of negative emissions. However, synthetic fuels or a fully electrified process could be used instead of fossil fuels, but the use of synthetic fuels would increase the primary energy demand and costs of the process. (Fasihi, Efimova and Breyer, 2019, pp. 959, 968–977)

This thesis focuses on solid adsorbent-based LT DAC, because it offers significant advantages and potential over other DAC technologies. Solid adsorbents can usually be regenerated at much lower temperatures of around 80-100°C, providing more heating options and allowing the use of cheaper low-grade heat sources, such as heat pumps and waste heat, reducing the costs related to regeneration. LT DAC systems also offers better modularity than the more complex HT DAC systems that consists of separate adsorption and regeneration units. In addition, solid adsorbents have reported to have better kinetic properties and they rise less environmental concerns related to the evaporation and leakage of the sorbent material to the air (Shi et al., 2020, pp. 6986–6987). As for water consumption, LT DAC does not require water to operate, while HT DAC may consume water up to 50 tons per ton CO_2 captured depending on the process and operating conditions. However, the cyclic stability of the promising recently studied solid adsorbents is still a problem as many materials have been reported to lose a significant part of their adsorption capacity after a few cycles, although they should last up to tens of thousands of cycles (Jahandar Lashaki, Khiavi and Sayari, 2019). (Fasihi, Efimova and Breyer, 2019, pp. 959, 968–977)

The DAC concept was first introduced for climate change mitigation by Lackner in 1999 (Lackner, Ziock and Grimes, 1999). Thereafter, the number of scientific publications on the topic has increased rapidly. Currently, there are 19 small-scale DAC plants operating worldwide capturing more than 10 kt_{CO2}/year, as listed in Appendix 1. In most of the cases, the captured CO_2 is used rather than stored. The leading companies in the field of DAC are Climeworks, Carbon Engineering and Global Thermostat. Many of these operating plants are only pilot and demonstration facilities, but commercial plants with capture capacities of

several kilotons also exist and are being developed. The world's largest DAC plant is capturing 4 kt_{CO2}/year operated by Climeworks in Iceland. Carbon Engineering has the first large-scale DAC plant under development in the United States capable of capturing up to 1 Mt_{CO2}/year. In the Net Zero Emissions 2050 scenario made by IEA, DAC accounts for 10% of the captured CO_2 in 2050, scaling up from current pilot projects to 90 Mt_{CO2}/year in 2030 and to around 1 Gt_{CO2}/year by 2050 (IEA, 2021b, p. 80). IEA's Sustainable Development Scenario as well as IPCC's SR1.5 Scenario limiting temperature increase to 1.5°C, predict smaller levels for DAC relying more on other emission reduction measures such as BECCS (IEA, 2020a, pp. 77–88). However, all these scenarios highlight the importance of CO_2 removal from the atmosphere. (IEA, 2021a)

Despite of the benefits and high estimated potential of DAC, its costs are currently too high for large-scale deployment. Its viability for cost-effective reduction in atmospheric GHG levels has therefore been debated (Sanz-Pérez et al., 2016, p. 11865). The current costs of solid adsorbent-based LT DAC reported in the literature contains lots of uncertainty and varies somewhere between 100 and 850 €/t_{CO2}, as shown in Table 1 in Section 2.5.1. However, the lowest cost estimates have been obtained with very optimistic assumptions for theoretical processes that have not yet been tested in practice in a larger-scale, and thus the actual cost is probably closer to the upper limit of the estimate. By comparing this cost to the estimated cost of conventional flue gas capture, which is typically less than 100 €/t_{CO2}, it is clear that further development is needed in the field of DAC to overcome the technical issues and reduce the costs related to high energy requirement and short sorbent lifetime (Sanz-Pérez et al., 2016, p. 11865).

1.3 Objectives and scope of the thesis

The main objective of this thesis is to evaluate how the cost-effectiveness of the DAC process could be improved, especially through novel CO_2 adsorbent material development, but also through process parameter optimization. The focus is on solid-supported amine CO_2 adsorbents that have lately received lots of attention due to their promising performance at low CO_2 concentrations typical for DAC. Although the number of research articles and

patents related to DAC has grown exponentially, there are still many technical issues to be solved and critical research gaps to be covered before large-scale commercialization can happen (Zolfaghari et al., 2022). For example, comprehensive data related to the performance of amine-based adsorbents under different conditions are still somewhat lacking in the literature. Furthermore, the effects of various adsorbent-related parameters on the performance of the DAC process have not been comprehensively investigated with process models capable of taking into account adsorbent stability, co-adsorption of CO_2 and H_2O, and cycle optimization. To get better understanding, the properties and performance of a novel amine-based adsorbent material are investigated in this work under different conditions based on both experiments and modelling of the DAC process. The key results to be examined are CO_2 productivity and specific energy requirement of the process. In addition, this work provides an extensive evaluation of the effects of different CO_2 adsorbent parameters on the CO_2 capture from air that can be used as a help in the adsorbent development.

1.4 Thesis structure

Chapter 2 gives the reader an overview of the low-temperature DAC process. First, the adsorption process is described, after which the essential DAC process configurations, regeneration methods and adsorbent materials are presented. In addition to this, cost estimates, cost breakdowns and energy requirements of the DAC process are compiled from the literature. Chapter 3 first introduces the experimental set-up and methods used to examine the properties of the adsorbent sample. Next, the CO_2 adsorption models used in the simulation of the DAC process are presented, as well as energy consumption calculations, cycle optimization methods and methods for performing an adsorbent parameter-related sensitivity analysis. The experimental and modelled results are presented in Chapter 4. In the experimental results section, the experimentally obtained adsorption and desorption capacities of CO_2 are presented, while in the modelling results section the reliability of the used model is first evaluated, and then the simulated performance of the DAC process is presented for different conditions. In the sensitivity analysis, the effect of adsorbent-related parameters on DAC cost-effectiveness is discussed. Finally, the conclusions of this work are given in Chapter 5.

2. Review of adsorbent-based DAC process

The cyclic solid adsorbent-based DAC process involves the adsorption and desorption (i.e. regeneration) phases as illustrated in Figure 2. In the adsorption phase, the fans blow air through a contactor unit, where the CO_2 molecules and possible co-adsorbing species are adsorbed on the surface of the solid adsorbent material under ambient conditions. At the same time the CO_2 depleted air leaves the contactor. Electrical fans are required to overcome the pressure drop in the contactors (Erans et al., 2022, p. 17). The adsorption phenomenon is explained in more detail in Section 2.1. (National Academies of Sciences, 2019, pp. 146–147; McQueen et al., 2021, pp. 4–5)

Once the adsorbent material is sufficiently saturated with CO_2 and the target capacity is reached, the device switches from adsorption mode to regeneration mode. The purpose of the regeneration phase is to recover the adsorbed CO_2 through desorption and return the adsorbent material close to its original state allowing for another cycle. The CO_2 molecules are desorbed from the adsorbent surface using one of the alternative regeneration methods presented in Section 2.2. In this phase, the residual CO_2 depleted air may be first evacuated from the contactor by a vacuum enabling higher purity CO_2 recovery. Furthermore, a condenser is needed if the desorbed gas stream contains notable amounts of water vapour. Finally, the concentrated CO_2 stream is often compressed to higher pressure allowing for transport, utilization, or geological storing. (National Academies of Sciences, 2019, pp. 146–147; McQueen et al., 2021, pp. 4–5)

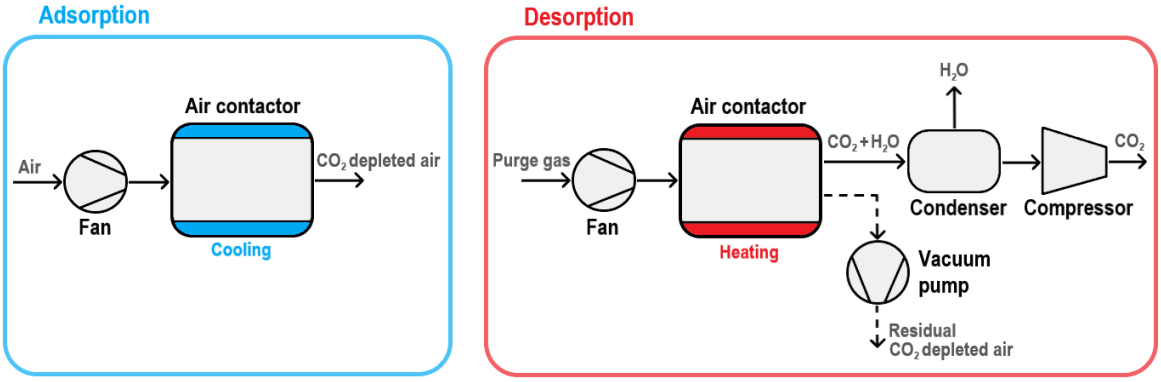

Figure 2. Simplified flowsheet of adsorbent-based two-step DAC process.

The aim of this chapter is to give an overview of the solid adsorbent-based DAC process. In addition to the explanation of the adsorption and regeneration processes, the typical process configurations for DAC are introduced in Section 2.3. Next, the most relevant types of solid adsorbent materials used for CO_2 capture under DAC conditions are presented in Section 2.4 with their typical properties. At the end of this chapter, the costs and energy requirements of the DAC process are evaluated in Section 2.5.

2.1 Adsorption process

Adsorption is a process, in which molecules, atoms, or ions from the gas or liquid phase diffuse and bind to the surface of a solid adsorbent material, as illustrated in Figure 3. The solid, often in the form of packed granular or powdery material, can either be the adsorbent itself, or it can act as a support material for a thin layer of adsorbent on it. The adsorbed solute is called as adsorbate. Adsorption can be used for selective separation of low-concentration species from a multi-component fluid flow because every component in the fluid has different adsorption affinities. In the case of DAC, the adsorption and separation of CO_2 molecules from other species in air (N_2, O_2, H_2O) is promoted by choosing favourable reaction conditions and suitable adsorbent materials with e.g. high enough selectivity for CO_2 (Oschatz and Antonietti, 2018, p. 59). (Seader, Henley and Roper, 2011, pp. 13, 568–571)

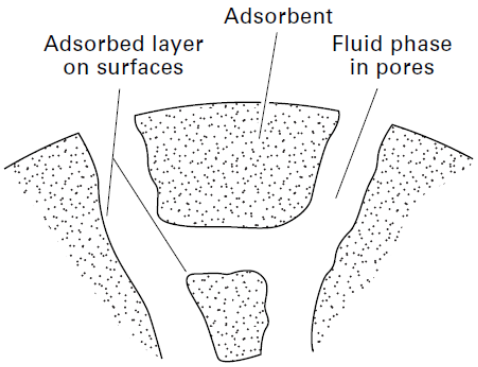

Figure 3. Adsorption on the surface of a porous adsorbent material (Seader, Henley and Roper, 2011, p. 569).

2.1.1 Adsorption equilibrium and isotherms

An adsorption equilibrium determines the distribution of the adsorbing solute between the fluid and the adsorbent surface when there has been a contact between them for a sufficient time. The equilibrium cannot be estimated directly, and therefore equilibrium data has to be obtained for the specific solute and adsorbent material in question to predict their interaction. Thus, modelling of the equilibrium data is of great importance when predicting adsorption mechanisms and modelling adsorption systems, such as DAC (Al-Ghouti and Da'ana, 2020, p. 2). Typically the equilibrium data is expressed at constant temperature in terms of adsorption isotherm, as illustrated in Figure 4. In the case of DAC, the adsorption isotherm makes it possible to predict how much CO_2 can be adsorbed on the adsorbent material (i.e. adsorption capacity) in a range of CO_2 partial pressure at a specific temperature. The shape of the adsorption isotherm depends on the adsorbate, adsorbent, and physical properties of the fluid, such as temperature. (Seader, Henley and Roper, 2011, p. 578)

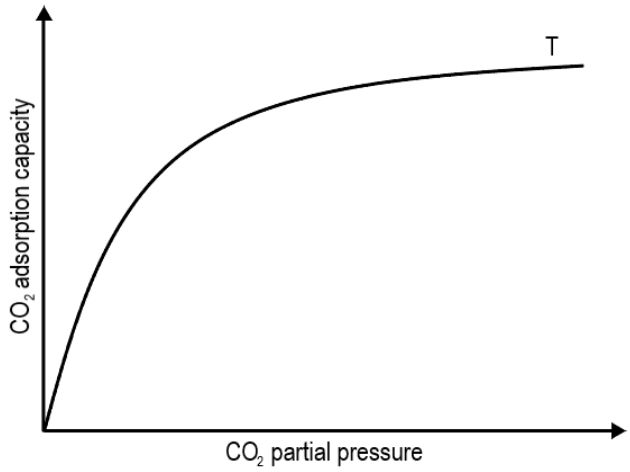

Figure 4. CO_2 adsorption isotherm.

Many empirical and theoretical approaches have been developed to model and correlate adsorption isotherms. There are adsorption isotherm models for both pure gases and multi-component gas mixtures. The isotherms for gas mixtures are much more complex than those of single-component gases because they have to take into account the effect of each gas component on the adsorption capacity and the adsorption promoting or hindering influences on other components. However, if all but one gas components are insignificant, the isotherm of pure gas can be used. Generally, an isotherm model is chosen that most accurately predicts the adsorption performance of a particular adsorbate and adsorbent under certain conditions (Al-Ghouti and Da'ana, 2020, p. 2). (Seader, Henley and Roper, 2011, p. 582)

Sing et al. (1985, pp. 611–612) have categorized six experimentally observed adsorption isotherms based on their shape, as shown in Figure 5. The Type I isotherm is rather simple demonstrating monomolecular layer adsorption. Due to the upwards convex shape, this isotherm is highly favourable representing strong adsorption even with low partial pressures of adsorbing solute in the fluid. An advantage of the favourable isotherm is the sharpening effect on the solute concentration wave front allowing for larger utilization of the adsorbent bed (Seader, Henley and Roper, 2011, p. 605). The Type II isotherm is favourable as well corresponding to multimolecular layer adsorption. The Type III isotherm is corresponding to multimolecular layer adsorption, where the heat of adsorption increases after the first molecular layer. This isotherm is highly unfavourable due to its downwards convex shape

resulting in low adsorption capacities except at high partial pressures. However, this type of isotherm is uncommon. Types IV and V isotherms represents the Types II and III isotherms with a difference that they consider the capillary condensation, which is a mechanism where the pores of the adsorbent get filled with the adsorbate via capillary effects. As a result of the capillary condensation, the Types IV and V isotherms involve a hysteresis loop. The Type VI isotherm represents stepwise multilayer adsorption on a uniform non-porous adsorbent surface. (Sing et al., 1985, pp. 611–612; Seader, Henley and Roper, 2011, pp. 571, 578–579)

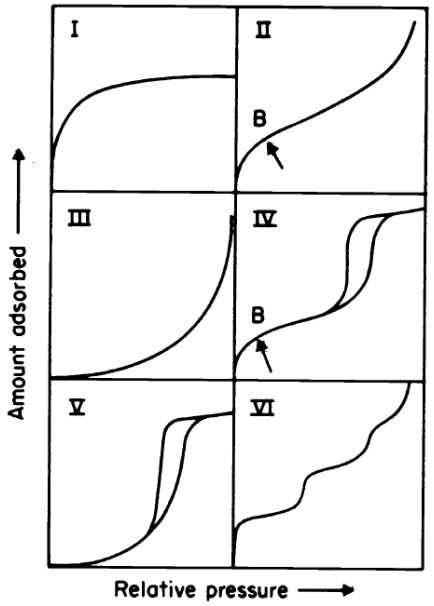

Figure 5. Basic types of adsorption isotherms (Sing et al., 1985, p. 612).

Due to the differences between adsorbate-adsorbent interactions, various adsorption isotherm models have been developed with differing number of parameters. Some of the single-component isotherm models often reported in the literature are linear, Langmuir, Freundlich, Sips, and Toth. (Al-Ghouti and Da'ana, 2020, pp. 2–3)

The linear isotherm, also knowns as Henry's isotherm, is the simplest isotherm possible. In linear isotherm model, the adsorbate loading develops linearly as a function of partial pressure of the adsorbate. At some cases, other isotherms may also resemble linear isotherm

if the adsorption capacity remains very low at all partial pressures due to special conditions such as very high adsorption temperature. The linear isotherm model is given as:

$$q_i = kp_i \tag{1}$$

where q_i is the adsorption capacity of species i, k is an empirical temperature-dependent constant and p_i is the partial pressure of species i. (Seader, Henley and Roper, 2011, pp. 579–580)

Freundlich and Langmuir equations are the most widely used correlations for modelling non-linearly behaving adsorption performance because they can simply correlate Type I isotherms. Freundlich isotherm model is given as:

$$q_i = kp_i^{\frac{1}{n_{\mathrm{Fr}}}} \tag{2}$$

where n_{Fr} is a temperature-dependent exponential parameter. (Seader, Henley and Roper, 2011, pp. 579–580)

Langmuir isotherm model is restricted to monomolecular layer adsorption and Type I isotherms. It assumes homogeneous adsorption along the adsorbent material (Al-Ghouti and Da'ana, 2020, p. 6). Langmuir model is given as:

$$q_i = \frac{q_{\mathrm{m}} b p_i}{1 + b p_i} \tag{3}$$

where q_{m} is the maximum adsorption capacity corresponding to complete adsorbent surface coverage and b is the adsorption affinity coefficient. (Seader, Henley and Roper, 2011, p. 581)

Sips isotherm model has been obtained by combining the Langmuir and Freundlich models. It can resolve some of the limitations concerning the previous models and predict the heterogeneity of the adsorption systems (Al-Ghouti and Da'ana, 2020, p. 10). Sips isotherm model is given as:

$$q_i = \frac{q_{\mathrm{m}}(bp_i)^{\frac{1}{n_{\mathrm{Sips}}}}}{1 + (bp_i)^{\frac{1}{n_{\mathrm{Sips}}}}} \tag{4}$$

where n_{Sips} is a temperature-dependent exponential parameter (Do, 1998, pp. 57–58).

The Toth isotherm model has been developed to fix the limitations of the Sips and Freundlich models related to the incomplete correlation at low- or high-end pressures ranges. The Toth isotherm model has found to predict accurately the CO_2 adsorption at low atmospheric CO_2 partial pressures thus being suitable for DAC modelling (Elfving, Bajamundi and Kauppinen, 2017, p. 6087). Toth isotherm model is given as:

$$q_i = \frac{q_{\mathrm{m}} bp_i}{[1 + (bp_i)^{t_{\mathrm{Toth}}}]^{\frac{1}{t_{\mathrm{Toth}}}}} \tag{5}$$

where t_{Toth} is a temperature-dependent exponential parameter. (Do, 1998, pp. 64–65)

In practical adsorption processes, multi-component gas mixtures are often present instead of pure single-component gases. Some co-adsorbing components may noticeably affect the adsorption of the primary component. This also applies to the DAC process, where the adsorption of CO_2 is the primary focus, but its adsorption is also affected by the adsorption of other components present in air (e.g. H_2O) (Oschatz and Antonietti, 2018, p. 59). Sometimes the CO_2 adsorption experiments are carried out using dry air, but in practice the air contains humidity. Especially the co-adsorption of H_2O is essential due to its ability to promote or hinder the CO_2 adsorption depending on conditions and adsorbents used (Kolle, Fayaz and Sayari, 2021, pp. 7281–7282). Since the single-component isotherm models cannot handle multiple components, one solution is to extend and modify these adsorption isotherm models to incorporate multiple gas components. The multiple-component modifications are possible for some models, such as Langmuir and Toth. In a model developed by Wurzbacher et al. (2016, p. 1332) the effect of water on CO_2 capture is described with an empirical enhancement factor that is a function of CO_2 partial pressure and relative humidity. The Guggenheim-Anderson de Boer (GAB) isotherm model has been

commonly used to describe the H_2O adsorption in DAC conditions as a function of relative humidity, given as:

$$q_{\mathrm{H2O}} = \frac{q_{\mathrm{m,mono}} C K \left(\frac{p_{\mathrm{H2O}}}{p_{\mathrm{H2O,sat}}}\right)}{\left(1 - K\left(\frac{p_{\mathrm{H2O}}}{p_{\mathrm{H2O,sat}}}\right)\right)\left(1 + K\left(\frac{p_{\mathrm{H2O}}}{p_{\mathrm{H2O,sat}}}\right)(C-1)\right)} \tag{6}$$

where $q_{\mathrm{m,mono}}$ is the maximum monolayer adsorption capacity of water, p_{H2O} is the partial pressure of water and $p_{\mathrm{H2O,sat}}$ is the saturation vapour pressure of water (Quirijns et al., 2005, p. 1807; Stampi-Bombelli, van der Spek and Mazzotti, 2020, pp. 1186–1187). (Seader, Henley and Roper, 2011, p. 582)

Temperature dependent GAB isotherm parameters C and K are calculated by:

$$C = C_0 \exp\left(\frac{\Delta H_{\mathrm{C}}}{R_{\mathrm{id}} T}\right) \tag{7}$$

$$K = K_0 \exp\left(\frac{\Delta H_{\mathrm{K}}}{R_{\mathrm{id}} T}\right) \tag{8}$$

where C_0 and K_0 are dimensionless parameters, ΔH_{C} is the enthalpy difference between mono- and multilayer adsorption, ΔH_{K} is the enthalpy difference between H_2O condensation and multilayer adsorption, R_{id} is the ideal gas constant and T is the temperature (Quirijns et al., 2005, p. 1807).

2.1.2 Transport mechanisms and dynamics

The mass transfer processes in a contactor unit, which is a column filled with adsorbent particles or consists of monolithic adsorbent structures, resist the instantaneous adsorption of species from the feed stream to the surface of the adsorbent, as shown in Figure 6. The external transport of the solute in the bulk flow between the adsorbent particles takes place by means of convection and dispersion. From the bulk flow, the solute diffuses through the boundary layer surrounding the particle into the tiny pores of the adsorbent. Within the pores, the solute can transport by diffusion, and finally it is adsorbed to the vacant adsorption site

on the surface of the pore. The adsorption process is typically exothermic, and the amount of energy it releases is measured as a heat of adsorption. The desorption reaction, which is endothermic, follows the opposite order of transportation of species. (Seader, Henley and Roper, 2011, pp. 571, 587–588)

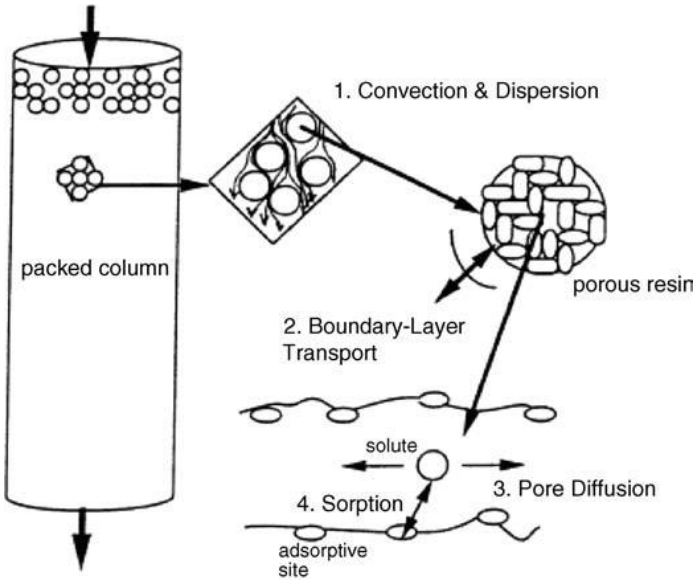

Figure 6. The mass transfer processes in adsorption (Seader, Henley and Roper, 2011, p. 587).

The concentration of the adsorbing solute in the adsorbent bed changes with time during adsorption process, as illustrated in the concentration-distance profile in Figure 7. When the clean adsorbent bed is exposed to feed containing adsorbing species, the fluid-phase solute concentration begins to rise within the bed. The solute concentration first rises at the inlet of the bed, from where the solute wave front begins to spread forward in the flow direction as the proportion of the vacant adsorption sites decreases. The concentration of adsorbing solute in a particular part of the bed rises until that part becomes fully saturated and reaches dynamic balance (i.e. equilibrium) with the feed. The mass transfer resistances lead to a broadening of the solute wave front. The more favourable is the shape of the isotherm, the sharper is the achieved concentration wave in the bed. In the modelling of the DAC process, the speed of the adsorption reaction dynamics is analysed with the breakthrough curve, which tells how close the outlet concentration of the solute is to the feed concentration. The breakthrough curve reaches its maximum value when the adsorbent bed is completely saturated. (Seader, Henley and Roper, 2011, pp. 602–605)

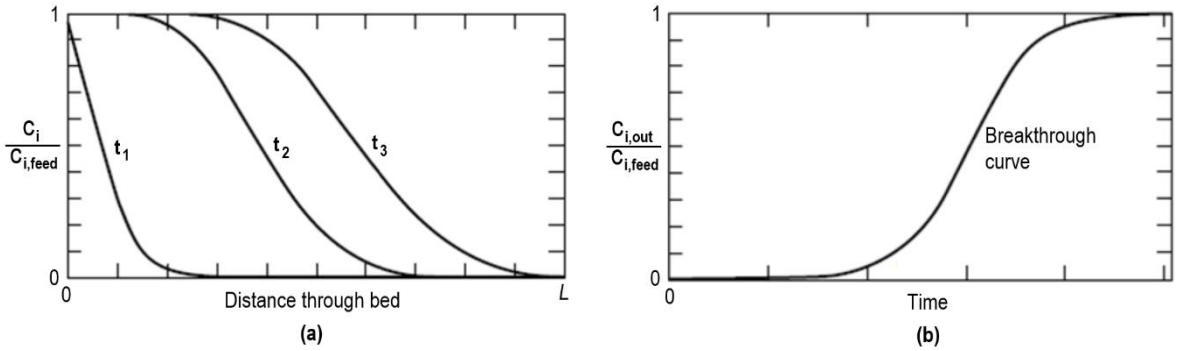

Figure 7. Solute concentration profiles in the adsorbent bed. (a) Concentration-distance profiles. (b) Breakthrough curve. Reproduced from (Seader, Henley and Roper, 2011, p. 602).

2.2 Regeneration methods

To recover the CO_2 adsorbate and to reuse the adsorbent bed after the adsorption step, the bed must be regenerated by desorption (Seader, Henley and Roper, 2011, p. 569). Several regeneration methods have been developed for solid adsorbent materials. Unlike adsorption, regeneration is accomplished by increasing the equilibrium driving force for the adsorbed species to desorb from the solid adsorbent (Green and Perry, 2008, p. 1836). CO_2 can be desorbed from the adsorbent by shifting the adsorption equilibrium by increasing the temperature or decreasing the partial pressure of CO_2. This comes out from the adsorption isotherm, which expresses the CO_2 adsorption capacity as a function of temperature and CO_2 partial pressure, as described in Section 2.1.1. Desorption of CO_2 at some specific part of the bed only occurs when the equilibrium capacity is less than the current loading of the bed in these conditions. The various regeneration swings evaluated in this section and their achievable equilibrium working capacities are illustrated in Figure 8. Equilibrium working capacity of the adsorbent means the difference between the equilibrium loading at adsorption and desorption conditions, telling the maximum achievable working capacity (Sabatino et al., 2021, p. 2055). However, typically the adsorption and desorption phases are interrupted before reaching the equilibrium state in order to shorten the cycle time and improve the productivity of the DAC process. (Bos et al., 2018, pp. 11141, 11147)

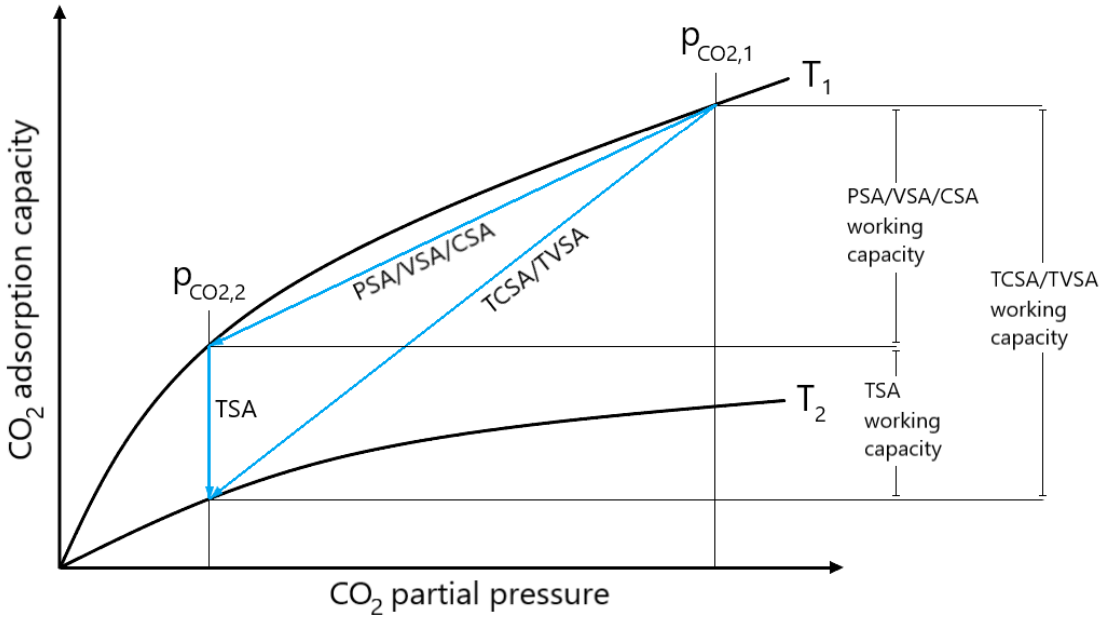

Figure 8. Various regeneration swings and their working capacities. Reproduced from (Seader, Henley and Roper, 2011, p. 610; Elfving, 2021, p. 37).

Attempts have been made to maximize the working capacity of the adsorbent and the rate of desorption and to minimize the energy consumption and the loss of adsorption capacity between consecutive cycles by choosing proper regeneration conditions, such as temperature, pressure, and flow rate of the possible purge gas (Serna-Guerrero, Belmabkhout and Sayari, 2010, pp. 4166–4171). Cost-effective CO_2 recovery by regeneration is a key feature that enables practical large-scale DAC systems (Goeppert et al., 2012, p. 7847). In most cases, the storage and utilization applications require the production of high-purity CO_2, and this restricts the choice of regeneration method (Erans et al., 2022, pp. 7, 19).

2.2.1 Pressure (PSA) and vacuum swing adsorption (VSA)

Pressure swing adsorption (PSA) is a type of process in which the adsorption of CO_2 takes place at elevated pressure, while the desorption is executed by reducing the pressure so that the partial pressure of CO_2 decreases, and CO_2 is released from the bed (McQueen et al., 2021, p. 9). The temperature remains constant during the cycle. The advantage of PSA is the short cycle time (Yang et al., 2019, p. 284). PSA is also the most mature cyclic process for solid adsorbents (Sabatino et al., 2021, p. 2053). Vacuum swing adsorption (VSA) is another

method relying solely on pressure change (Yang et al., 2019, p. 284). In VSA, desorption is accomplished under vacuum. However, both PSA and VSA are not considered suitable for DAC, because reaching a sufficiently high working capacity would require either a very high pressurization of the high flow-rate feed or an unpractically high vacuum during regeneration (Elfving et al., 2017, p. 274). This would result in unreasonably high energy requirements and capital expenditures due to vacuum pumps and compressors. (Wijesiri et al., 2019, p. 15607)

2.2.2 Concentration swing adsorption (CSA)

Concentration swing adsorption (CSA) is an approach, in which desorption is performed at the same temperature and total pressure as adsorption either by reducing the CO_2 partial pressure using an inert purge gas that sweeps CO_2 from the adsorbent or by displacing adsorbed CO_2 with another adsorbable gas (Green and Perry, 2008, p. 1839). Inert purge gases such as N_2, Ar, He, and air have been used in DAC-related laboratory-scale adsorption studies to desorb CO_2 from the adsorbent (Wijesiri et al., 2019, p. 15607; Yang et al., 2019, pp. 281–282). The disadvantage of using an inert purge gas is that it cannot be removed from the product gas, and thus the CO_2 is obtained in a dilute form (Yang et al., 2019, p. 284).

2.2.3 Temperature swing adsorption (TSA)

Temperature swing adsorption (TSA) process relies on temperature change. The adsorbent is heated during regeneration by heating the purge gas before it enters to the adsorption column or by heating elements located inside the column or covering it (Green and Perry, 2008, p. 1837; Goeppert et al., 2012, p. 7847). The energy demand of TSA is significantly increased due to heating of inactive components of the DAC system, such as support and packing materials of the adsorbents (Erans et al., 2022, p. 19). Temperature swing process is the most effective regeneration method for CO_2 capture with supported amine adsorbents due to the high energy needed to break the bonds between CO_2 and amines (Li et al., 2010, p. 899). Pure TSA could be a suitable method to produce CO_2 for utilization applications

that accept CO_2 at lower concentrations and are not impeded by the other gas components in air (Elfving et al., 2017, p. 276).

2.2.4 Temperature-concentration swing adsorption (TCSA)

To achieve more efficient regeneration processes, approaches combining the earlier mentioned methods have been investigated (Bos et al., 2018, p. 11141). In the temperature-concentration swing adsorption (TCSA) process, the adsorbent is desorbed by both heating and purging with gas (Wijesiri et al., 2019, p. 15606). TCSA has been the most widely used desorption method in laboratory-scale adsorbent studies (Wijesiri et al., 2019, pp. 15606–15607; Yang et al., 2019, pp. 281–282). The rate of desorption is increased at higher temperatures (Wang et al., 2015, p. 978; Bos et al., 2018, p. 11147). However, the maximum allowable temperature is limited. Amine-functionalized adsorbents have found to be susceptible to degradation at temperatures higher than 120°C, which limits the applicable range of thermal swing and thus the achievable CO_2 production (Gebald, Repond and Wurzbacher, 2017, p. 11).

To face the problem of dilute CO_2 product caused by using inert purge gases, the use of CO_2 as a purge gas has been assessed to produce high-purity CO_2 (Wijesiri et al., 2019, p. 14607). However, CO_2 as a purge gas may cause deactivation of the amine-based adsorbents at elevated temperatures and thus lead to loss of adsorption capacity (Jahandar Lashaki, Khiavi and Sayari, 2019, p. 3348). In addition, the CO_2 purge gas may slow down the desorption rate due to keeping the CO_2 partial pressure high close to the adsorbent (Hoffman et al., 2014, p. 187).

Another more commonly used method for producing a high-purity CO_2 is to use steam as a purge gas, which can be easily removed later by condensation. This process is known as steam-stripping. Steam as a purge gas provides both thermal energy for desorption and a partial pressure driving force. Steam-stripping has shown faster desorption kinetics and

better stability with solid amine sorbents compared to utilization of inert purge gases (Sandhu et al., 2016, p. 2219). (Li et al., 2010, p. 899)

2.2.5 Temperature-vacuum swing adsorption (TVSA)

Temperature-vacuum swing adsorption (TVSA) is a promising method used by the first commercial solid adsorbent DAC systems to produce nearly pure CO_2 from air (Deutz and Bardow, 2021, pp. 203–204). In the TVSA process, adsorption is first performed at ambient conditions, followed by blowdown, where the air inlet is closed, and the residual air is evacuated from the column by applying a vacuum. After that, the desorption is conducted either by heating the column with an external heating mechanism under a vacuum or by using a hot steam purge. A regeneration temperature of around 100°C is typically sufficient (Sabatino et al., 2021, p. 2054). After the desorption step, the adsorption column is repressurized and cooled by opening the air inlet, returning the column to its initial conditions. The advantage of TVSA is that it does not require that high vacuum level for DAC application than pure VSA due to the simultaneous heating (Wijesiri et al., 2019, p. 15607). However, smaller achievable working capacities have been reported with TVSA compared to TCSA with an inert gas purge. The desorption rate could be improved by higher temperatures and stronger vacuum levels. (Wurzbacher, Gebald and Steinfeld, 2011, pp. 3588–3590; Stampi-Bombelli, van der Spek and Mazzotti, 2020, p. 1188; Elfving et al., 2021)

Steam-assisted temperature-vacuum swing adsorption (S-TVSA) has also been proposed for DAC (Gebald, Repond and Wurzbacher, 2017). Steam purge enhances the desorption rate of CO_2 because the adsorption of H_2O during the steam purge release additional energy for CO_2 desorption. Higher steam flow results in faster desorption and decreases the costs related to vacuuming, but it increases the thermal energy costs (Stampi-Bombelli, van der Spek and Mazzotti, 2020, p. 1183). The steam could be supplied at temperatures lower than 100°C allowing for utilization of low-grade waste heat or solar energy. (Zhu et al., 2021, pp. 2–3)

2.3 DAC process configurations

The design of the contactor unit is of great importance for achieving efficient CO_2 capture (Erans et al., 2022, pp. 16–17). Fixed bed, monolithic, moving bed, fluidized bed, and fibre contactor designs have been investigated for solid adsorbent DAC systems (Zhang et al., 2014; Sinha et al., 2017; Sujan et al., 2019; Yu and Brilman, 2020).

Adsorption in DAC process relying on solid adsorbents is typically performed in a fixed bed (McQueen et al., 2021, p. 9). The fixed bed is a cylindrical column filled with adsorbent particles. To achieve continuous operation, multiple batch-wise operated fixed beds are often used periodically, with some beds adsorbing while the others are regenerating, as shown in Figure 9 (Seader, Henley and Roper, 2011, p. 13). The fixed bed contactor offers some advantages over the fluidized bed for DAC, including a more compact size and potential for lower pressure drop (Yu and Brilman, 2020, p. 2).

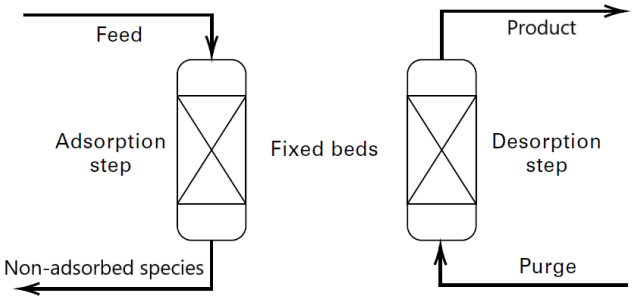

Figure 9. Fixed bed adsorption process. Reproduced from (Seader, Henley and Roper, 2011, p. 610).

Like in the fixed bed design, the adsorption and desorption steps are similarly periodically switched in the monolithic, fibre, and some fluidized bed designs (Erans et al., 2022, p. 18). Monolithic contactors contain monolithic channels that are covered inside with an adsorbent film (Sinha et al., 2017, p. 752). The advantages of monolithic contactor structure are lower pressure drop and higher mass transfer rate compared to most other contactors (Sinha et al., 2017, p. 751). Sujan et al. (2019) have estimated the potential of fibre contactors for DAC. The fibre contactors are densely packed monolithic structures that contain adsorbing

material, such as amines (Sujan et al., 2019, p. 5267). Fibre contactors can also provide a low pressure drop with solid adsorbents (Sujan et al., 2019, p. 5267).

By contrast to stationary batch-wise operating contactors, moving bed and some fluidized bed designs involve continuous replacement of the bed material through adsorbent circulation, as shown in Figure 10 and Figure 11 (Erans et al., 2022, p. 18). The circulation enables continuous running, and it is accomplished by moving the saturated adsorbent bed material from the adsorber to the regenerator, while constantly replenishing the adsorber with the regenerated adsorbent (Seader, Henley and Roper, 2011, pp. 621–623; Yang et al., 2019, p. 283). The potential advantages of moving bed systems are the avoided time-consuming heating and cooling steps and reduced pressure drop, but the operation is more complicated and more mechanical energy is needed (Yang et al., 2019, p. 283; McQueen et al., 2021, p. 9). In addition, both bubbling fluidized bed (BFB) and circulating fluidized bed (CFB) configurations are possible for DAC, but the high pressure drop is a result of high fluidizing velocities needed to suspend and circulate the bed particles (Zhang et al., 2014, p. 306). In a CFB system the riser acts as the adsorber and the return leg as the regenerator (Zhang et al., 2014, p. 312).

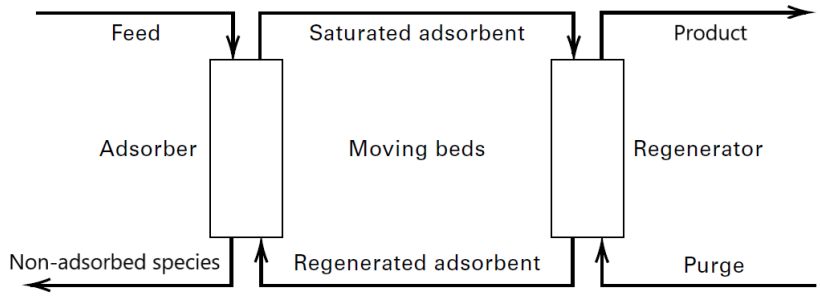

Figure 10. Moving bed adsorption process. Reproduced from (Seader, Henley and Roper, 2011, p. 610).

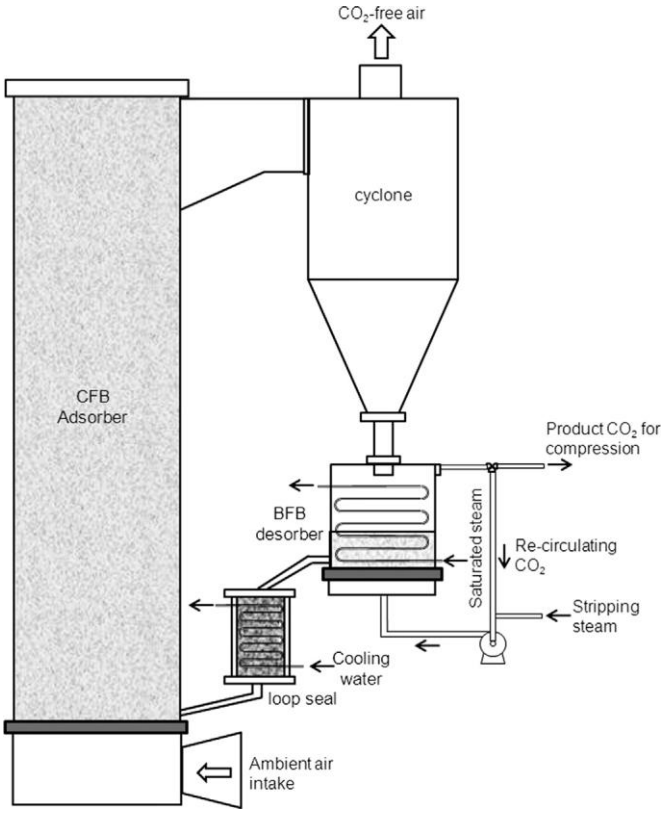

Figure 11. Circulating fluidized bed DAC process (Zhang et al., 2014, p. 313).

2.4 Adsorbent materials

Solid adsorbent materials for DAC can be divided into physisorbent and chemisorbent materials depending on the type of interaction between the adsorbent material and the adsorbate (CO_2). Chemisorption involves the formation of covalent or ionic chemical bond between the adsorbate and adsorbent material, whereas physisorption is based on weaker physical interactions without changing the chemical bonding structure. Thus, the binding energy between the CO_2 molecules and the adsorbent material, i.e. isosteric heat of adsorption, is only about 8-50 kJ/mol for physisorbents, while chemisorbents require 40-800 kJ/mol (Nakao et al., 2019, p. 47; Abd et al., 2020, p. 3). The weak interaction of physisorbents decreases the CO_2 selectivity and adsorption capacity, while the high chemical binding energy of chemisorbents results in easy capture of CO_2 even from the low atmospheric concentrations. Thus, chemisorbent materials have been found to be much more effective for DAC process (Sanz-Pérez et al., 2016, p. 11843). However, the regeneration of

chemisorbent materials requires much more energy compared to regeneration of physisorbents due to the stronger bond. (Shi et al., 2020, p. 6987)

In the sections below the most important adsorbent properties and their effects on CO_2 capture have been described as well as the most popular solid adsorbent materials have been presented. The solid-supported amine-functionalized chemisorbent materials are one of the most promising group of solid adsorbent materials for DAC and thus the greatest attention has been given to them (Sanz-Pérez et al., 2016, p. 11849). In addition, couple of other solid adsorbent materials based on other mechanisms have been shortly reviewed.

2.4.1 Desirable adsorbent properties

There are many favourable properties that make the adsorbent suitable for commercial use in the DAC process. First of all, the adsorbent should have a high selectivity for CO_2, to be able to sharply separate CO_2 from the feed air, which has a very low CO_2 concentration of around 400 ppm (Shi et al., 2020, pp. 6987, 7001). High adsorption capacity is another crucial property because it determines the amount of adsorption material needed and consequently the size of the process equipment (Abd et al., 2020, p. 3). The good selectivity and adsorption capacity features originates from a high enough binding energy, i.e. heat of adsorption, between the CO_2 molecules and the adsorbent material. For example, the high heat of adsorption of amine-functionalized adsorbents enables strong adsorption performance even at low partial pressures of CO_2 (Gelles et al., 2020, pp. 8–11).

The adsorption materials are expensive, and the refilling of adsorption columns is rather onerous, so these materials should have a long operational lifetime (Abd et al., 2020, p. 3). Hence, the adsorbent should have a high mechanical strength and resistance against crushing and fouling and no tendency to promote undesirable chemical reactions (Abd et al., 2020, p. 3). In addition, the adsorbent material may degrade due to feed gas composition and operational parameters. The high temperatures in the regeneration phase can cause thermal degradation of the adsorbent material, for example due to the leaching and evaporation of

the amine in the case of amine-functionalized adsorbents. Another issue is the oxidative degradation, which can occur in the presence of oxygen at high temperatures, for example if the feed gas contains lots of oxygen or air is used to cool the column. The adsorbent can also deactivate if it is exposed to CO_2 in high concentrations during the adsorption phase or if CO_2 or steam are used as purge gas in the regeneration. Therefore, the material needs a high chemical and thermal stability to withstand many adsorption cycles. Jahandar Lashakai et al. (2019, pp. 3330–3383) have reported that many amine-based adsorbent materials lose significant parts of their adsorption capacities already after a few cycles, although they should last up to tens of thousands of cycles. (Jahandar Lashaki, Khiavi and Sayari, 2019; Shi et al., 2020, pp. 6987, 7001)

The adsorbent should also have favourable adsorption/desorption kinetics and transport properties to allow for rapid adsorption/desorption and mass transfer within the porous adsorbent material. The reaction kinetics control the cycle time and fast kinetics enable an efficient use of the adsorbent bed as the adsorbent is saturated easily, which is expressed as a sharp breakthrough curve. Thus, shorter adsorption and desorption phases can be used if the kinetics are fast, which improves the productivity of the DAC process. The regenerability, i.e. the capability of being regenerated easily, is important for the operating cost of the DAC process by the means of energy costs. The amount of energy required for regeneration varies depending on the strength of CO_2 binding, the used regeneration method, and the energy losses due to heating of the inert support material. (Abd et al., 2020, p. 3; Shi et al., 2020, pp. 6987, 7001)

Since adsorption occurs at the adsorption sites on the surface of the pores, the structure of the adsorbent material is of great importance for CO_2 capture. A high porosity of the adsorbent material and better accessibility of the sites are desirable to enable higher amine loading in the case of amine-functionalized adsorbents and to increase the rate of adsorption (Shi et al., 2020, p. 6991). High porosity also increases the specific surface area of the adsorbent material, reducing the size of the adsorbent bed. After all, the adsorbent material itself should be affordable. All these properties together affect the costs and competitiveness of the adsorption-based DAC process. (Seader, Henley and Roper, 2011, pp. 13, 568–571)

2.4.2 Amine-functionalized adsorbents

In CO_2 capture, aqueous amine-based solutions have been widely used in industry since 1930 in the process called amine scrubbing (Nakao et al., 2019, pp. 3–4). Although amine scrubbing is a mature technology, it has some drawbacks, such as appropriateness only for high concentration CO_2 capture and high energy demand during regeneration due to evaporation of liquid (Kolle, Fayaz and Sayari, 2021, p. 7281). To improve the CO_2 capture process and to decrease the costs associated to regeneration energy, amines and polyamines functionalized on porous solid supports have been proposed instead. The supported amine adsorbents are typically prepared by post-functionalization of the solid support with amines. These amine-functionalized materials can be categorized into three classes, as depicted in Figure 12, depending on their preparation methods: 1) physical amine impregnation into porous support materials, 2) chemical amine grafting onto the support surface, and 3) chemical amine grafting from the support through in situ polymerization. (Shi et al., 2020, pp. 6989–6990)

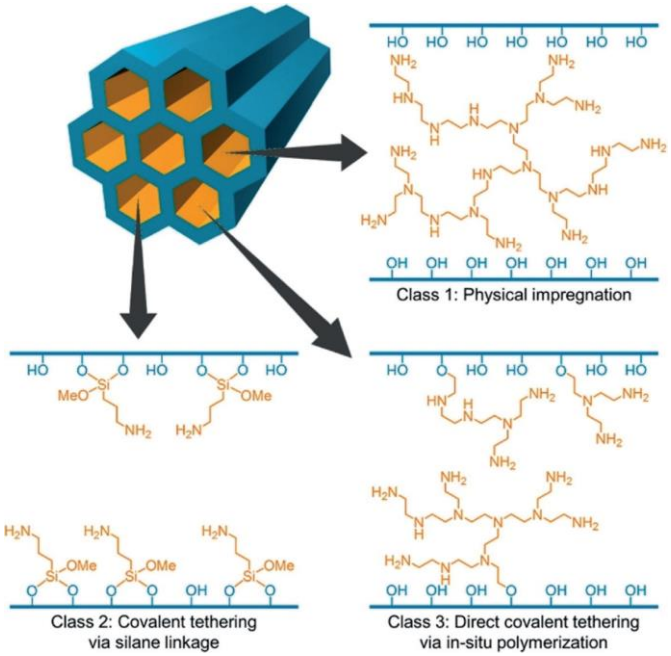

Figure 12. The three different preparation methods of amine-functionalized adsorbents (Shi et al., 2020, p. 6991).

Amines are chemical compounds that have been used for CO_2 capture due to their effective take up of CO_2 molecules through a reversible chemical reaction. More specifically, amines are functional groups that consist of a nitrogen atom and a lone pair of electrons, and form three bonds either with hydrogen atoms or with other organic groups. Amines are classified into primary, secondary and tertiary amines based on the number of organic groups attached to the nitrogen, as shown in Figure 13. A rough generalization is that primary amines have the highest reactivity towards CO_2 and tertiary amines have the worst. (Nakao et al., 2019, pp. 3–6; Shi et al., 2020, pp. 6990–6991)

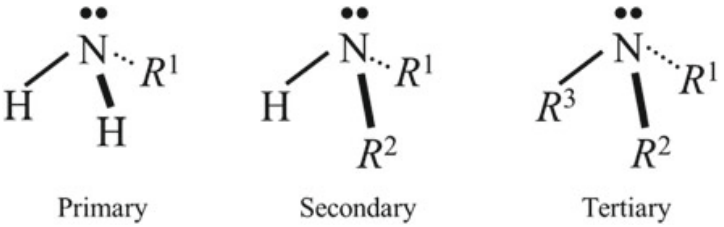

Figure 13. Classification of amines (Nakao et al., 2019, p. 5).

Amines can adsorb CO_2 in different ways depending on the reaction conditions, especially humidity. Generally, in dry conditions the reaction produces carbamate or carbamic acid carried out by primary and secondary amines, while in humid conditions the reaction can also produce bicarbonate or hydronium carbamate by also tertiary amines (Li, Kress and Mebane, 2016, pp. 23683–23686; Chen et al., 2018). However, the precise CO_2 capture mechanism in humid conditions is still ambiguous in the literature. Due to the changes in the CO_2 capture reaction mechanism, humidity has often a promoting effect on the CO_2 adsorption capacity of amine-functionalized adsorbents (Kolle, Fayaz and Sayari, 2021, p. 7282). Under dry conditions, two moles of amine are required to capture one mole of CO_2, while under humid conditions, only one mole of amine is needed to capture one mole of CO_2 and H_2O (Sanz-Pérez et al., 2016, p. 11849). Thus, humidity could theoretically up to double the maximum CO_2 adsorption capacity compared to dry conditions. However, in some cases the CO_2 capacity improvement in humid conditions may be even higher due to changes in adsorption kinetics (Sujan et al., 2019, p. 5269).

Probably the most popular support material for amines in CO_2 capture is silica due to its high porosity and thus high surface area (Halliday and Hatton, 2021, p. 9323). Widely used silica supports are for example MCM-41, SBA-15, KIT-6, MCF and silica gel (Sanz-Pérez et al., 2016, pp. 11850–11854; Ünveren et al., 2017, p. 39). Also variety of other porous support materials have been investigated, such as carbon, alumina, zeolites, and metal-organic frameworks (MOFs) (Fan and Jia, 2022, p. 1252). Especially, MOFs have shown remarkable potential as support materials for amines (McDonald et al., 2012, p. 7056; Pettinari and Tombesi, 2020, p. 14). Each of these support materials has advantages and disadvantages for the DAC process. For example, some support materials are more stable when exposed to humidity (Shi et al., 2020, p. 6994).

Amine-functionalized adsorbents, in general, offers good CO_2 adsorption capacity and selectivity for DAC process. The adsorption capacity depends largely on the amine loading of the support material. In addition, the structure of the adsorbent material, especially the accessibility of the amine sites, affects greatly the CO_2 capture ability of the adsorbent. Although increasing the amine loading typically improves the adsorption capacity, excessive amine loading begins to limit the transport within the pores (Bollini et al., 2012b, p. 15153). (Shi et al., 2020, pp. 6990–6993)

Amine-impregnated adsorbents, also called as class 1 adsorbents, are prepared by physically impregnating amines into pores of the porous support materials e.g. by wet-impregnation. Class 1 adsorbents can typically hold more amines than class 2 adsorbents, so higher adsorption capacity may be achieved. However, the weaker physical bond between amines and the support material with amine-impregnated adsorbents lead to severe stability problems over several cycles due to leaching of the amines during adsorption and regeneration steps. The problem is the most serious with low molecular weight amines, such as monoethanolamine (MEA) and diethanolamine (DEA). This will lead to more frequent replacement of the material and may cause environmental problems. High molecular weight amines are more stable, but the weight may affect negatively on CO_2 adsorption by decreasing the adsorption capacity. Thus, medium-weight amines are typically good alternatives offering a compromise between stability and adsorption capacity. Probably the

most commonly used polymeric amines in class 1 adsorbents are polyethylenimine (PEI), tetraethylenepentamine (TEPA), and polyallylamine (PAA), as depicted in Figure 14 (Sanz-Pérez et al., 2016, p. 11851). (Shi et al., 2020, pp. 6990–6993)

Elfving (2021, pp. 123–124) and Sanz-Perez et al. (2016, p. 11852) have summarized the experimental CO_2 adsorption capacities of recently studied class 1 adsorbent materials found from the literature, and their capacities are ranging from 0.5 $mmol_{CO2}/g_{adsorbent}$ to slightly over 3 $mmol_{CO2}/g_{adsorbent}$ under DAC conditions. For example, Kwon et al. (2019) reported on a PEI impregnated silica support that achieved adsorption capacity of 2.6 $mmol_{CO2}/g_{adsorbent}$ in dry DAC conditions and even 3.4 $mmol_{CO2}/g_{adsorbent}$ in the presence of humidity.

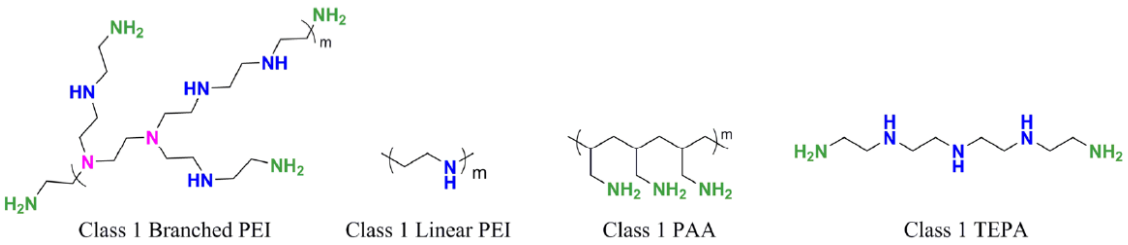

Figure 14. Molecular structures of commonly used class 1 amines for DAC adsorbents (Sanz-Pérez et al., 2016, p. 11850).

Class 2 amine-functionalized adsorbents are prepared by chemically grafting the amine functional groups onto the surface of porous support material. For DAC process, the amine-grafted adsorbents are typically prepared by covalently tethering amine-containing silanes to the support material through chemical reaction. Since the amines are tethered to the support with strong covalent bonds, these adsorbent materials are more stable during regeneration compared to class 1 adsorbents. The commonly used amines in DAC applications for class 2 adsorbents are depicted in Figure 15. (Shi et al., 2020, p. 6995)

The experimental adsorption capacities of some relevant class 2 adsorbents summarized by Elfving (2021, p. 125) and Sanz-Perez et al. (Sanz-Pérez et al., 2016, p. 11854) are ranging

between 0.17 $mmol_{CO2}/g_{adsorbent}$ and 3.89 $mmol_{CO2}/g_{adsorbent}$ under DAC conditions. The best among them (Mg_2(dobdc)) reported by Liao et al. (2016), uses hydrazine diamine to functionalize a MOF support. It has shown excellent performance under dry DAC conditions at 25°C achieving CO_2 adsorption capacity of 3.89 $mmol_{CO2}/g_{sorbent}$ with amine loading of 6.01 $mmol_N/g_{sorbent}$ (Liao et al., 2016, p. 6528). However, this value is clearly above the typical adsorption capacities of class 2 adsorbents and therefore it should be viewed with a little skepticism.

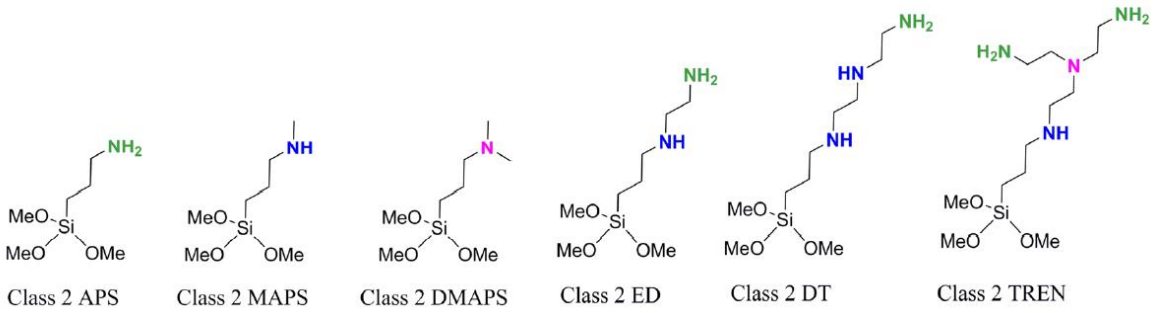

Figure 15. Molecular structures of commonly used class 2 amines for DAC adsorbents (Sanz-Pérez et al., 2016, p. 11850).

Class 3 amine-functionalized adsorbents are prepared through in-situ polymerization of amine-containing monomers on solid support material resulting in polyamine structures covalently bound to the material surface. Like class 2 adsorbents, class 3 adsorbent materials are also stable over multiple adsorption and regeneration cycles due to strong chemical bond between the amine and support material. According to Choi et al. (2011, p. 2421), they are also easy to manufacture and potentially cost-effective. (Shi *et al.*, 2020, pp. 6990, 6998)

Choi et al. (2011, pp. 2423–2425) have evaluated the performance of hyperbranched aminosilica (HAS) materials on porous silica supports in atmospheric CO_2 concentrations. By increasing the amine loading to 9.9 $mmol_N/g_{adsorbent}$, they achieved CO_2 adsorption capacity of 1.72 $mmol_{CO2}/g_{adsorbent}$. The report concluded that HAS adsorbents could provide a higher adsorption capacity compared to class 2 adsorbents with larger amine loading and without significant degradation of the material. A poly(L-lysine) brush-mesoporous silica hybrid is another class 3 adsorbent material evaluated by Chaikittisilp et al. (2011) lately,

but its adsorption capacity did not outperform HAS materials. The molecular structures of these class 3 amines are illustrated in Figure 16.

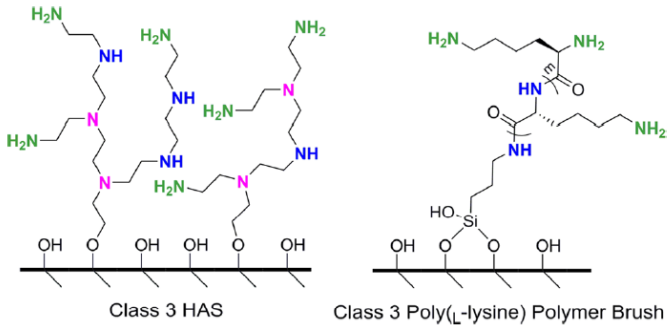

Figure 16. Molecular structures of commonly used class 3 amines for DAC adsorbents (Sanz-Pérez et al., 2016, p. 11850).

2.4.3 Other adsorbent materials

The well-known solid physisorbent materials, such as activated carbon, zeolites, and metal organic frameworks (MOFs) have not shown a remarkable potential for DAC process without modification and amine-functionalization. Their main disadvantage is the poor selectivity and thus low adsorption capacity in the atmospheric CO_2 concentrations due to their low heat of adsorption, making them unfavourable choices for DAC. They are also often negatively affected by moisture that always exist in the ambient air, as the water may strongly compete with CO_2 for physical adsorption sites (Kolle, Fayaz and Sayari, 2021, pp. 7281–7282). However, the regeneration of these physical adsorbents is faster and less energy consuming compared with amine-based chemisorbents, for example. These physisorbents can be modified by e.g. amine-functionalization to change them to chemisorb CO_2 and hence improve their performance. The applicability of some novel physisorbent materials, such as boron nitride nanomaterials and graphene, has also been investigated for CO_2 capture. (Abd et al., 2020, p. 15; Shi et al., 2020, pp. 6988–6989)

In addition to solid adsorbent materials, separation by recently studied polymeric membranes could be a potential option for DAC. Membranes could offer some advantages over

adsorbent-based CO_2 separations, such as easier scalability and higher energy-efficiency. However, this method reported by Fujikawa et al. (2021) could produce CO_2 only at around 40% concentration, which makes it suitable only for CCU applications and not for geological storage. (Fujikawa, Selyanchyn and Kunitake, 2021, pp. 111–117)

2.5 Economics

The costs of the solid adsorbent-based DAC process consist of capital expenditures (Capex) and operating expenditures (Opex). The capital expenditures involve process equipment costs and financing costs, while the operating expenditures include energy costs, adsorbent costs, labour costs, maintenance costs as well as CO_2 transport and storage costs. Levelized cost of DAC (LCOD) is a measure that makes it possible to compare the costs of various DAC applications reported in the literature that all involve different capacities, lifetimes and interest rates. The LCOD expresses the annual discounted expenditures of DAC per tonne of CO_2 captured, and it can be calculated as: (IEAGHG, 2021, pp. 9–10)

$$LCOD = \frac{Capex \cdot CRF + annual\ fixed\ Opex + variable\ Opex \cdot annual\ CO_2\ capture}{annual\ CO_2\ capture} \quad (9)$$

The capital recovery factor (CRF) is calculated with interest rate (i) and plant lifetime (n) by (IEAGHG, 2021, p. 10):

$$CRF = \frac{i(1+i)^n}{(1+i)^n - 1} \quad (10)$$

In the sections below, the current and projected costs of solid adsorbent-based DAC systems reported in the literature are first presented and the main ways to reduce the costs are suggested. Also, the comparability and uncertainties related to cost literature are discussed. Next, a cost breakdown of the LT DAC system is presented giving typical ranges for each cost component. Lastly, the energy requirement of the LT DAC plants is assessed in more detail based on literature.

2.5.1 Cost estimates of DAC systems

The cost estimates for DAC in the literature range from about 15 to 850 €/t_{CO2} depending on the process, scale and underlying assumptions, as shown in Table 1. Costs expressed in US dollars ($) have been converted into euros by using a 10-year average conversion rate (1 $ = 0.8478 €) (European Central Bank, 2022). Some sources have reported DAC costs as the costs of captured CO_2 ignoring the emissions from operating the DAC process, while the others have reported the cost of avoided CO_2, resulting in high deviation in cost estimates (Fuss et al., 2018, pp. 17–18). If fossil fuels are used to produce energy in the DAC system, the costs of net CO_2 removed should be considered, as the combustion process produces CO_2 emissions (National Academies of Sciences, 2019, p. 154). The studies are also focusing on different DAC technologies with differing process conditions as well as differing output CO_2 purities and pressures (Fasihi, Efimova and Breyer, 2019, p. 966). In most cases, the studies only cover the CO_2 capture and regeneration processes excluding the compression and transport that are relevant for all end-use options as well as storage that is required for DACCS. The period covered by the studies may be the present or the future, and sometimes it is not even precisely defined. It is also often unclear whether the cost is reported as LCOD. Furthermore, the assumptions related to energy prices, interest rates and lifecycle emissions have a very large impact on the resulting cost estimate. This makes the direct comparison of the reported costs very difficult. (IEAGHG, 2021, p. 5)

Table 1. DAC costs reported in the literature.

Technology	Indicated time of cost [year]	Cost reported [€/t_{CO2}]	Reference
LT DAC based on solid adsorbent	2017	51-161[1] (60-190 $)	(Sinha et al., 2017, p. 761)
	2018	75-744[1] (89-877 $)	(National Academies of Sciences, 2019, p. 154)
	2018	509-678 (600-800 $)	(Tollefson, 2018; Birnbaum, 2021) (**Climeworks**)
	2020	464-593[1,2] (547-699 $)	(IEAGHG, 2021, p. 14)
	First plant	120-291[2] (142-343 $)	(Larsen et al., 2019, pp. 49–50)
	2030	170-254 (200-300 $)	(Birnbaum, 2021) (**Climeworks**)
	2040	85 (100 $)	(Tollefson, 2018; Birnbaum, 2021) (**Climeworks**)
	2050	148-214[1,2] (174-253 $)	(IEAGHG, 2021, p. 16)
	First commercial-scale plant	127 (150 $)	(Climate Advisers, 2022) (**Global Thermostat**)
	2050	32-54	(Fasihi, Efimova and Breyer, 2019, p. 957)
	n/a	13-42 (15-50 $)	(Kintisch, 2014) (**Global Thermostat**)
DAC based on MSA in solid adsorbent	2009	170 (200 $)	(Lackner, 2009)
	Long-term	25 (30 $)	(Lackner, 2009)
Generic DAC (process not specified)	2011	848[1] (1000 $)	(House et al., 2011, p. 20433)
	2018	509-848 (600-1000 $)	(Fuss et al., 2018, p. 20)
	2020	110-288 (130-340 $)	(IEA, 2020b, p. 147)
	2050	< 254[1] (300 $)	(House et al., 2011, p. 20433)
	Long-term	85-254 (100-300 $)	(Fuss et al., 2018, p. 20)
	2050	39-139 (46-164 $)	(Larsen et al., 2019, p. 28)
	Long-term	34-119 (40-140 $)	(Broehm, Strefler and Bauer, 2015, p. 15)

[1]Cost of net CO_2 captured. [2]Cost of DACCS.

The current costs of solid adsorbent-based LT DAC reported in the literature varies roughly between 100 and 850 €/t_{CO2}. The extreme lower bound estimate of 51-161 €/t_{CO2} comes from a modelling-based economic assessment performed by Sinha et al. (2017, p. 761), in which they analysed two MOF adsorbents in a TVSA cycle. However, this estimate does not include all the necessary cost components such as compression stage. House et al. (2011, p. 20433) have given a sceptical upper limit estimate of 848 €/t_{CO2} based on an empirical

analysis of operating commercial processes, suggesting that the costs of CO_2 capture have been underestimated. Climeworks, one of the leading companies in the field of LT DAC, has stated that the cost of its operating plant is currently around 509-678 €/t_{CO2} (Tollefson, 2018; Birnbaum, 2021). Another company, Global Thermostat, estimates that its first commercial scale plant will cost 127 €/t_{CO2} (Climate Advisers, 2022). In the other economic analyses listed in Table 1, the current DAC costs are estimated to range mainly between 200-700 €/t_{CO2}. The lower net CO_2 capture cost estimates are for low-cost renewable energy powered systems with higher capacities of around 1 Mt_{CO2}/a (National Academies of Sciences, 2019, p. 154; IEAGHG, 2021, p. 14).

The cost of DAC is expected to decrease significantly in the future due to the economies of scale and optimization of the systems (Broehm, Strefler and Bauer, 2015, p. 15). Solid adsorbent-based LT DAC may have more room for cost reductions since it utilizes more novel processes compared to more mature liquid adsorbent-based HT DAC. LT DAC systems also allow for easier mass production due to their higher modularity. Decreasing adsorbent prices and improving performance are likely to be the most important factors in the reduction of the LT DAC costs, making this thesis highly relevant. In addition, the lifetime of the DAC plants is expected to increase from around 10 years to 25 years, further reducing the costs. (IEAGHG, 2021, pp. 4, 21)

However, making cost estimates for DAC is very challenging due to the high extent of uncertainty. Because the technology is still relatively novel and large-scale DAC plants do not yet exist, major assumptions are required about plant scaling factors, interest rates, adsorbent cost-performance development and future cost reduction through learning and innovation. The wider construction of DAC pilot plants will further clarify the cost estimates (Fasihi, Efimova and Breyer, 2019, p. 959). The long-term cost estimates for DAC reported in the literature are highly speculative because they are commonly based on learning rates observed in other relevant sectors. The learning rate describes how much the cost of a certain technology decreases as the installed capacity doubles. The IEAGHG's technical report estimates that the learning rate for solid adsorbent-based DAC is about 12%. (IEAGHG, 2021, pp. 6, 19, 21)

As shown in Table 1, some economic assessments and review articles state that the cost of DAC will fall from the current first-of-a-kind plant costs to 34-254 €/t_{CO2} for nth-of-a-kind plant through market scale-up under both optimistic and pessimistic assumptions. The companies operating in the field of DAC have also presented rather ambitious cost reduction targets. Climeworks expects that they could drop the costs to 170-254 €/t_{CO2} by 2030 and around 85 €/t_{CO2} by 2040 (Tollefson, 2018; Birnbaum, 2021). Global Thermostat estimates that the costs will fall as low as 13-42 €/t_{CO2}, but they have not specified any time frame for that (Kintisch, 2014). Fasihi et al. (2019, p. 957) have presented a scenario where the LT DAC is powered by hybrid PV-wind-battery systems in Moroccan conditions and the cost of this system will reach 32-54 €/t_{CO2} by 2050 depending on the availability of free waste heat. Lackner (2009) has proposed that very low cost of 25 €/t_{CO2} could be achieved in the long-term by using moisture swing adsorption (MSA) for solid adsorbents relying on moisture changes instead of temperature or pressure swings.

2.5.2 Cost breakdown of DAC systems

As mentioned earlier, the capital expenditures of the DAC process involve process equipment costs and financing costs. The financing costs are influenced by the interest rate as well as lifetime and availability of the plant. Since the LT DAC plants based on solid adsorbents are rather Capex intensive, it is beneficial to run them on high full-load hours as it lowers the LCOD (Fasihi, Efimova and Breyer, 2019, p. 969). According to the IEAGHG's sensitivity analysis, the lifetime of the plant has a strong impact on the LT DAC costs. It has also been mentioned that current LT DAC plants have a higher Capex than HT DAC plants due to their typically shorter plant lifetimes. As a result, the investment must be recovered in a shorter time. However, the lifetime of the LT DAC plant is assumed to more than double by 2050 through technological development, especially through development of more stable adsorbent materials. The interest rate used in that study varied between 5 and 10%. (IEAGHG, 2021, pp. 14–18, 43)

The base Capex of the DAC system consist of acquiring and upgrading costs of process equipment, property (e.g. buildings) and technology (e.g. patents) (Fernando, 2022). The LT DAC system requires several process equipment, such as air contactor units, air fans, vacuum pumps, compressors, condensers as well as heating and cooling systems (Sabatino et al., 2021, p. 2054). The equipment related Capex is estimated to fall in the long term due to mass production and technology development (Fasihi, Efimova and Breyer, 2019, p. 966).

The economic data available for solid adsorbent-based LT DAC systems is rather limited compared to more mature HT DAC systems. Fasihi et al. (2019, pp. 965, 968) have estimated that the Capex for LT DAC will drop from the current assumed level of 730 €/t_{CO2} to either 199 €/t_{CO2} or 84 €/t_{CO2} by 2050 under the conservative and base case scenarios. On the other hand, IEAGHG's economic model is using much lower Capex of 173-194 €/t_{CO2} (204-229 \$/t_{CO2}) for current LT DAC plants, which is predicted to fall as low as 42-47 €/t_{CO2} (50-55 \$/t_{CO2}) by 2050 (IEAGHG, 2021, pp. 14–16). However, it is worth noting that in some sources the adsorbent costs are included in the Capex, increasing its share significantly, while in this work they are included in the Opex instead because the need to renew the adsorbent depends on the operating time of the DAC device.

The operational expenditures include adsorbent costs, energy costs, labour costs, maintenance costs as well as CO_2 transport and storage costs. Fasihi et al. (2019, p. 965) have estimated that the Opex for LT DAC are approximately 4% of the total Capex per year.

The CO_2 adsorbent costs often cover the largest share of the operational expenditures in the case of LT DAC, in contrast to HT DAC, whose costs are more dominated by energy costs (National Academies of Sciences, 2019, pp. 142–152; IEAGHG, 2021, pp. 14–16). This is because solid adsorbents, such as amine-functionalized materials, require frequent replacement due to degradation (Realmonte et al., 2019, p. 9). Deutz and Bardow (2021) have reported an amine-based adsorbent consumption of 7.5 g per kg CO_2 captured in the TVSA process based on experimental data provided by Climeworks, and they estimate that the future consumption could be limited to 3 g per kg CO_2 captured. Adsorbent development can significantly reduce CO_2 capture costs by improving the lifetime, cost and performance

of the adsorbent. Sinha et al. (2017, p. 758) estimate the purchase costs of their two MOF adsorbents to be between 13-42 €/kg (15-50 $/kg). National Academies of Sciences (2019, p. 152) estimate the purchase cost of generic solid adsorbent to be approximately 42 €/kg (50 $/kg) and the share of the adsorbent costs to be around 80% of the total costs of the LT DAC process. The report by IEAGHG (2021, p. 43) assumes that the adsorbent cost per ton CO_2 captured is 153 €/t_{CO2} (180 $/$t_{CO2}$) for current first-of-a-kind LT DAC plants, being around 30-40% of the total costs, and it is predicted fall to around 61 €/t_{CO2} (72 $/$t_{CO2}$) by 2050.

In the LT DAC process, the second most significant operational expenditures are related to energy. According to IEAGHG, the energy costs cover about 10-25% of the levelized cost of LT DAC systems. Therefore, accessibility of cheap energy is important for the competitiveness of these systems. Since emissions from energy production affect the net CO_2 removal costs of DAC, the use of lowest cost renewable energy sources (e.g. solar PV, wind power, hydropower, waste heat and geothermal energy) is favourable. (IEAGHG, 2021, pp. 10–16, 27–30)

In order to store or utilize CO_2 after capture, it often needs to be transported over various distances. The transportation can be done by pipelines, or by ships, trucks and trains. Pipelines are a safe and suitable option for large transport capacities within distances up to about 500 km. The cost of transportation by onshore pipelines is estimated to be 1.5-10 €/t_{CO2} and even higher for offshore pipelines. Longer than 2000 km distances require transportation by ship, which costs about 11-20 €/t_{CO2}. Transport by trucks and trains become economical for smaller CO_2 quantities (Karjunen, Tynjälä and Hyppänen, 2017, p. 40). (Fasihi, Efimova and Breyer, 2019, p. 973)

CO_2 storing brings some additional costs. According to the model made by IEAGHG (2021, p. 25), the CO_2 transport and storage costs can be up to 6-15% of the total DAC costs for stand-alone plants, and 53 €/t_{CO2} in the worst-case scenario. However, these costs can be significantly reduced to 4 €/t_{CO2} by using shared infrastructure and low-cost storage locations. Larsen et al. (2019, p. 50) assumes that it costs roughly 15 €/t_{CO2} to compress and

sequester the captured CO_2. Chen and Tavoni (2013, pp. 66–67) have estimated that the cost of storing CO_2 could be less than 10 €/t_{CO2} for the best storage locations in the world with a cumulative capacity of around 400 Gt_{CO2}.

2.5.3 Energy requirement

Production of high-purity CO_2 typically requires more energy-demanding cycles, such as TVSA. In the various temperature swing cycle modifications, heating of the adsorbent bed during regeneration is the most energy consuming step. Solid chemisorbents, such as amine-functionalized adsorbents, have high heats of adsorption, which increases the need for thermal energy to desorb the adsorbed species. There are also significant heat losses due to heating of inactive components such as support and packing materials of the adsorbents (Erans et al., 2022, p. 19). There may also be a trade-off between energy consumption and productivity. With solid amine-based adsorbents, the co-adsorption of H_2O in the presence of humidity can increase the CO_2 productivity. On the other hand, if energy consumption is to be minimized, H_2O adsorption should be limited because it increases the energy demand during the regeneration step. (Sabatino et al., 2021, pp. 2050, 2065–2069)

Regeneration of solid adsorbents can be performed at much lower temperatures of around 80-100℃ compared to liquid absorbents. This low-temperature heat is cheaper to produce and can be supplied by heat pumps from low-grade waste heat sources such as power plants and industrial facilities (Fasihi, Efimova and Breyer, 2019, pp. 959, 977). Even though some LT DAC systems can run solely on electricity, it is often cheaper to use this low-grade heat alongside electricity (IEAGHG, 2021, pp. 10–16, 27–30).

The electricity consumption in the LT DAC process comes mainly from air fans, vacuum pumps, compressors, control systems and possible electric heaters. Fans are needed to overcome the pressure drop in the contactor units and their electricity consumption is rather high because large volumes of air have to be processed due to very low CO_2 concentration in the ambient air. The CO_2 production rate of the process can be affected by adjusting the

flow rate of the feed air. With a vacuum pump, a lower vacuum pressure results in more efficient removal of gas components from the contactor unit, but it leads to higher electricity consumption. The evacuation of residual air from the contactor consumes less electricity than the CO_2 recovery phase. As mentioned in Section 2.2, some regeneration methods, such as pure PSA and VSA, have been found to be economically impractical for DAC due to their too extreme pressure and vacuum requirements. In addition to the electricity consumed by compressors in the pressure swing cycles, the efficient transportation of the CO_2 product for utilization or storage requires compression of the gas to a higher pressure. Simon et al. (2011, p. 2895) have reported that the minimum energy requirement for CO_2 compression to 138 bar is 0.225 GJ/t_{CO2} and in practice around 0.375 GJ/t_{CO2} with a 60% compression efficiency. The estimate made by Erans et al. (2022, p. 8) is very similar saying that 0.28 GJ/t_{CO2} is required to compress the CO_2 from 1 bar to 150 bar. (Sabatino et al., 2021, p. 2065)

The electrical and thermal energy requirements vary significantly depending on the adsorbent and DAC process configuration. Table 2 summarizes the specific energy requirements (SER) of LT DAC systems found from the literature, divided into the shares of electrical and thermal energy. The total SER in these estimates varies in a range of 3.6-13.1 GJ/t_{CO2}. The upper limit SER estimate of 13.1 GJ/t_{CO2} given by IEAGHG (2021, p. 42) is for first-of-a-kind hybrid LT DAC plants, and it is predicted to fall to 6.5 GJ/t_{CO2} for Nth-of-a-kind plants. The SER estimates given by LT DAC companies, such as Climeworks and Global Thermostat, correspond well to other estimates presented in the literature.

Table 2. Specific energy requirements of LT DAC systems reported in the literature.

Adsorbent	Thermal energy requirement [GJ/t_{CO2}]	Electrical energy requirement [GJ/t_{CO2}]	Specific energy requirement [GJ/t_{CO2}]	Reference
Generic solid adsorbent	3.4-4.8 GJ/t_{CO2}	0.56-1.13 GJ/t_{CO2}	3.96-5.93	(National Academies of Sciences, 2019, p. 148)
Generic solid adsorbent	4.9-10.8	1.6-2.3	6.5-13.1	(IEAGHG, 2021, p. 42)
Generic solid adsorbent	-	3.6-6.6	3.6-6.6	(IEAGHG, 2021, p. 42)
Amine-based	4.4-7.2	0.6-1.1	5.0-8.3	(Realmonte et al., 2019, p. 3)
Amine-based	4.4	0.58	4.98	(Ishimoto et al., 2017, p. 9) (**Global Thermostat**)
Amine-based	5.4-7.2	0.72-1.08	6.12-8.28	(Fasihi, Efimova and Breyer, 2019, p. 963) (**Climeworks**)
Amine-based (TRI-PE-MCM-41)	5.96	0.78	6.75	(Kulkarni and Sholl, 2012)
Amine-based (MIL-101(Cr)-PEI-800)	-	5.11	5.11	(Sinha et al., 2017, pp. 757–758)
Amine-based (mmen-Mg_2(dobpdc))	-	3.59	3.59	(Sinha et al., 2017, pp. 757–758)
Ion-exchange resin	-	1.1	1.1	(Lackner, 2009, p. 102)

In hybrid DAC systems, where both electricity and heat are used, the thermal energy consumption accounts for the largest share of 3.4-10.8 GJ/t_{CO2}, whereas the electrical energy accounts only for 0.6-2.3 GJ/t_{CO2}. In contrast, electricity only DAC systems have much higher electrical energy consumption of 3.6-6.6 GJ/t_{CO2}, but in general, their total SER is in the same range as hybrids. One exception is the ion-exchange resin reported by Lackner (2009, p. 102), which operates in the MSA cycle and requires only around 1.1 GJ/t_{CO2} of electricity to operate.

3. Experimental and modelling methods

In this study, the performance of amine-functionalized CO_2 adsorbent for DAC was evaluated based on both experimental and modelling work. The experimental and modelling methods used are described in the sections below.

3.1 Experimental methods

The CO_2 adsorption and desorption experiments have been done with a laboratory-scale fixed-bed DAC device located at VTT's office in Jyväskylä. The device can be used to determine, for example, the adsorption capacity, CO_2 adsorption isotherms, cyclic stability, as well as adsorption kinetics and dynamics of the adsorbent material. The obtained measurement data can be further utilized in the validation of DAC process models.

3.1.1 Adsorbent sample

An adsorbent consisting of polystyrene resin functionalized with primary amine groups delivered by Oy Hydrocell Ltd. was used as an adsorbent sample in this study. Elfving et al. (2017) have previously studied the physical and chemical properties of this adsorbent. The adsorbent particles have been found to be spherical with a median size of 0.60 mm and a low specific surface area of 32 $m^2/g_{adsorbent}$. In addition, chemisorption has found to be the main interaction mechanism between the adsorbent and the adsorbing species at DAC conditions.

3.1.2 Fixed-bed adsorption/desorption device and experimental setup

The adsorbent sample (0.5-1 g) was placed inside an adsorption column, which can be heated or cooled by circulating either hot or cold liquid in its jacket with two manually controlled Julabo Corio CD 200 F circulators. Different CO_2/N_2 gas mixtures can be fed to the column along two alternative routes. The CO_2/N_2 composition of the feed gas mixture was controlled

by several flow rate controllers with operating ranges from 0.01 to 10 l/min, allowing the CO_2 concentration to vary from ppm level up to 100%. The feed gas can also be humidified with Hovacal Digital 122-SP humidity calibrator. The adsorption column can be bypassed along two routes, allowing the adsorption gas and purge gas compositions to be measured without changing the conditions in the adsorption column. The upper bypass route can also be utilized in the desorption step to purge the post-column piping, where part of the desorbed species tends to get stuck. Pressure in the adsorption column was controlled by two pressure control valves and a vacuum pump, which allows operation under vacuum (< 1 bar) or normal/overpressure (1-5 bar). The process scheme is shown in Figure 17.

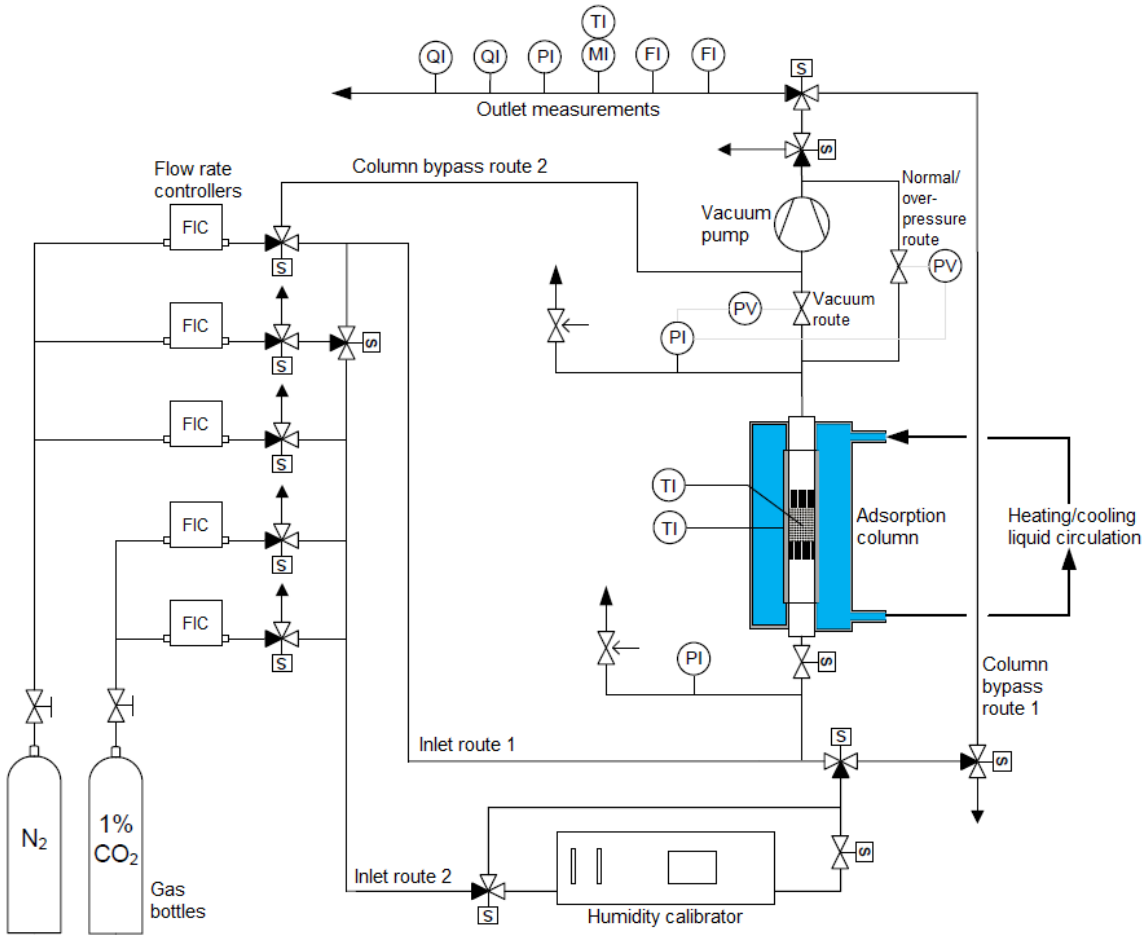

Figure 17. Process scheme of the fixed-bed adsorption/desorption device.

The temperature, pressure, flow rate, CO_2 concentration and relative humidity of the exiting gas mixture were measured with sensors and detectors located in the outlet route. Of the two flow rate sensors, one has a calibrated operating range of 0-21 ml/min and the other 0-2100 ml/min. The outlet CO_2 concentration can be measured either on the ppm- or %-scale. The operating ranges of the ppm- and %-scale measurements are between 0-5000 ppm and 0-50%. In addition to the outlet measurements, the pressure was measured both before and after the column. The temperature of the adsorption column can be measured with thermocouples either from the wall of the column or from the bed inside the column.

The experimental DAC device was operated by a Labview software on a computer connected to the experimental device. Labview is a graphical programming environment used for data acquisition and development of automated experiment systems. The setpoints for the controllable equipment (including flow rate controllers, magnetic valves, pressure control valves and vacuum pump) can be adjusted in the software either manually or by uploading a self-made spreadsheet file that defines the adjustments to be made in a step-by-step sequence. This automated sequence makes the experiments less time consuming and the results more reproducible. However, some of the valves (e.g. gas bottle valves) and equipment (such as humidity calibrator as well as heating and cooling circulators) had to be switched on manually and controlled on site. At the end of the experiment, Labview creates an experiment data file that can be processed on a computer.

3.1.3 Experiments

Two CO_2 adsorption/desorption processes, closed TVSA and TCSA, were used in the experiments as shown in Table 3. The experimental cycle of both processes consisted of three phases: pre-desorption, adsorption and desorption. Pre-desorption phases were the same for both processes, whereas the conditions and methods used in the adsorption and desorption phases varied between them. The main difference was that in the closed TVSA process the column inlet was closed during the whole desorption step, while in the TCSA process it remained open.

Table 3. The conditions, durations and methods used in each cycle step of the two experimental CO_2 adsorption/desorption processes.

Process & conditions	Pre-desorption	Adsorption	Pre-vacuum/ purge	Temperature swing	Desorption of remaining species
TVSA closed:					
Inflow	N_2 purge	400 ppm CO_2, 0-2 vol-% H_2O	No inflow	No inflow	N_2 purge
Temperature	100 ℃	25 ℃	25 ℃	60/100 ℃	60/100 ℃
Method	TCSA, TVCSA	-	VSA	TVSA	TVCSA
Duration	1 h 10 min	5 h	1 h	2 h	1 h 15 min
TCSA:					
Inflow	N_2 purge	400 ppm CO_2, 0-2 vol-% H_2O	N_2 purge	N_2 purge	N_2 purge
Temperature	100 ℃	25 ℃	25 ℃	25-100 ℃	100 ℃
Method	TCSA, TVCSA	-	CSA	TCSA	TVCSA
Duration	1 h 10 min	2 h	0.5 h	~3 h	0.5 h

In the pre-desorption phase, the adsorbent was completely regenerated using the TCSA method with 1000 ml/min N_2 purge gas flow for 40 min and after that TVCSA with 100 ml/min N_2 purge and around 50 mbar vacuum for 30 min. In this phase all the pre-adsorbed species were removed and measured. The pre-desorption phase was required only for a fresh sample.

Before the adsorption phase, the CO_2 and H_2O concentrations of the feed gas were measured by bypassing the adsorption column. As the experiments were performed under both dry and humid conditions, the composition of the feed gas varied depending on the experiment. In the dry experiments, a feed gas mixture representing dry ambient air containing N_2 and about 400 ppm CO_2 was used, while in the humid experiments the feed gas was humidified to contain 2 vol-% H_2O. In addition, the N_2 purge gas was measured to be able to do the baseline corrections for CO_2 and H_2O concentrations. In the adsorption phase, the feed gas with a total flow rate of 500 ml/min was fed into the adsorption column at ambient pressure and a temperature of 25 ℃ for 2-5 hours.

The desorption phase depended significantly on the regeneration method used. Most of the experiments conducted in this work were based on the closed TVSA method. The steps during the closed TVSA experimental cycle are illustrated in a CO_2 concentration profile in

Figure 18. In the closed TVSA experiments, desorption began with a pre-vacuum step, in which the adsorption column was evacuated of the gas phase or weakly-bound molecules (mainly N_2 but also H_2O to some extent in humid experiments) using a vacuum that could reach up to 11-14 mbar. The pre-vacuum step lasted 30 min, during which the column inlet was kept closed. Next, the column was heated to 60 or 100 °C in the closed TVSA step, still using the vacuum and keeping the column inlet closed for 1 hour. Finally, a TVCSA method was used to desorb all CO_2 and H_2O remaining in the column by opening the column inlet and purging the column with 500 ml/min N_2 purge gas flow for 1 hour. However, the TVCSA step was only intended for checking the share of CO_2 uptake that remained undesorbed in the closed TVSA process and therefore it was not part of the actual closed TVSA process.

Since significant part of the desorbed CO_2 and H_2O tended to get stuck into the post-column pipeline, these evolved species were measured by purging the piping with 100 ml/min N_2 gas flow through the upper column bypass route 2 for 15-60 min after each regeneration step. As shown in Figure 18, flushing the pipeline may lead to high CO_2 concentration measurement peaks, because the N_2 purge flow carried the trapped desorbed gases suddenly to the measurements. The pipeline flushing was important so that the amount of CO_2 desorbed by each desorption step could be specified.

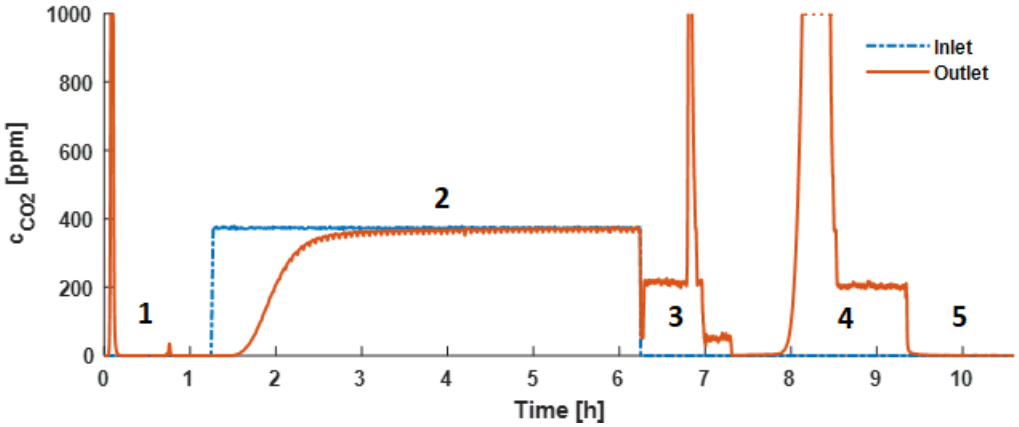

Figure 18. The steps of closed TVSA experiment in a CO_2 concentration profile: 1) pre-desorption, 2) adsorption, 3) pre-vacuum (VSA), 4) temperature swing using vacuum (TVSA), and 5) desorption of remaining species using TVCSA.

The experiments performed by using the TCSA process were only used for model validation. In this case the desorption started with a CSA step, in which N_2 purge of 1000 ml/min flowed through the adsorbent bed for 30 min. After that the TCSA regeneration method was used, and the column was heated step by step from 25 °C to 100 °C, still purging with N_2. This temperature ramping made it possible to validate the heat transfer and kinetics of the model by comparing the experimental and modelled temperature and concentration profiles within the column at each temperature step. The temperature ramping stage took about 100 minutes, including a 10-15-minute waiting time after each temperature change. The TCSA step with 1000 ml/min purge flow continued for 1 hour after the last temperature change, after which a lower purge flow of 100 ml/min was used for 15 min. Finally, the same TVCSA step was performed as in the closed TVSA experiment to check the share of CO_2 uptake that remained undesorbed in the TCSA process.

The adsorption and desorption experiments were performed using 0.5 g and 1 g adsorbent samples under both dry and humid conditions. In addition, humid closed TVSA experiments were repeated at both 60 and 100 °C regeneration temperatures to reveal the effect of regeneration temperature on working capacity and specific energy costs. The experiments performed are listed in Table 4.

Table 4. The performed experiments and their differing conditions.

Experiment number	Process	Feed gas CO_2 concentration [ppm]	Feed gas H_2O concentration [vol-%]	Adsorbent weight [g]	Regeneration temperature [°C]
1	TVSA closed	400 ppm CO_2	-	0.5	100
2	TVSA closed	400 ppm CO_2	-	1.0	100
3	TVSA closed	400 ppm CO_2	-	-	100
4	TVSA closed	400 ppm CO_2	2 vol-% H_2O	0.5	100
5	TVSA closed	400 ppm CO_2	2 vol-% H_2O	0.5	60
6	TVSA closed	400 ppm CO_2	2 vol-% H_2O	1.0	100
7	TVSA closed	400 ppm CO_2	2 vol-% H_2O	1.0	60
8	TVSA closed	400 ppm CO_2	2 vol-% H_2O	-	100
9	TCSA	400 ppm CO_2	2 vol-% H_2O	0.5	25-100*
10	TCSA	400 ppm CO_2	2 vol-% H_2O	-	25-100*

* Temperature ramping step by step from 25 to 100°C.

Each experiment was performed using only one cycle, except for the three experiments (3, 8 and 10) in which the capacities caused by the empty column were measured. Empty column capacities were measured by performing two experiments without an adsorbent sample for both dry and humid closed TVSA cases as well as humid TCSA cases from which an average was taken for each case. The empty column capacities measured were then subtracted from the experimental capacities obtained with the adsorbent samples.

3.1.4 CO_2/H_2O capacity calculation

The experiment-based adsorption and desorption capacities for CO_2 and H_2O were calculated by numerically integrating the mass balances of the gas components in the adsorption column with respect to time. The equation for calculating the volume of adsorbed or desorbed species $V_{i,\mathrm{exp}}$ varied depending on the phase of the cycle. In the case of adsorption phase, the volume of adsorbed species was calculated by:

$$V_{i,\mathrm{exp}} = \int_{t_0}^{t} \dot{V}_{\mathrm{tot}}\left(y_{i,\mathrm{in}} - y_{i,\mathrm{out}}\right) \tag{11}$$

where t is time, $\dot{V}_{\mathrm{tot}}$ is the total flow rate, $y_{i,\mathrm{in}}$ and $y_{i,\mathrm{out}}$ are the volume fractions of species i in the gas coming into the adsorption column and exiting the column respectively. In the desorption phase, the volume of desorbed species was calculated by integrating the flow rate of species i exiting the column against zero:

$$V_{i,\mathrm{exp}} = \int_{t_0}^{t} \dot{V}_{\mathrm{tot}} y_{i,\mathrm{out}} \tag{12}$$

In the closed TVSA process, the volume of desorbed CO_2 during the temperature swing step could be calculated based on its volume fraction as explained above. However, by keeping the column inlet closed, the volume flow rate at the outlet became very small after pre-vacuuming step, in which majority of gas phase species were evacuated from the column. This may easily lead to an error related to flow rate measurement. To achieve a larger volume flow peak that is more in the range of the flow rate meters, either a larger sample mass or a

higher regeneration temperature can be used. On the other hand, another way to obtain the volume of desorbed species was to integrate only the total flow rate exiting the adsorption column, assuming that the flow was already pure CO_2 after pre-vacuuming step:

$$V_{i,\mathrm{exp}} = \int_{t_0}^{t} \dot{V}_{\mathrm{tot}} \tag{13}$$

With this calculation method based solely on the total volume flow rate, it was possible to detect a larger part of the desorbed CO_2 even before the pipeline was flushed with N_2 purge gas, because the volume flow rate sensors were located in the pipeline at an earlier stage than the concentration sensors. However, the flow still contained some H_2O, which would have been detected as CO_2 if the rather radical assumption was applied, and therefore this way of measurement could not be considered very accurate.

In the calculation method based on concentration measurement, according to equation 12, almost all desorbed CO_2 during the TS desorption phase was detected only in the pipeline flushing phase in the end of the TS phase, when the N_2 purge gas carried the desorbed gas components to the concentration measurements. In this case, the real reaction dynamics of the TS desorption phase could not be found out, because the desorbed species were detected with a delay. Nevertheless, this way of calculation provided a more accurate result for the volume of the desorbed species in the TS phase of the closed TVSA process.

After determining the adsorbed or desorbed volume of species i, the experimental capacity of the adsorbed or desorbed species $q_{i,exp}$ was then calculated by using an ideal gas law:

$$q_{i,\mathrm{exp}} = \frac{P_{\mathrm{tot}} V_{i,\mathrm{exp}}}{R_{\mathrm{id}} T m_{\mathrm{a}}} \tag{14}$$

where P_{tot} is the total pressure, R_{id} is the ideal gas coefficient, T is the temperature, and m_{a} is the mass of the adsorbent.

The measured CO_2 volume fractions and flow rates as well as calculated H_2O volume fractions at the outlet were corrected by using the methods reported by Elfving (2021, pp.

51–53). Thus, the measured CO_2 volume fractions were corrected to standard ambient temperature and pressure (SATP) conditions to compensate for the total pressure and temperature variations, while the effect of humidity on adsorption was compensated by using a correction factor. The volume fraction of H_2O was calculated from relative humidity and temperature measurements. The baselines of the measured CO_2 and calculated H_2O volume fractions were then corrected to zero level by using the baseline volume fraction measurements of these two gas components. The measured flow rates had to be corrected by multiplying them by gas conversion factors. The flow rate correction was made because the flow rate meters were calibrated for air and the density and composition of the measured gas varied during the experiments. Under humid conditions, another flow rate correction was required to correct the flow rate measurement from a dry gas mixture to a humid gas mixture. In contrast to Elfving's calculation methods, the water saturation temperature and some thermodynamic properties of the gas components have been calculated using available correlations and constant values at constant conditions, rather than being solved with REFPROP software.

3.2 Modelling methods

In this work, the closed TVSA and TCSA DAC processes were modelled in Matlab using the kinetic and dynamic models for CO_2 adsorption from air proposed by Elfving and Sainio (2021). The kinetic model represents the CO_2 adsorption and desorption on solid amine-functionalized adsorbent based on the reaction mechanisms in dry and humid conditions. The kinetic model could be used to calculate the CO_2 adsorption/desorption capacities and to model humid CO_2 adsorption equilibrium isotherms. In addition, the kinetic model was used in the dynamic model together with mass and heat balance equations to describe the reaction dynamics in a fixed bed adsorption column. The experimental data was utilized to validate the model by comparing the results obtained from experiments with the simulation results. Because the high energy consumption of the DAC process causes a significant part of the total costs, the calculation of specific energy requirement (SER) of the process was complemented to the model. To improve the cost-performance of the modelled DAC process, a mechanism to optimize the durations of the adsorption and desorption phases was added to the model. In addition, a sensitivity analysis of the adsorbent related parameters

was performed, in which the effects of different parameters on CO_2 capture from air were evaluated. The sections below introduce the used models and the ways how the DAC process was analysed and optimized in more detail.

3.2.1 Kinetic CO_2 adsorption model

As explained in Section 2.4.2, the CO_2 capture reactions on amine functionalized adsorbents depend on humidity. Under dry conditions, two moles of amine are theoretically required to capture one mole of CO_2, while under humid conditions, only one mole of amine is needed to capture one mole of CO_2 and H_2O. The enhancing effect of humidity on CO_2 adsorption on amine functionalized adsorbents is taken into account in the kinetic model proposed by Elfving and Sainio (2021). In the model, two separate reaction rate equations have been derived for the reactions in dry and humid conditions referred to as subscripts 1 and 2, respectively. These equations consist of forward and backward reaction terms. In the forward reaction term, the available amine site concentration for CO_2 adsorption is calculated from balance q_{m}-2$q_{1,\mathrm{CO2}}$-$q_{2,\mathrm{CO2}}$, where q_{m} is the maximum capacity of amine sites being available for both reactions, while $q_{1,\mathrm{CO2}}$ and $q_{2,\mathrm{CO2}}$ are the CO_2 uptakes for reactions 1 and 2, i.e. solid-phase concentrations of CO_2 in adsorbent. The exponents of the available amine site concentration can be based on the reaction stoichiometry, in which case they would be t_1 = 2 and t_2 = 1. This is called the 5-parameter model. Another way, which was primarily used in this work, is to fit the exponential parameters t_1 and t_2 from the experimental data, and the obtained model is called the 7-parameter model. The gas-phase concentrations of CO_2 and H_2O can be replaced with their partial pressures, and the kinetic constants of backward reactions (k_{b}) can be written as a ratio of forward kinetic constant k_{f} and adsorption affinity b in the form of k_{f}/b. The resulting reaction rate equations are:

$$\frac{dq_{1,\mathrm{CO2}}}{dt} = k_{\mathrm{f},1}\left(q_{\mathrm{m}} - 2q_{1,\mathrm{CO2}} - q_{2,\mathrm{CO2}}\right)^{t_1} p_{\mathrm{CO2}} - \frac{k_{\mathrm{f},1}}{b_1} q_{1,\mathrm{CO2}} \tag{15}$$

$$\frac{dq_{2,\mathrm{CO2}}}{dt} = k_{\mathrm{f},2}\left(q_{\mathrm{m}} - 2q_{1,\mathrm{CO2}} - q_{2,\mathrm{CO2}}\right)^{t_2} p_{\mathrm{CO2}} p_{\mathrm{H2O}} - \frac{k_{\mathrm{f},2}}{b_2} q_{2,\mathrm{CO2}} \tag{16}$$

where $k_{\mathrm{f},1}$ and $k_{\mathrm{f},2}$ are the forward reaction kinetic constants, p_{CO2} and p_{H2O} are the partial pressures of CO_2 and H_2O, and b_1 and b_2 are the adsorption affinities. The total CO_2 uptake

rate in the adsorbent is calculated by summing the reaction rate equations 15 and 16 as $dq_{\mathrm{tot,CO2}}/dt = dq_{1,\mathrm{CO2}}/dt + dq_{2,\mathrm{CO2}}/dt$. The adsorption affinities for dry and humid reactions are calculated as:

$$b_1 = b_{0,1} \exp\left(\frac{-\Delta H_1}{R_{\mathrm{id}} T_0}\left(\frac{T_0}{T} - 1\right)\right) \tag{17}$$

$$b_2 = b_{0,2} \exp\left(\frac{-\Delta H_2}{R_{\mathrm{id}} T_0}\left(\frac{T_0}{T} - 1\right)\right) \tag{18}$$

where $b_{0,1}$ and $b_{0,2}$ are the reference adsorption affinities at reference temperature T_0, while $-\Delta H_1$ and $-\Delta H_2$ are the isosteric heats of adsorption for reactions 1 and 2.

The 7-parameter model is used in this work to describe the CO_2 adsorption kinetics in humid conditions. In addition, a method to describe H_2O adsorption kinetics needs to be implemented to the model. The adsorption kinetics of H_2O are described with the linear driving force (LDF) model:

$$\frac{d\bar{q}_{\mathrm{H2O}}}{dt} = k_{\mathrm{H2O,LDF}}\left(q_{\mathrm{H2O,eq}} - \bar{q}_{\mathrm{H2O}}\right) \tag{19}$$

where $\bar{q}_{\mathrm{H2O}}$ is the average uptake of H_2O in the adsorbent particle, $k_{\mathrm{H2O,LDF}}$ is the linear driving force model kinetic constant of H_2O and $q_{\mathrm{H2O,eq}}$ is the local equilibrium adsorption capacity of H_2O (Sircar and Hufton, 2000, p. 137). Of the alternative ways of describing H_2O adsorption, the single-component GAB-isotherm model, presented in equation 6, has been chosen as the most suitable option to calculate the equilibrium adsorption capacity of H_2O due to its temperature dependence and ability to depict the multilayer type III adsorption of H_2O. The temperature dependent GAB-isotherm parameters C and K are calculated by equations 7 and 8.

The 7-parameter model is used to calculate the equilibrium CO_2 adsorption capacity in humid conditions by integrating until equilibrium state is reached using the 'ODE15s'-solver in Matlab. The same parameters that Elfving (2021, pp. 73, 78) used in his work for the same adsorbent material are used here to describe adsorption equilibrium in the case of 7-

parameter model (q_{m}, $b_{0,1}$, $b_{0,2}$, $-\Delta H_1$, $-\Delta H_2$, t_1, t_2) and the GAB-isotherm model ($q_{\mathrm{m,mono}}$, C_0, K_0, ΔH_{C}, ΔH_{K}). The 7-parameter model parameters, listed in Table 5, are obtained by fitting the kinetic model to experimental CO_2 isotherms measured in humid conditions. Similarly, the GAB-isotherm model parameters, listed in Table 6, are fitted from experimental single-component H_2O isotherms. The equilibrium parameter fitting is done by using the 'lsqnonlin' optimization function in Matlab. The upper limits of t_1 and t_2 are set to 3 to limit the computational effort. Since kinetics do not matter in equilibrium, the forward reaction kinetic constants $k_{\mathrm{f},1}$ and $k_{\mathrm{f},2}$ can be set to 1 during equilibrium parameter fitting. At a later stage, the kinetic constants are obtained by fitting the dynamic model to experimental fixed-bed CO_2 and H_2O breakthrough curves.

Table 5. Parameters of the 7-parameter model fitted from experimental CO_2 isotherms (Elfving, 2021, p. 78).

q_{m}	$b_{0,1}$	$b_{0,2}$	$-\Delta H_1$	$-\Delta H_2$	t_1	t_2
[$\mathrm{mmol_{amine}/g_{adsorbent}}$]	[$\mathrm{bar^{-1}(mol/kg)^{1-t1}}$]	[$\mathrm{bar^{-2}(mol/kg)^{1-t2}}$]	[kJ/mol]	[kJ/mol]	[-]	[-]
2.63	400.39	$2.38 \cdot 10^4$	84.35	124.02	3	3

Table 6. Parameters of the GAB model fitted from experimental single-component H_2O isotherms and the isosteric heat of H_2O adsorption at zero loading (Elfving, 2021, p. 73).

$q_{\mathrm{m,mono}}$	C_0	K_0	ΔH_{C}	ΔH_{K}	$-\Delta H_{\mathrm{H2O,0}}$
[$\mathrm{mmol_{H2O}/g_{adsorbent}}$]	[-]	[-]	[kJ/mol]	[kJ/mol]	[kJ/mol]
2.58	0.155	0.871	6.63	0	50.73

3.2.2 Dynamic CO_2 adsorption model

The reaction dynamics in a fixed-bed adsorption column can be described with the dynamic 1D model proposed by Elfving and Sainio (2021) using the 'ODE15s'-solver in Matlab for the integration of the mass and heat balance equations. Separate ODE-functions are used for cases with either an open or closed adsorption column inlet during regeneration phase, representing the TCSA and closed TVSA processes, respectively. Some of the process parameters, such as feed gas flow rate during desorption, are different for these two cases.

However, the model representing an open inlet is only used for model validation, while the closed-inlet model is used to produce other results. The simplified flowsheet of mass and heat transfer in the adsorption column is illustrated for closed-inlet model in Figure 19.

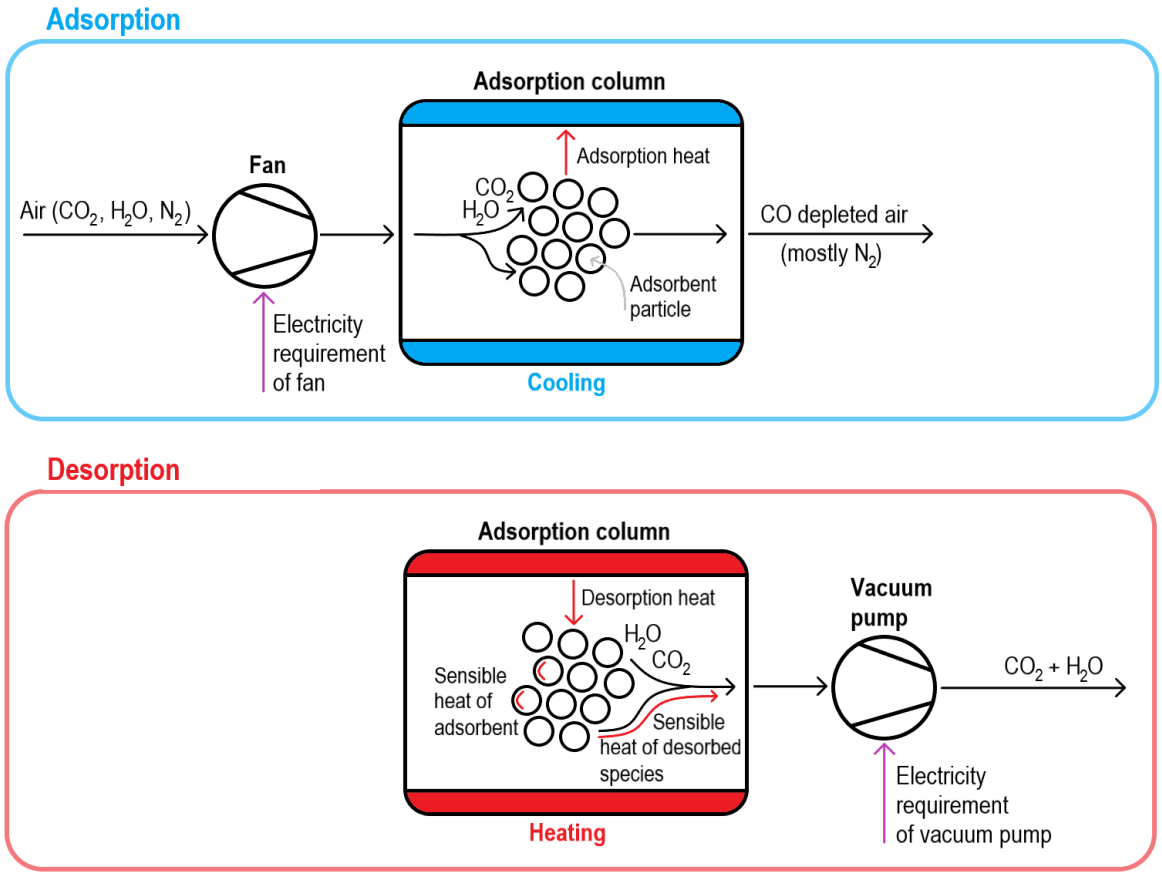

Figure 19. Simplified flowsheet of mass and heat transfer in the fixed-bed adsorption column in the closed-inlet model.

The dynamic model includes some assumptions and simplifications. The gas flow within the column is represented by an idealized plug flow model, meaning that the concentration varies continuously in axial direction, but no concentration, temperature and pressure variations exist in radial direction. In addition, only the adsorption of CO_2 and H_2O is taken into consideration, while the adsorption of N_2 is neglected due to its minimal effect. The gas velocity inside the column is assumed to be constant during adsorption, while during desorption it is approximated with a mechanism based on the difference between total pressure and vacuum pressure. Otherwise, the gas phase is described by the ideal gas law.

The heat transfer is simplified by assuming that a thermal equilibrium between the gas and solid phases is instantaneously formed. Furthermore, the wall temperature is assumed to be uniform along axial and radial directions. The enhanced heat transfer by the two times higher flow rate in the desorption phase of the open-inlet ODE-function, is taken into account by assuming twice as high heat transfer coefficient for the desorption phase compared to the adsorption phase. Adsorbent bed is assumed to be homogeneous, and its properties are kept constant during simulation. Also kinematic viscosity for the gas mixture is assumed to be constant.

The mass balance equation consisting of diffusion, convection and source terms is written for gas component i as:

$$\frac{\partial c_i}{\partial t} = D_{\mathrm{L}} \frac{\partial^2 c_i}{\partial z^2} - v_{\mathrm{i}} \frac{\partial c_i}{\partial z} - \frac{\rho_{\mathrm{B}}}{\varepsilon} \frac{\partial q_i}{\partial t} \tag{20}$$

where c_i si the concentration of species i, t is time, D_{L} is the axial dispersion coefficient, z is the axial dimension of the column, v_{i} is the interstitial velocity within the column, ρ_{B} is the adsorbent bulk density and ε is the adsorbent bed porosity (Bollini et al., 2012a, p. 15147). The kinetic models for CO_2 and H_2O are used in the dynamic model to obtain the adsorption source terms $\partial q_i / \partial t$ for each gas component. The axial dispersion coefficient is calculated using the Chung and Wen empirical correlation reported by Rastegar and Gu (2017, p. 134):

$$D_{\mathrm{L}} = \frac{d_{\mathrm{p}} v_{\mathrm{i}} \varepsilon}{0.2 + 0.011 Re^{0.48}} \tag{21}$$

where d_{p} is the adsorbent particle diameter and Re is the Reynold's number calculated by $Re = d_{\mathrm{p}} v_{\mathrm{i}} \varepsilon / \nu$, where ν is the kinematic viscosity of the gas mixture.

Based on the model used by Haghpanah et al. (2013), a simplified heat balance equation is derived that takes into account the convection and diffusion along the axial direction of the bed, sensible heat of the adsorbed species, heat of adsorption and the heat transfer between the bed and column walls:

$$\left[\rho_{\mathrm{g}} c_{\mathrm{p,g}} + \frac{1-\varepsilon}{\varepsilon}\rho_{\mathrm{p}}\left(c_{\mathrm{p,a}} + c_{\mathrm{p,CO2}} q_{\mathrm{tot,CO2}} + c_{\mathrm{p,H2O}} q_{\mathrm{H2O}}\right)\right]\frac{\partial T}{\partial t} =$$
$$\frac{K_{\mathrm{z}}}{\varepsilon}\frac{\partial^2 T}{\partial z^2} - \rho_{\mathrm{g}} c_{\mathrm{p,g}} v_{\mathrm{i}} \frac{\partial T}{\partial z} - \frac{1-\varepsilon}{\varepsilon}\rho_{\mathrm{p}}\left(c_{\mathrm{p,CO2}}\frac{dq_{\mathrm{tot,CO2}}}{dt} + c_{\mathrm{p,H2O}}\frac{dq_{\mathrm{H2O}}}{dt}\right)T -$$
$$\frac{1-\varepsilon}{\varepsilon}\rho_{\mathrm{p}}\left[-\Delta H_1\frac{dq_{1,\mathrm{CO2}}}{dt} + (-\Delta H_2)\frac{dq_{2,\mathrm{CO2}}}{dt} + \left(-\Delta H_{\mathrm{H2O,0}}\right)\frac{dq_{\mathrm{H2O}}}{dt}\right] - \frac{2h}{\varepsilon R_{\mathrm{bed}}}(T - T_{\mathrm{w}}) \quad (22)$$

where ρ_{g} is the gas density, $c_{\mathrm{p,g}}$ is the specific heat capacity of the gas, ρ_{p} is the adsorbent particle density, $c_{\mathrm{p,a}}$ is the specific heat capacity of the adsorbent, $c_{\mathrm{p,CO2}}$ and $c_{\mathrm{p,H2O}}$ are the specific heat capacities of CO_2 and H_2O, K_{z} is the axial effective heat conductivity, $-\Delta H_{\mathrm{H2O,0}}$ is the isosteric heat of H_2O adsorption at zero loading, h is the heat transfer coefficient between the bed and column walls, R_{bed} is the bed radius and T_{w} is the wall temperature. The axial effective heat conductivity is calculated according to Ruthven (1984, p. 216) by:

$$K_{\mathrm{z}} = D_{\mathrm{L}}\rho_{\mathrm{g}} c_{\mathrm{p,g}} \quad (23)$$

In the model, a column of length L_{bed} packed with amine-functionalized adsorbent is considered. The calculation within the column is based on finite difference method and therefore the column is divided into a grid with N number of cells as shown in Figure 20.

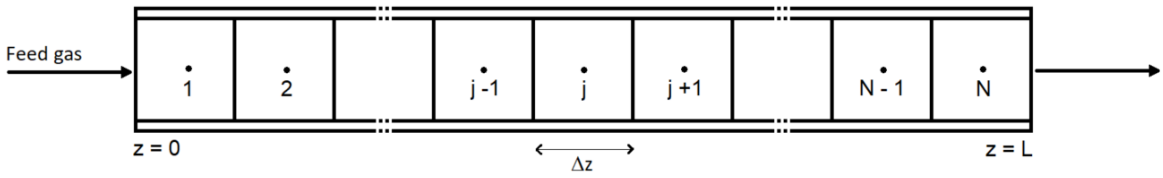

Figure 20. Schematic of the adsorption column and finite difference scheme

To be able to numerically compute the mass and heat balance equations for each cell, the partial differential equations need to be transformed into discrete difference equations. For this purpose, discretization methods are needed. The convection terms of mass and heat balance equations are discretized using the first order backward difference scheme:

$$\frac{\partial x}{\partial z} = \frac{x_{\mathrm{j}} - x_{\mathrm{j-1}}}{\Delta z} \quad (24)$$

where x is either concentration or temperature and j is the cell under consideration. The diffusion terms are discretized using the second order central difference scheme:

$$\frac{\partial^2 x}{\partial z^2} = \frac{x_{\mathrm{j}+1} - 2x_{\mathrm{j}} + x_{\mathrm{j}-1}}{\Delta z^2} \tag{25}$$

As the variable values in a particular cell j depend on the values in the previous $j-1$ and the following cell $j+1$, the inlet and outlet boundary conditions must be defined so that the first and the last cell can be computed. The concentration of species i at the inlet boundary ($c_i|_{\mathrm{z}=0}$) can be calculated with equation 27 that is derived from the Danckwert's boundary condition (equation 26) as:

$$D_{\mathrm{L}} \left.\frac{\partial c_i}{\partial z}\right|_{\mathrm{z}=0} = -v_{\mathrm{i}}\left(c_{i,\mathrm{feed}} - c_i|_{\mathrm{z}=0}\right) \tag{26}$$

$$c_i|_{\mathrm{z}=0} = \frac{c_{i,\mathrm{feed}} + \frac{D_{\mathrm{L}}}{v_{\mathrm{i}}\Delta z} c_{i,1}}{1 + \frac{D_{\mathrm{L}}}{v_{\mathrm{i}}\Delta z}} \tag{27}$$

where $c_{i,\mathrm{feed}}$ is the feed concentration of species i and $c_{i,1}$ is the concentration in the first cell (Haghpanah et al., 2013, p. 4263). Similarly, the gas temperature at the inlet boundary ($T|_{\mathrm{z}=0}$) can be calculated with equation 29 that is obtained by the analogy of mass and heat transfer from the Danckwert's boundary condition (equation 28) as:

$$K_{\mathrm{z}} \left.\frac{\partial T}{\partial z}\right|_{\mathrm{z}=0} = -\varepsilon v_{\mathrm{i}} \rho_{\mathrm{g}} c_{\mathrm{p,g}} (T_{\mathrm{feed}} - T|_{\mathrm{z}=0}) \tag{28}$$

$$T|_{\mathrm{z}=0} = \frac{T_{\mathrm{feed}} + \frac{K_{\mathrm{z}}}{\varepsilon v_{\mathrm{i}} \rho_{\mathrm{g}} c_{\mathrm{p,g}} \Delta z} T_1}{1 + \frac{K_{\mathrm{z}}}{\varepsilon v_{\mathrm{i}} \rho_{\mathrm{g}} c_{\mathrm{p,g}} \Delta z}} \tag{29}$$

where T_{feed} is the feed gas temperature and T_1 is the gas temperature in the first cell (Haghpanah et al., 2013, p. 4263). The concentration of species i remains unchanged after the last cell ($c_{i,\mathrm{N}+1} = c_{i,\mathrm{N}}$), so the boundary condition at the outlet can be written for concentration as:

$$c_i|_{\mathrm{z}=\mathrm{L}} = c_{i,\mathrm{N}} \tag{30}$$

Similarly, the outlet boundary condition for gas temperature is given as:

$$T|_{z=L} = T_N \tag{31}$$

As initial conditions, the adsorbent bed is regenerated and emptied ($q_{tot,CO2}$ = 0; q_{H2O} = 0; c_{CO2} = 0; c_{H2O} = 0) as well as the column temperature is set equal to column wall and feed gas temperature ($T = T_w = T_{feed}$). At later timesteps as the simulation progresses, the feed gas temperature during adsorption or pre-vacuum/purge phases is set equal to the measured bed temperature during adsorption. In the desorption phase, the gas-heating effect of the inlet part of the column (such as the easily heated grate on which the adsorbent sample is placed and through which the air passes) is considered by approximating the feed gas temperature to be equal to the bed temperature measurement of the experiment performed without an adsorbent sample.

The dynamic model can also be used to model multiple consecutive cycles by making a loop that sets the simulated values of the last time point of the previous cycle as initial values for the next cycle. This makes it possible, for example, to examine the cyclic stability of the adsorbent and check whether a cyclic steady state is reached during several cycles. The cyclic steady state is reached when successive cycles are identical. Thus, the achievement of the cyclic steady state is evaluated in the model on the basis of the differences in average CO_2 uptakes and gas temperatures of successive cycles. The criterion is that consecutive cycles can differ by only $1 \cdot 10^{-6}$%. The cyclic drops in CO_2 and H_2O adsorption and desorption capacities are taken into account in the model by a fixed cyclic capacity drop (CCD) coefficient. The coefficient reduces the maximum capacity of amine sites q_m being available for CO_2 capture reactions as well as the maximum monolayer adsorption capacity of water $q_{m,mono}$ after each cycle. A cyclic CO_2 capacity drop coefficient of 0.36 %/cycle reported by Elfving (2021, p. 88) for the same adsorbent is used in this work as the CCD coefficient for both CO_2 and H_2O. However, this coefficient was measured using dry air instead of humid air. On the other hand, CO_2 uptake losses between 0-6.5 %/cycle have been reported by Jahandar Lashaki et al. (2019, pp. 3332–3341) in a summary of thermal stability data on different amine-functionalized adsorbents under various conditions. Nevertheless, this only includes thermal stability, not chemical or hydrothermal stability.

In dynamic modelling, the forward kinetic constants ($k_{f,1}$, $k_{f,2}$, $k_{H2O,LDF}$) are obtained by fitting the dynamic model to experimental fixed-bed CO_2 and H_2O breakthrough curves using the 'lsqcurvefit' function in Matlab. Similarly, the heat transfer coefficient h is gained by fitting the dynamic model to experimental fixed-bed column temperature data. The fitted kinetic constants and heat transfer coefficient are listed in Table 7. Due to the significant concentration of H_2O in the feed gas, the effect of H_2O dispersion must be accounted in the breakthrough curve fitting. This is done by modelling the empty column adsorption capacity with Langmuir isotherm model (equation 3), and by adding it to the H_2O equilibrium capacity, as proposed by Elfving and Sainio (2021). The parameters of Langmuir isotherm are obtained by fitting the isotherm model to measured empty column H_2O adsorption capacities.

Other model parameters used in the dynamic model validation and experiment-based calculations of CO_2 productivity and SER are listed in Appendix 2. In these cases, many of the used model parameters are case-dependent, such as feed gas concentrations, temperature and pressure. However, the subsequent sensitivity analysis must be performed using the same model parameters all the time. Therefore, the case-dependent model parameters are replaced with slightly modified and rounded parameters that are typical for a laboratory-scale DAC device. The chosen model parameters replacing the case-dependent parameters in the sensitivity analysis are listed in Appendix 3. Without changes to the model, the model would not completely work in a real-scale DAC process, e.g. with much higher amounts of adsorbent or much larger adsorption column sizes, due to the simplifications of the model. For example, the idealization of the heat transfer would not work well in a large-scale column, in which the temperature variations in radial direction should also be considered.

3.2.3 Specific energy requirement modelling

The outputs from the kinetic and dynamic models are used to calculate the specific energy requirement (SER) of the modelled DAC process to be able to compare it with the values reported in the literature and to assess the effects of parameter variations on SER. However, the calculated SER values are ideal because energy losses are not taken into account. The

SER is calculated by dividing the total energy requirement of a cycle by the amount of CO_2 produced during that cycle. The total energy requirement consists of the mechanical energy related to the air blowers (E_{fan}) and the vacuum pump (E_{vac}), as well as the thermal energy related to the sensible heat of the adsorbent and the adsorbed species ($E_{\mathrm{sen,a}}$, $E_{\mathrm{sen,CO2}}$, $E_{\mathrm{sen,H2O}}$) and desorption enthalpies of the adsorbed species ($E_{\mathrm{des,CO2}}$, $E_{\mathrm{des,H2O}}$). The energy consumed by cooling the column, condensing the co-adsorbed H_2O out of the product gas, and compressing the product gas to the final pressure is not considered in this report. The total energy requirement E_{tot} for the cycle is obtained by summing all the energy requiring elements during adsorption and desorption phases:

$$E_{\mathrm{tot}} = E_{\mathrm{fan}} + E_{\mathrm{vac}} + E_{\mathrm{sen,a}} + E_{\mathrm{sen,CO2}} + E_{\mathrm{sen,H2O}} + E_{\mathrm{des,CO2}} + E_{\mathrm{des,H2O}} \tag{32}$$

The mechanical energy required by air blowers, when blowing feed air into the column during adsorption is calculated by:

$$E_{\mathrm{fan}} = \int_0^t \Delta p \dot{V}_{\mathrm{tot}} dt \tag{33}$$

where Δp is the pressure drop along the adsorbent bed and $\dot{V}_{\mathrm{tot}}$ is the total volume flow rate of the gas. The pressure drop along the bed is caused by viscous energy losses and a decrease in kinetic energy as the gas flows through the voids between the adsorbent particles. This pressure drop can be calculated using the Ergun equation:

$$\Delta p = \frac{150 \rho_{\mathrm{g}} \nu L_{\mathrm{bed}} (1-\varepsilon)^2 v_{\mathrm{s}}}{{d_{\mathrm{p}}}^2 \varepsilon^3} + \frac{1.75\, L_{\mathrm{bed}} \rho_{\mathrm{g}} (1-\varepsilon) {v_{\mathrm{s}}}^2}{d_{\mathrm{p}}\, \varepsilon^3} \tag{34}$$

where ρ_{g} is the gas density, ν is the kinematic viscosity of the gas mixture, L_{bed} is the length of the adsorbent bed, ε is the adsorbent bed porosity, v_{s} is the superficial velocity of the gas and d_{p} is the adsorbent particle diameter (Shafeeyan, Wan Daud and Shamiri, 2014, p. 984). The mechanical energy required by the vacuum pump to withdraw gases from the column during regeneration is calculated as follows:

$$E_{\mathrm{vac}} = -P_{\mathrm{ext}} \int_0^t \dot{V}_{\mathrm{tot}} dt \left(\frac{P_1}{P_{\mathrm{ext}}} - \frac{P_2}{P_{\mathrm{ext}}} + ln\left(\frac{P_2}{P_1}\right) \right) \tag{35}$$

where P_{ext} is the external pressure, P_1 is the pressure in the column before vacuuming and P_2 is the vacuum pressure at given time point (Kulkarni and Sholl, 2012, p. 8635). Sensible heat of the dry adsorbent is calculated as:

$$E_{\text{sen,a}} = m_{\text{a}} c_{\text{p,a}} \Delta T \tag{36}$$

where m_{a} is the adsorbent mass, $c_{\text{p,a}}$ is the specific heat capacity of the adsorbent and ΔT is the temperature difference in the temperature swing. Sensible heats of desorbed CO_2 and H_2O are calculated as:

$$E_{\text{sen,CO2}} = m_{\text{CO2}} c_{\text{p,CO2}} \Delta T \tag{37}$$

$$E_{\text{sen,H2O}} = m_{\text{H2O}} c_{\text{p,H2O}} \Delta T \tag{38}$$

where m_{CO2} and m_{H2O} are the masses of desorbed CO_2 and H_2O, while $c_{\text{p,CO2}}$ and $c_{\text{p,H2O}}$ are the specific heat capacities of CO_2 and H_2O. The desorption enthalpies of CO_2 and H_2O are calculated as:

$$E_{\text{des,CO2}} = \int_0^t \left((-\Delta H_1) \dot{n}_{1,\text{CO2}} + (-\Delta H_2) \dot{n}_{2,\text{CO2}} \right) dt \tag{39}$$

$$E_{\text{des,H2O}} = \int_0^t (-\Delta H_{\text{H2O,0}}) \dot{n}_{\text{H2O}} dt \tag{40}$$

where $-\Delta H_1$ and $-\Delta H_2$ are the isosteric heats of adsorption for reactions 1 and 2, $-\Delta H_{\text{H2O,0}}$ is the isosteric heat of H_2O adsorption at zero loading, $\dot{n}_{1,\text{CO2}}$ and $\dot{n}_{2,\text{CO2}}$ are the molar flow rates of desorbed CO_2 for reactions 1 and 2, and $\dot{n}_{\text{H2O}}$ is the molar flow rate of desorbed H_2O.

3.2.4 Cycle time optimization

To keep the CO_2 capture costs per kilogram of CO_2 produced as low as possible in the modelled DAC process, a mechanism to optimize the durations of the cycle phases is implemented to the model. The durations of the adsorption, pre-vacuum, and TS desorption phases are determined by setting cut-off criteria, rather than allowing the phases to continue longer than necessary. When the cut-off criterion is reached, the phase is terminated, and the

next phase begins. The adsorption phase is cut off when 90% or 99% of the equilibrium adsorption capacity is reached. On the other hand, the cut-off criterion for the TS desorption phase is that 90% or 99% of the working capacity must be desorbed. The pre-vacuum phase is cut off after 99.9% of the desirable vacuum pressure is reached and this criterion is kept constant throughout the work. An example of an optimized cycle is given in Figure 21. The effect of different cut-off criteria on CO_2 productivity and SER is examined. However, in the sensitivity analysis, the 99% cut-off criteria are selected in order to obtain comparable results.

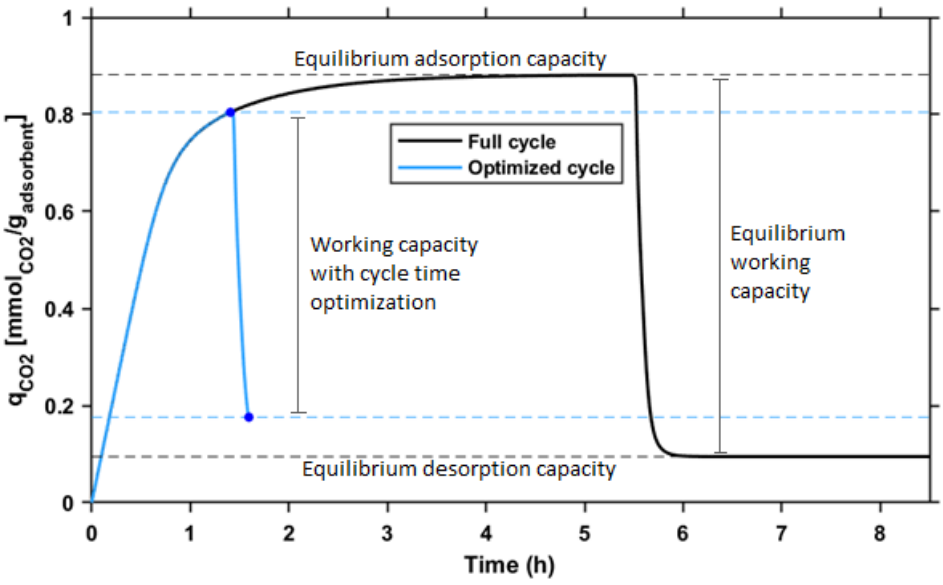

Figure 21. An example of cycle time optimization using the 90% cut-off criterion. The blue dots describe the end points of the adsorption and desorption phases of the optimized cycle.

Due to the cutting of the cycle phases, a cyclic steady state cannot be reached during one cycle, and therefore the results of the sensitivity analysis are presented for the first cycle that has reached the cyclic steady state in order to preserve the comparability of the results. Typically, the sufficient cyclic steady state that meets the criterion of $1 \cdot 10^{-6}$% similarity between consecutive cycles is reached after 3-5 cycles.

3.2.5 Execution of the sensitivity analysis

After validating the model, a sensitivity analysis of the adsorbent-related parameters is performed. The adsorbent-related sensitivity analysis focuses on parameters, such as isotherm parameters, adsorbent material properties as well as heat transfer and kinetic parameters. The effect of each parameter on CO_2 productivity and SER is evaluated. First, the effects of all parameters are roughly assessed by changing them by +/- 80% and 40%. After that, the most important and most uncertain parameters are examined one by one in more detail. When examining each parameter one at a time, all other parameters are kept at their basic levels, so that the results show only the effect of the change in that parameter. The volume of the adsorption column and the bed are kept constant.

4. Results and discussion

The performance of the novel amine-functionalized CO_2 adsorbent material is evaluated in the sections below based on the experimental and modelling methods presented in Section 3. The key results to be analyzed are CO_2 working capacity, CO_2 productivity and specific energy requirement in different operating conditions and with different adsorbent-related parameters. These results are compared with the available and relevant values reported in the literature.

4.1 Experimental results

In this section, the experimentally obtained adsorption and desorption capacities of CO_2 and H_2O of the solid amine-functionalized adsorbent are presented. In addition, the effect of different operating conditions as well as the magnitude and source of the possible error have been evaluated.

4.1.1 Experimental CO_2 working capacity

The experimentally obtained CO_2 and H_2O adsorption and desorption capacities for the amine-functionalized adsorbent sample, using different regeneration methods, operating conditions, and masses of samples, are shown in Figure 22. It can be seen from Figure 22a that the CO_2 working capacity is increased in humid conditions due to co-adsorption of H_2O. CO_2 adsorption capacities of 0.71-0.77 $mmol_{CO2}/g_{adsorbent}$ were measured in humid conditions, while in dry conditions the adsorption capacities were only about half of that, being 0.43-0.47 $mmol_{CO2}/g_{adsorbent}$. This is consistent with the humidity-dependent CO_2 capture mechanism of amine functionalized adsorbents explained in Section 2.4.2 that was implemented to the model as well, meaning that in dry conditions the CO_2 capture reaction consumes twice as much amines as in humid conditions. H_2O adsorption capacities of 3.21-3.78 $mmol_{H2O}/g_{adsorbent}$ were measured in humid conditions, as shown in Figure 22b, which means that H_2O and CO_2 capture ratio was around 4.2-5.3 mol_{H2O}/mol_{CO2}. The adsorption

capacities under the same experimental conditions are quite similar with some exceptions. The H_2O adsorption capacity of the closed TVSA experiment with 1 g sample and 100 °C TS is clearly a bit too low, for example.

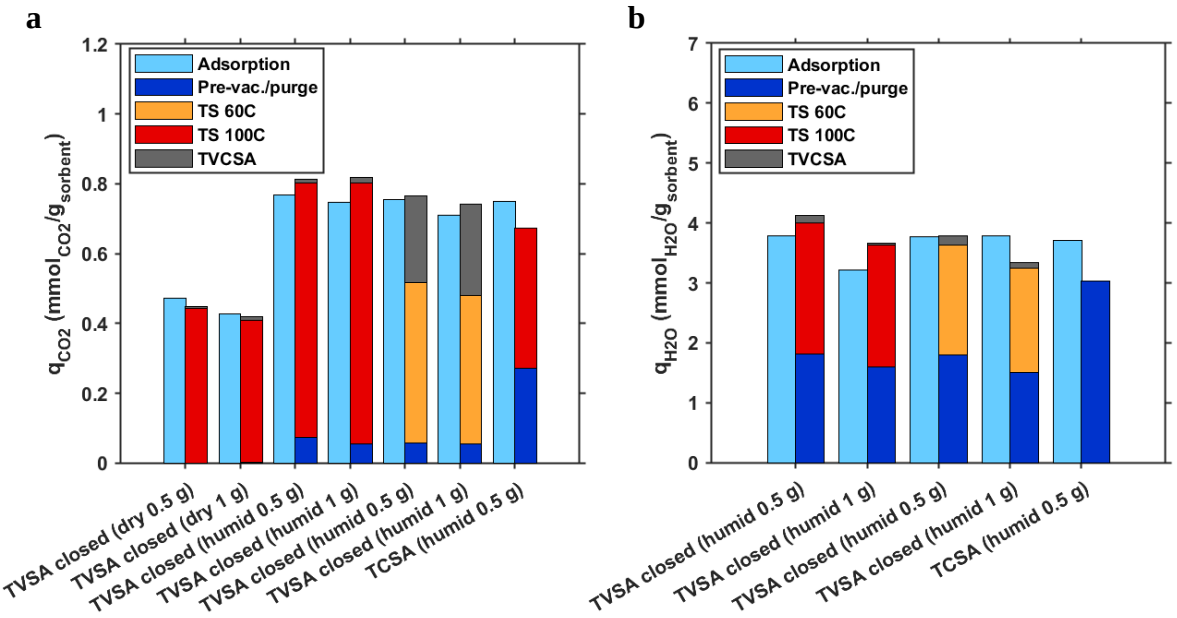

Figure 22. Experimental adsorption and desorption capacities of the amine-functionalized adsorbent for a) CO_2 and b) H_2O.

When examining the results, it should be noted that the actual desorption capacities (i.e. working capacities) of the closed TVSA and TCSA processes are the sums of the desorption capacities of the pre-vacuum/purge and TS phases. The total desorption capacities of the experiments, on the other hand, were obtained by adding the desorption capacity of the TVCSA phase to the actual working capacities of the processes. The TVCSA phase was only intended for checking the share of CO_2 and H_2O uptake that remain undesorbed in these processes.

In the closed TVSA experiments, working capacities of 0.41-0.44 mmol$_{CO2}$/g$_{adsorbent}$ and 0.80 mmol$_{CO2}$/g$_{adsorbent}$ were achieved by the TS desorption phase at 100°C under dry and humid conditions, corresponding to almost the entire total CO_2 desorption capacity. The closed TVSA experiments conducted in a lower regeneration temperature and humid conditions revealed that working capacities of 0.48-0.52 mmol$_{CO2}$/g$_{adsorbent}$ were already reached at

60°C. In dry conditions, a noteworthy CO_2 desorption capacity was not achieved in the pre-vacuum phase, while in humid conditions, 0.06-0.07 $mmol_{CO2}/g_{adsorbent}$ was desorbed only by vacuuming.

TCSA experiments differed from closed TVSA experiments so that N_2 purge gas was initially used for desorption instead of vacuuming. The use of purge gas turned out to be a much more efficient regeneration method than vacuuming in humid conditions, giving CO_2 desorption capacity of 0.27 $mmol_{CO2}/g_{adsorbent}$ for the purge phase. An even greater proportion of CO_2 desorption would have been achieved with purge if the duration of that phase had been extended. The regeneration was completed in the TCSA experiments by the TS phase at 100°C, after which a working capacity of 0.67 $mmol_{CO2}/g_{adsorbent}$ was achieved. Based on the CO_2 isotherms, a higher working capacity should have been obtained from the TCSA experiments than from the closed TVSA experiments at the same humidity levels and TS phase temperatures, because a lower CO_2 partial pressure was achieved within the adsorbent bed by purging the bed with the N_2 purge gas instead of vacuuming. This did not appear in the experiment results due to the experimental uncertainty. Even though the adsorption time in the TCSA experiment was set to less than half of what it was in the closed TVSA experiments, the adsorption capacity of the TCSA experiment seems to have almost reached the same level as in other humid experiments.

By comparing Figure 22a and Figure 22b, it is noticed that in the pre-vacuum and purge phases, a much larger share of desorption was achieved for H_2O than for CO_2. This is probably due to the faster desorption kinetics of H_2O and the fact that the H_2O molecules are more weakly bound to the adsorbent material than CO_2 molecules.

The total desorption capacities of most of the closed TVSA experiments somewhat exceed the measured adsorption capacities. The capacity overshoot was up to 0.08 $mmol_{CO2}/g_{adsorbent}$ for CO_2 and up to 0.45 $mmol_{H2O}/g_{adsorbent}$ for H_2O. In theory, the desorption capacity cannot be higher than the adsorption capacity if the sample is properly pre-desorbed. The error is probably partly due to the fact that the desorption period was divided into several measurement phases, each of which contained at least a small error, for example due to

imprecise calibration or limited operation range of the used meter. The CO_2 desorption capacities of the pre-vacuum and TS desorption phases of the closed TVSA cycle were measured with a less accurate %-scale meter instead of ppm-scale meter because the desorbed CO_2 concentration peak exceeded momentarily 5000 ppm, which is the upper operation limit of the ppm-scale meter. A %-scale CO_2 measurement may wrongly show around 80-250 ppm even at its zero level and thus is not accurate at low concentrations. Due to the incorrect zero level of the %-scale measurement, the CO_2 desorption capacities calculated based on that measurement rose even after they should have levelled off due to a long desorption tail measured by the %-scale meter. Therefore, the proportion of incorrect infinitely rising capacity has been removed from the desorption capacities of these phases by visual examination. The results of the experiments that were performed with a larger adsorbent sample seem more realistic, because the desorption capacities were slightly lower and thus to a greater extent below the average adsorption capacity level.

Since several experiments were performed using the same adsorbent sample, it is also possible that degradation of the adsorbent influences the capacities of subsequent experiments, or that the sample is not fully regenerated before the next experiment. By repeating the experiments several times always with a fresh sample, the capacity variations between experiments could be eliminated.

4.2 Modelling results

In this section, the results obtained by modelling are presented. First, the dynamic fixed-bed CO_2 adsorption model is validated by comparing the simulated results with experimental data. At this point, the input parameters of the model are adjusted to match the fixed-bed experiments conducted using the amine-functionalized adsorbent sample. Then, the performance of the closed TVSA DAC process is evaluated by comparing the simulated CO_2 productivity and SER under different conditions. The impact of various cycle time optimization mechanisms on performance is also evaluated. Finally, the effects of different adsorbent-related parameters on the performance of the DAC process are presented in the form of a sensitivity analysis.

4.2.1 Model validation

The dynamic model that simulates the closed TVSA and TCSA processes using either a closed or open-inlet ODE-functions is referred to as a closed or open-inlet model depending on the function used. These dynamic closed- and open-inlet models are validated by comparing the simulated temperature, concentration and capacity profiles with the profiles of the experiments conducted with 0.5 g adsorbent sample and 100°C regeneration temperature in humid conditions. The input parameters used in the simulation are adjusted to match the experiments so that the results are comparable. Although the results presented in the later sections have only been produced with the closed-inlet model, the validation of the open-inlet model is needed especially for the validation of the desorption phase. This is because in the desorption phase the concentration and capacity profiles of the closed TVSA experiments are not comparable with the closed-inlet model as the actual reaction kinetics of these experiments cannot be measured because the CO_2 and H_2O tend to get stuck into the post-column pipeline. Only the profiles produced with open-inlet model are presented in this section, since the heat transfer and kinetic parameters have been fitted from them, and the closed-inlet model profiles are presented in the appendices.

The CO_2 and H_2O concentration profiles at the column outlet simulated using the open-inlet model, shown in Figure 23, represents relatively well the experimentally measured profiles both in the adsorption and desorption phases. According to Figure 23a, the model slightly underestimates the rate of CO_2 adsorption reaction, which appears as a delayed CO_2 concentration increase. On the other hand, the desorption phase CO_2 concentration profile in Figure 23c reveals that the CO_2 concentration is simulated higher than the experiment during the purge phase and the first temperature ramping steps. Based on that, the open-inlet model overestimates the share of the desorption capacity of the purge phase and the first temperature ramping steps. Due to this, the temperature required for nearly full regeneration is too low in the open-inlet model, being around 60-70 °C. According to Figure 23b and Figure 23d, the simulated H_2O concentration profiles follows more accurately the profiles of TCSA experiment. However, the rate of H_2O desorption is slightly overestimated. Moreover, by comparing the concentration profiles of CO_2 and H_2O in adsorption phase, it

is noticed that in the case of H_2O the saturation state is reached much earlier. The same phenomenon can also be seen in the desorption phase when nearly all H_2O is desorbed much faster than CO_2. This implies faster reaction kinetics of H_2O.

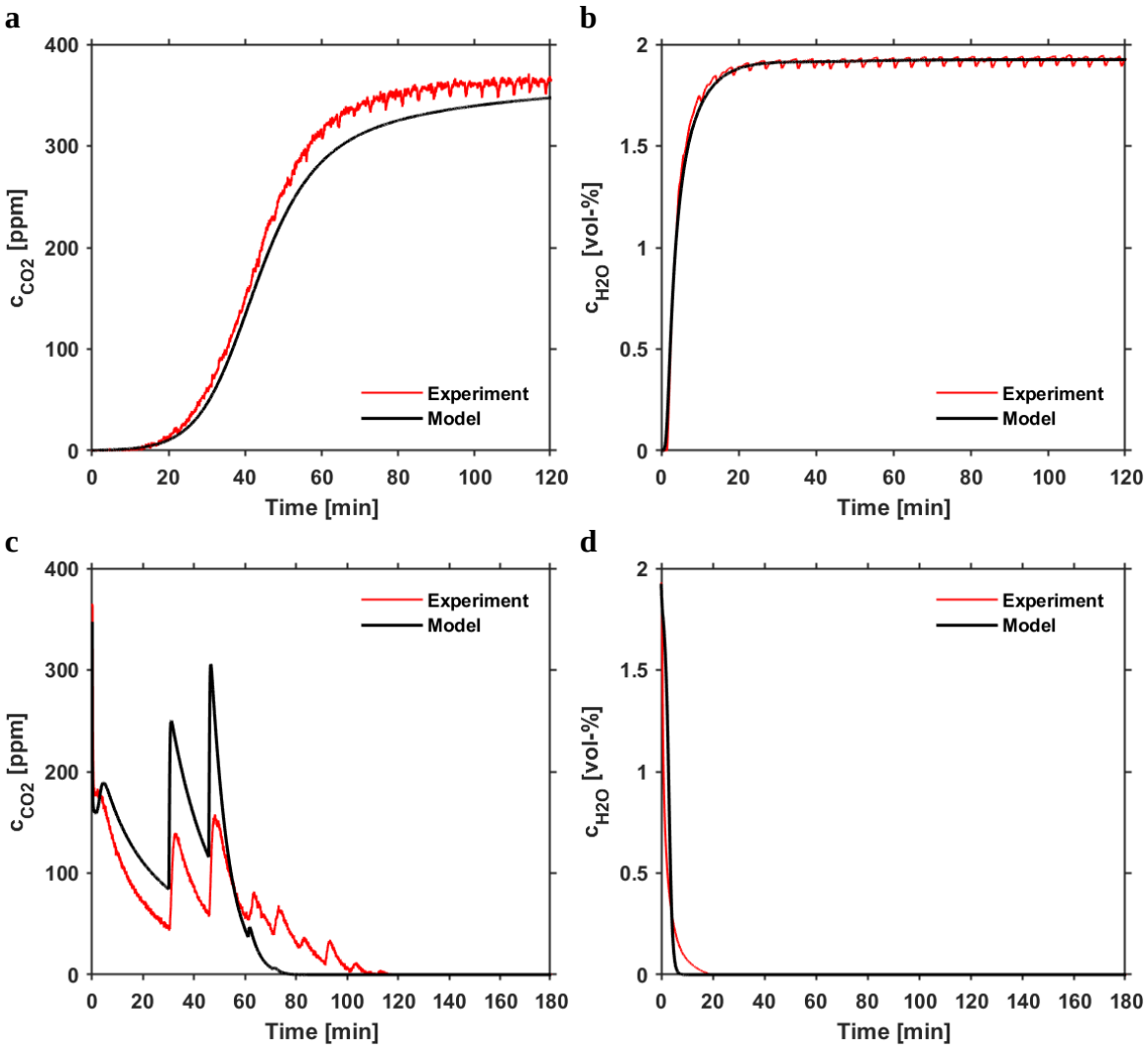

Figure 23. Experimental and simulated concentration profiles at the column outlet from the TCSA experiments and open-inlet model a) for CO_2 in the adsorption phase; b) for H_2O in the adsorption phase; c) for CO_2 in the desorption phase; d) for H_2O in the desorption phase.

Figure 24 shows that the gas temperature profiles simulated by the open-inlet model very closely follows the experimental bed temperature in both the adsorption and desorption phases. At the beginning of the adsorption phase, a gas temperature spike is observed as shown in Figure 24a, mainly due to the released heat of adsorption of H_2O. Due to the way higher concentration of H_2O in the gas, the energy released and bound by its reactions affects

the temperature of the gas much more than CO_2. As the column is cooled during the adsorption step and the rate of adsorption finally slows down, the gas temperature eventually reaches the wall temperature. At the beginning of the desorption phase, a small temperature spike to the opposite direction can be observed as shown in Figure 24b, mainly because of the energy bound by the endothermic desorption of H_2O. In the TS desorption phase, the column was heated step by step from 25 °C to 100 °C, which the modelled gas temperature follows closely.

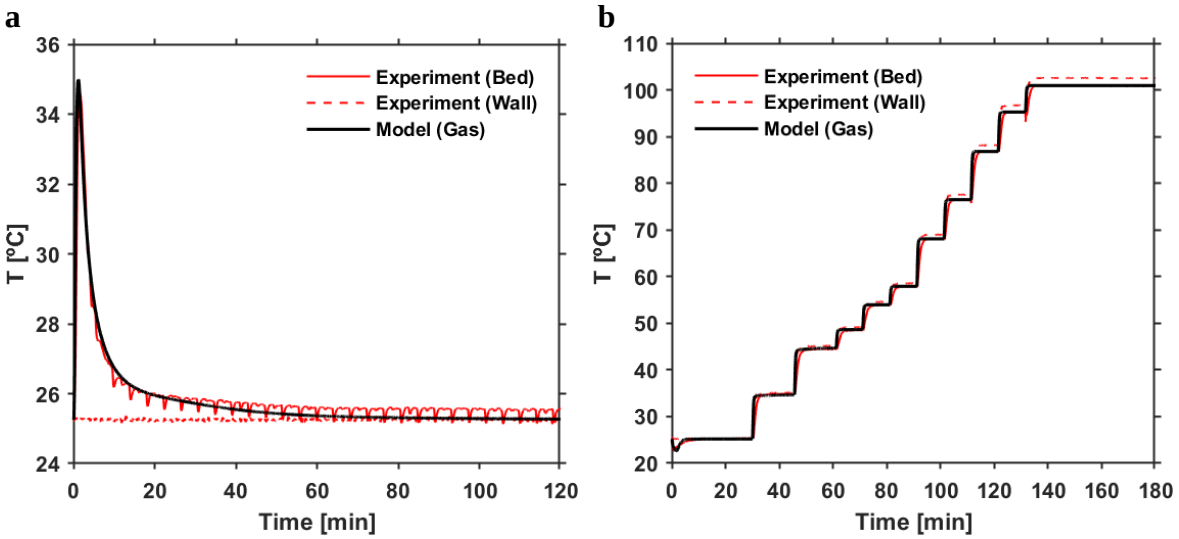

Figure 24. Experimental and simulated temperature profiles from the TCSA experiments and open-inlet model a) for the adsorption phase; b) for the desorption phase consisting of a 30 min purge step and a TS step limited to 150 min.

The heat transfer and kinetic parameters gained by fitting the open-inlet model to the experimental bed temperature (Figure 24) and concentration profiles (Figure 23) are listed in Table 7. The fitted heat transfer coefficient falls within the typical range of 10-500 W/(m^2K) for forced convection of air reported by Kosky et al (2021). The fitted heat transfer and kinetic parameters are also in the same order of magnitude as the values reported by Elfving (2021, p. 93) for the same adsorbent and similar conditions. Even though a constant heat transfer coefficient is assumed for each phase in the column, it would actually vary over time depending on the changes in e.g. gas density, viscosity and velocity. The effects of different heat transfer and kinetic parameters are evaluated in the sensitivity analysis.

Table 7. Heat transfer and kinetic parameters fitted from experimental data.

h	$k_{f,1}$	$k_{f,2}$	$k_{H2O,LDF}$
[W/(m^{2}K)]	[bar^{-1}s^{-1}(mol/kg)$^{1-t1}$]	[bar^{-2}s^{-1}(mol/kg)$^{1-t2}$]	[1/s]
30.84	0.41	6.19	0.13

The concentration and temperature profiles of the closed-inlet model and closed TVSA experiment are presented in Appendix 4. In general, the profiles simulated with the closed-inlet model match the experiment well. Greater similarity is achieved especially with regard to the CO_2 concentration profile in the adsorption phase. However, for an unidentified reason the closed-inlet model cannot desorb any noticeable CO_2 or H_2O capacity at the pre-vacuuming phase, and therefore no temperature spike is recognized at the beginning of the desorption phase. By contrast, in the closed TVSA experiments under humid conditions, CO_2 and H_2O capacities of 0.06-0.07 $mmol_{CO2}/g_{adsorbent}$ and 1.5-1.8 $mmol_{H2O}/g_{adsorbent}$ were desorbed during the pre-vacuuming phase. Fortunately, this fault in the closed model is not so problematic, because the duration of the pre-vacuum phase reduces to only a few tens of seconds after optimizing the durations of the cycle phases, and the capacity that should have been desorbed in this phase is simply transferred to the TS desorption phase, which is prolonged a little bit.

It can be seen from the Appendices 5 and 6 that the greatest differences between simulations and experimental results are found in the adsorption and desorption capacity profiles regardless of the model used. The models overestimate the CO_2 adsorption capacities by 0.06-0.09 $mmol_{CO2}/g_{adsorbent}$ and H_2O adsorption capacities by 0.23-0.29 $mmol_{H2O}/g_{adsorbent}$ compared to the experiments. The steepness of the adsorption capacity profiles is very similar at the beginning of the adsorption, but the simulated capacities end up at different levels. This is probably due to the fact that the previously fitted CO_2 and H_2O adsorption isotherm parameters, listed in Table 5 and Table 6, do not fully apply to the experiments anymore as the adsorbent sample has changed a bit over time. Especially, the simulated and experimental adsorption capacities should be closer to each other since the measurements of adsorption capacities can be considered quite accurate. The experimental desorption capacities, on the other hand, contain larger errors due to the reasons related to measurement accuracy introduced in Section 4.1.1, and therefore it is difficult to draw conclusions about

the reliability of the models based on the differences between the experimental and simulated desorption capacities. The desorption capacities of the closed-inlet model are fairly close to the experiments, but the open-inlet model overestimates the CO_2 desorption capacities by 0.14 $mmol_{CO2}/g_{adsorbent}$ and H_2O desorption capacities by 1.05 $mmol_{H2O}/g_{adsorbent}$ compared to the experiments. To make the comparison between the models and experiments even more accurate, the experiments should be repeated several times so that the differences between the experiments could be eliminated.

In this work, the modelled capacities have been calculated based on the changes in the solid-phase CO_2 and H_2O uptakes in the adsorbent bed during the adsorption and desorption phases. Another way would be to calculate the capacities based on the incoming and outgoing mass flows of the gas components, in other words based on the gas-phase balances of the species. However, the capacity calculation method based on the gas phase gives too high desorption capacity that may even exceed the adsorption capacity. Table 8 shows the effect of the chosen number of computing cells and the chosen capacity calculation method on CO_2 working capacity for both closed- and open-inlet models. The effect of the used capacity calculation method on the closed-inlet model is 0.17-0.19% of the working capacity, while the effect on the open-inlet model in only 0.01%. The effect of the number of used computing cells is a bit greater. The working capacity can change up to 0.33% when the column is divided into only 10 computing cells. On the other hand, the working capacity is not so significantly affected by increasing the number of computing cells to 100. Adding computing cells also leads to a considerable increase in simulation times. Thus, 50 computing cells are chosen to obtain accurate enough results with reasonable effort.

Table 8. Dependence of the simulated CO_2 working capacity on the capacity calculation method and the number of computing cells into which the column is divided.

Number of cells *N*	Working capacity (solid-phase balance)		Working capacity (gas-phase balance)	
	Closed-inlet model	Open-inlet model	Closed-inlet model	Open-inlet model
10	0.7735 (+0.33%)	0.8210 (-0.16%)	0.7748 (+0.31%)	0.8209 (-0.16%)
50	0.7710	0.8223	0.7725	0.8222
100	0.7706 (-0.05%)	0.8225 (+0.02%)	0.7721 (-0.05%)	0.8224 (+0.02%)

4.2.2 CO_2 productivity and specific energy requirement

The CO_2 productivity and SER were calculated with the closed-inlet model for different closed TVSA experiment cases based on the simulated working capacities, optimized cycle times and energy requirements in each case. The results obtained using 90% or 99% cut-off criteria for cycle time optimization are listed in Table 9. It can be seen from the table that the operating conditions and the choice of cut-off criterion significantly affects the performance of the DAC process.

Table 9. Working capacities, optimized cycle times, CO_2 productivities and specific energy requirements simulated under different conditions of closed TVSA cases at 90% and 99% cut-off criteria. The adsorbent samples of 0.5 g were used.

Case and conditions	Working capacity [$mmol_{CO2}/g_{adsorbent}$]		Cycle time [min]		CO_2 productivity [$kg_{CO2}/(kg_{adsorbent}\cdot d)$]		SER [MJ/kg_{CO2}]	
	90%	99%	90%	99%	90%	99%	90%	99%
TVSA closed (dry, 100°C)	0.329	0.399	50.2	78.4	0.416	0.322	11.5	10.0
TVSA closed (humid, 100°C)	0.612	0.735	96.0	222.0	0.404	0.210	16.2	14.8
TVSA closed (humid, 60°C)	0.273	0.329	183.9	316.3	0.094	0.066	25.1	23.1

According to the experimentally obtained CO_2 working capacities (see Section 4.1.1) and the modelled working capacities for optimized cycles shown in Table 9, it is evident that the working capacity in a closed TVSA cycle is highly affected by the humidity level and the extent of temperature-swing. The equilibrium working capacity is formed by the difference between the equilibrium capacities in the adsorption and desorption conditions, and therefore, to achieve a higher working capacity, the equilibrium capacity should be increased in the adsorption phase and decreased in the desorption phase. Based on Figure 25, the equilibrium adsorption capacity under ambient CO_2 partial pressure ($p_{CO2} \approx 0.0004$ bar) and temperature of 25°C is 36% higher in 2 vol-% humidity compared to dry air. This is a reason for the 84-86% higher simulated working capacities in the humid closed TVSA case compared with the dry case. In addition to changing the humidity level, the equilibrium

adsorption capacity could be increased by decreasing the adsorption temperature or increasing the feed gas pressure. Instead, the equilibrium capacity in the desorption phase can be reduced by increasing the regeneration temperature or decreasing the vacuum pressure even below the current 0.025 bar. Due to this, 123-124% higher working capacities were simulated in humid conditions for the closed TVSA experiment with a regeneration temperature of 100°C compared to the similar experiment with a regeneration temperature only of 60°C.

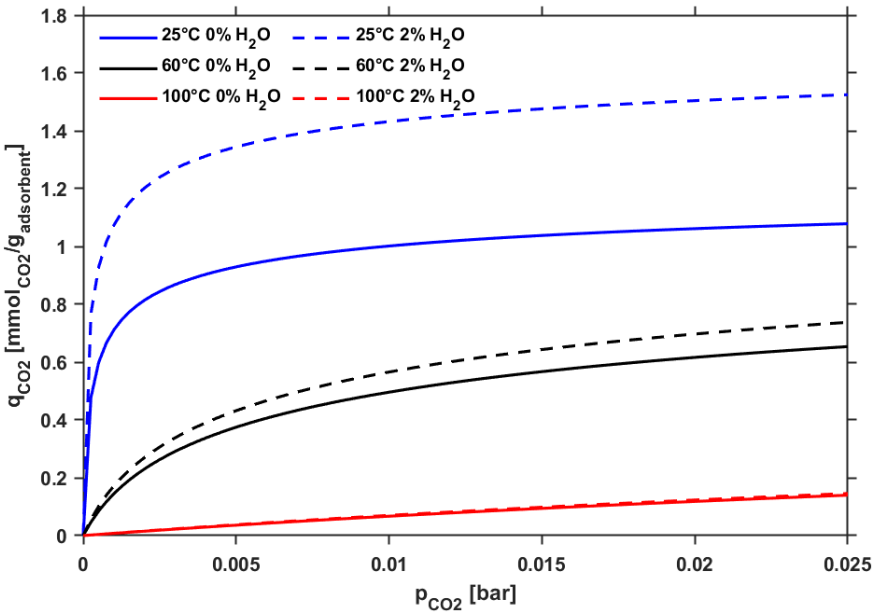

Figure 25. Modelled CO_2-isotherms under different temperature and humidity conditions.

The cut-off criteria define how close the equilibrium capacities of the adsorption and desorption phases can be reached during an optimized cycle. The adsorption phases of the simulated closed TVSA cases were cut off when 90% or 99% of the equilibrium CO_2 adsorption capacities were reached as shown in Figure 26. The SER is at its lowest at the beginning of the adsorption phase when the adsorption capacity rises quickly. After that, SER starts increasing more strongly as the increase in adsorption capacity slows down because the air fans consume electricity continuously regardless of whether more CO_2 can even be adsorbed. Therefore, it is reasonable to interrupt the adsorption phase before the full equilibrium adsorption capacity is reached. 0.07 $mmol_{CO2}/g_{adsorbent}$ higher adsorption capacities were achieved with the 99% cut-off criterion compared to the 90% criterion, but

the resulting adsorption-related SER became up to twice as high. Also, the durations of the adsorption phases with the 99% criterion became 21-121 min (52-141%) longer compared to the 90% criterion. In humid conditions, the adsorption times were more than twice longer than in dry conditions due to the higher adsorption equilibrium capacities.

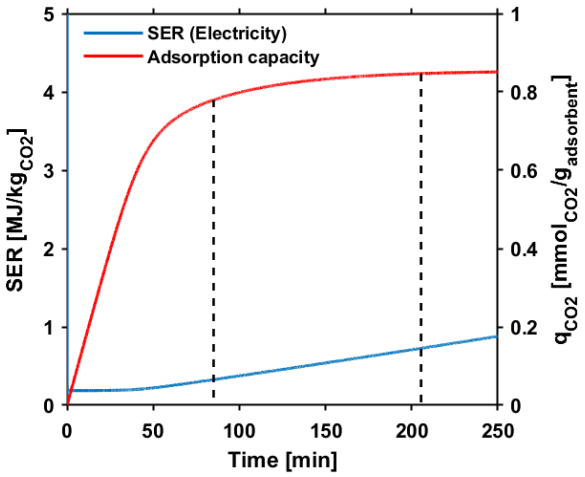

Figure 26. Modelled dynamic specific energy requirement and CO_2 adsorption capacity profiles during adsorption phase for humid closed TVSA case. The time steps when the 90% and 99% cut-off criteria are reached are illustrated with black dashed lines.

The desorption phases were cut off when 90% or 99% of the maximum attainable working capacity were desorbed as shown in Figure 27. The maximum attainable working capacities are higher with 99% criterion due to the higher adsorption capacities achieved in the adsorption phase, as explained earlier. The capacities that are in accordance with the cut-off criteria were reached much faster in the desorption phase than in the adsorption phase. The shares of the desorption phases were only 7-31% of the total cycle times if the cycle times are optimized in this way. In addition, the desorption phases consisted almost entirely of the TS desorption phases, as the pre-vacuum phases lasted only a few tens of seconds. SER is very high at the beginning of the desorption phase, especially in the pre-vacuum phase, because the energy consumption is high in relation to the amount of desorbed CO_2. At later stages, SER mainly consists of thermal energy. After the working capacity has reached its maximum value, SER will no longer change because no more heat-consuming desorption reactions occur, and the target vacuum pressure has already been reached. The benefit of using the 99% cut-off criterion is that 0.07-0.12 $mmol_{CO2}/g_{adsorbent}$ (20-21%) higher working

capacities and 1.3-2.0 MJ/kg_{CO2} (8-13%) lower SER were attained compared to the 90% criterion, as shown in Table 9. However, the drawback with the 99% criterion is 28-132 min (56-131%) longer required cycle time and thus 0.03-0.19 $kg_{CO2}/(kg_{adsorbent}\cdot d)$ (22-48%) lower CO_2 productivity.

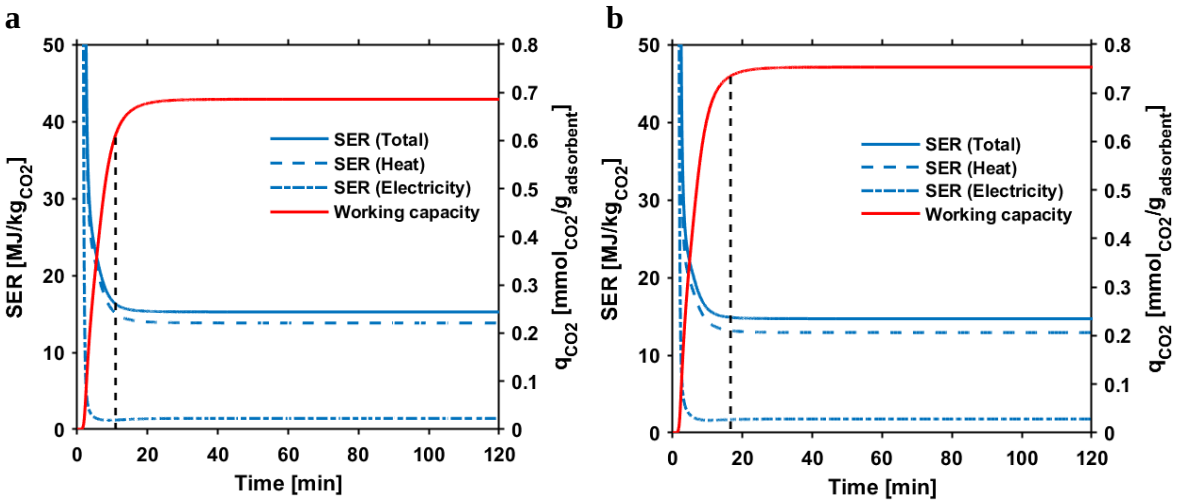

Figure 27. Modelled dynamic specific energy requirement and CO_2 working capacity profiles during desorption phase for humid closed TVSA case obtained with 100°C regeneration temperature. The time steps when the a) 90% and b) 99% cut-off criteria are reached are illustrated with black dashed lines.

In general, the CO_2 productivity has higher effect on the total costs of the DAC process than SER, and thus using a lower criterion could be beneficial, especially in the adsorption phase that takes long time. However, using a criterion much lower than 90% is probably not reasonable, because repeating several even shorter cycles to capture the same amount of CO_2 would degrade the adsorbent material more, and the adsorbent would lose its ability to capture CO_2 faster, which is already a substantial problem in the adsorbent design. In addition, lower criterion would cause higher energy losses due to cyclic heating and cooling of the bed. In the desorption phase, it is probably worth using a higher cut-off criterion than 90%, because the resulting increase in desorption time is small compared to the total cycle time. Therefore, the best option would be to use different optimized cut-off criteria for adsorption and desorption phases.

The detailed SER breakdowns showing the proportions of each energy requiring elements for different optimized closed TVSA cycles are shown in Figure 28. The electrical energy consumption of air fans and vacuum pump accounted for 11-16% of the total SER, being 1.2-3.7 MJ/kg_{CO2}, while the thermal energy consumption of 8.7-22.1 MJ/kg_{CO2} related to the sensible heats of the adsorbent and the adsorbed species as well as reaction heats of desorbing species accounted for most of the SER. The modelled SER compositions are very similar to the results presented by Sabatino et al. (2021, p. 2067) for different adsorbents in the closed TVSA cycle. Also, the modelled electrical and thermal energy consumptions are in some conditions within the ranges of 0.6-2.3 MJ/kg_{CO2} and 3.4-10.8 MJ/kg_{CO2} reported in the literature (see Table 2). However, the electricity requirement would be even higher if the energy consumption by cooling the column, condensing the co-adsorbed H_2O out of the product gas, or compressing the product gas is taken into account. The simulated SER values of the cases performed in humid conditions are higher than in dry conditions due to the high sensible and reaction heats of H_2O, corresponding to 3-5% and 42-53% of the total SER, respectively. As a result of this, the SER increases to 14.8-25.1 MJ/kg_{CO2} in 2 vol-% humidity depending on the cut-off criterion and regeneration temperature. By contrast, the lowest SER of 10.0-11.5 MJ/kg_{CO2} is achieved in dry conditions, and in that case the sensible heat of adsorbent plays the biggest role, corresponding to 68-71% of the total SER. SER is also much higher with a lower regeneration temperature of 60°C, because in that case longer cycles are needed, and the working capacities are reduced.

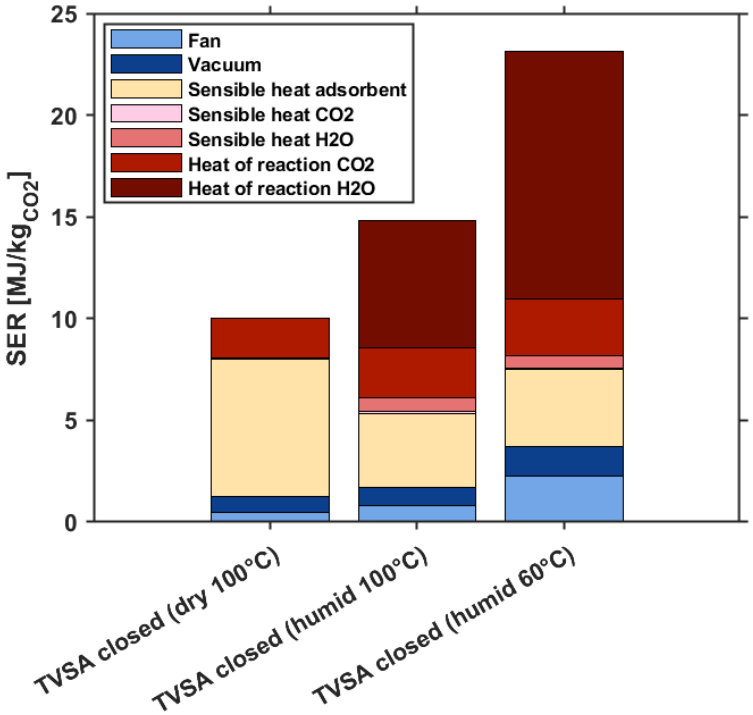

Figure 28. Breakdowns of the specific energy requirements simulated for the different closed TVSA cases. The adsorption and desorption phases were optimized with the 99% cut-off criteria.

In addition to changing the humidity level, temperature, pressure and cut-off criterion during the phases, the CO_2 productivity and SER can be affected by changing the flow rate of the feed gas or the length-to-diameter ratio of the adsorbent bed. Increasing the flow rate from the current 500 ml/min would improve CO_2 productivity, because the adsorption phase would be shortened due to higher CO_2 flow, but this would increase the electrical energy consumed by the air fans and thus also the SER. However, the flow rate in relation to the adsorbent mass is already several times higher with this laboratory-scale experimental setup compared to the larger-scale DAC processes, such as the DAC pilot unit reported by Vázquez et al. (2018, p. 237) operating with 1500 m^3/h feed gas flow and 480 kg adsorbent. With the same flow rate/adsorbent mass ratio, a feed gas flow rate of 26 ml/min should be used instead of 500 ml/min. Reducing the L/d-ratio from the current 2, on the other hand, would reduce the electrical energy consumed by the air fans due to the reduction of the pressure loss over the adsorbent bed. Therefore a lower L/d-ratio is typically used in process-scale DAC devices to keep the pressure drop reasonable, although laboratory-scale devices may have an L/d-ratio even greater than 2 (Vázquez et al., 2018, p. 238).

The CO_2 product gas purities of 11-31% were simulated for the different closed TVSA cases. If the co-adsorbed H_2O was separated from the product gas by condensation, a high-purity CO_2 stream of 96-99% could be reached. In dry conditions, the desorbed gas is almost pure CO_2, and no condensation is needed.

4.2.3 Sensitivity analysis of adsorbent-related parameters

Adsorbent-related parameters, such as heat transfer (K_z, h) and kinetic parameters ($k_{f,1}$, $k_{f,2}$, $k_{H2O,LDF}$), isotherm parameters of the 7-parameter model (q_m, $b_{0,1}$, $b_{0,2}$, $-\Delta H_1$, $-\Delta H_2$, t_1, t_2) and the GAB-model ($q_{m,mono}$, C_0, K_0, ΔH_C, ΔH_K, $-\Delta H_{H2O,0}$), as well as adsorbent material properties (ρ_p, d_p, $c_{p,a}$, CCD) are examined in the sensitivity analysis. The impacts of certain +/- changes in these adsorbent-related parameters on CO_2 productivity and SER are illustrated graphically in Figure 29 and Figure 30. The numeric results are provided in Appendix 7. Parameters that contain more uncertainty or are more important for the DAC process and adsorbent design have been evaluated one by one in more detail. Especially the kinetic parameters and the isotherm parameters of the 7-parameter model have huge impact on CO_2 productivity, while the SER is also highly affected by the GAB-model parameters and the adsorbent material properties. The results of the sensitivity analysis were produced using the 99% cut-off criterion.

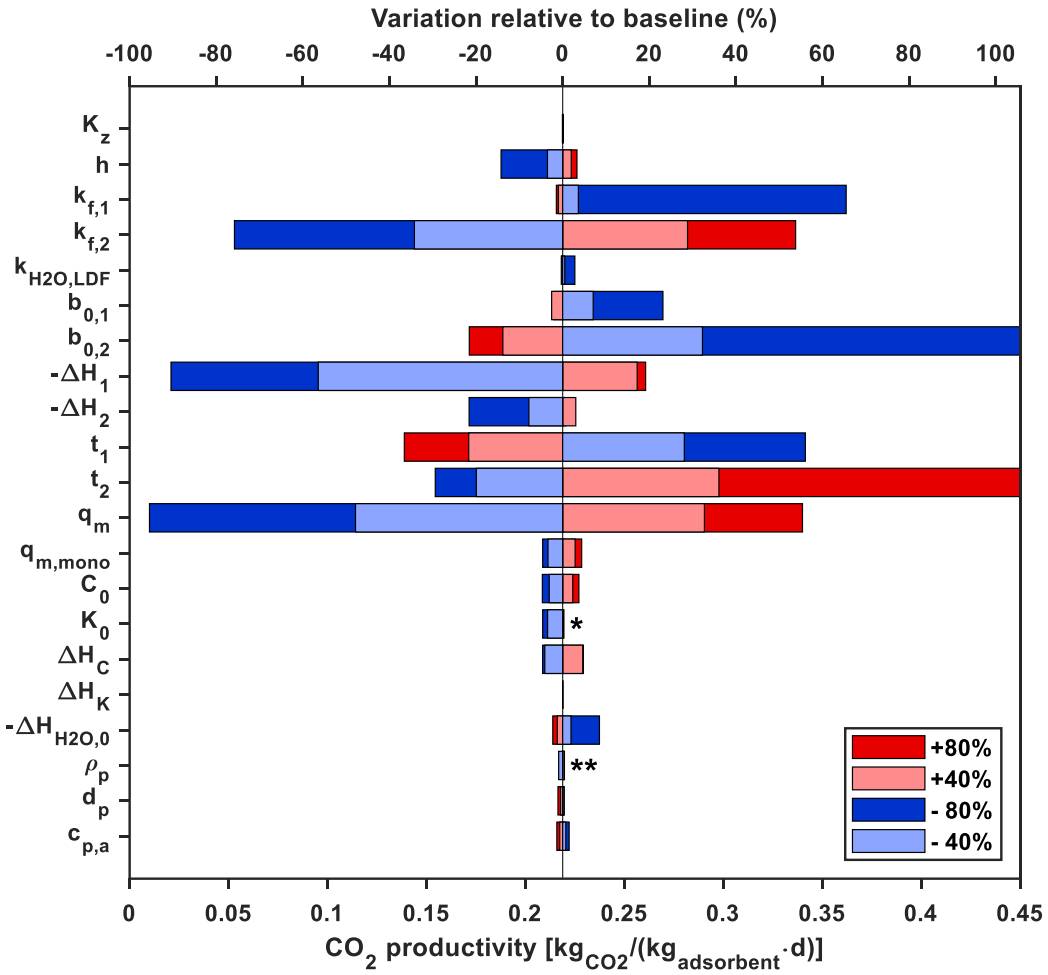

Figure 29. The effect of adsorbent-related parameters on CO_2 productivity in a simulated humid closed TVSA DAC process, when changing the parameters by +/- 80% and 40%. * No reasonable productivity is achieved when the K_0 is changed by +80% due to too high adsorption time. ** For ρ_p only -20% is used instead of -40 and -80%, because the adsorbent particle density cannot be lower than the defined bulk density.

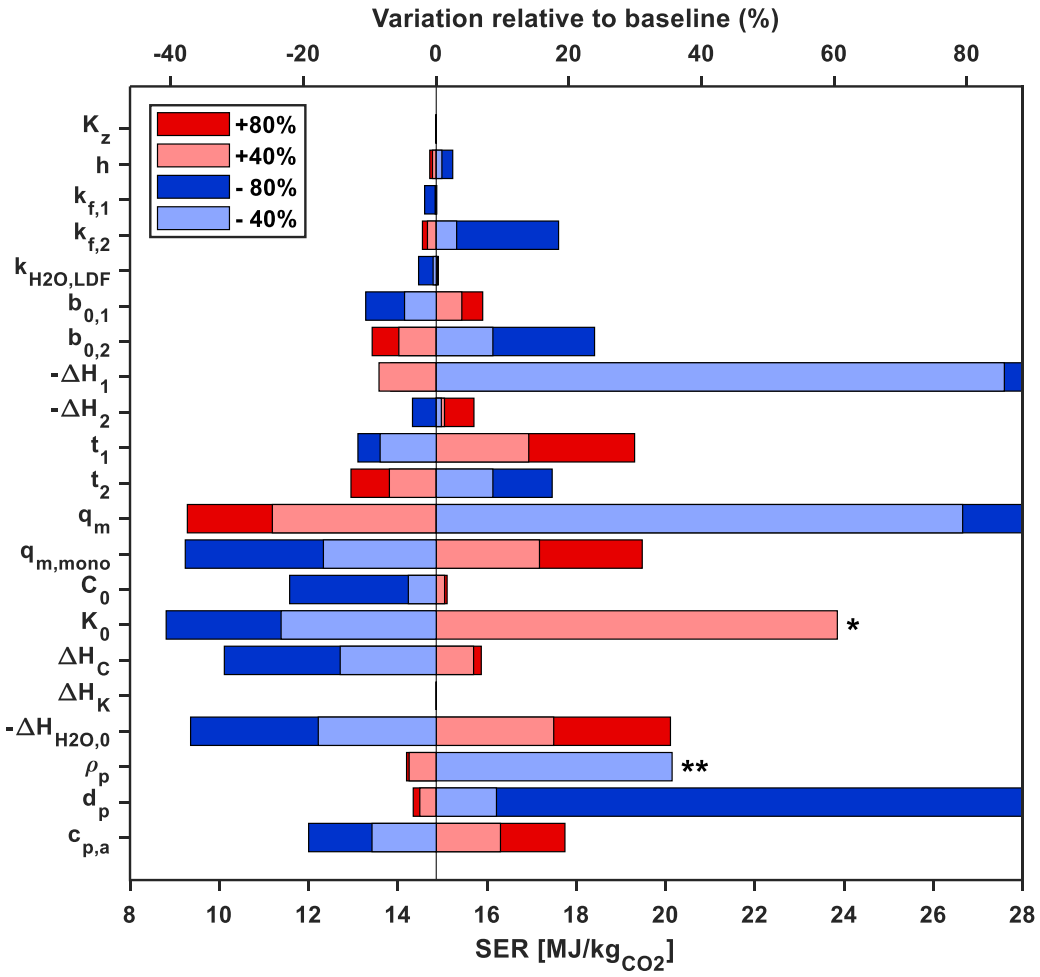

Figure 30. The effect of adsorbent-related parameters on specific energy requirement (SER) in a simulated humid closed TVSA DAC process, when changing the parameters by +/- 80% and 40%. * No reasonable SER is achieved when the K_0 is changed by +80% due to too high adsorption time. ** For ρ_p only -20% is used instead of -40 and -80%, because the adsorbent particle density cannot be lower than the defined bulk density.

As the availability of data and correlations on heat transfer coefficients are very limited for this type of amine-functionalized adsorbent, the heat transfer coefficient h of 30.84 W/(m^{2}K) was estimated by fitting the dynamic model to experimental bed temperature data. The fitted coefficient is comparable with the values of 6.7-35 W/(m^{2}K) used in the CO_2 adsorption simulation literature (Haghpanah et al., 2013, p. 4255; Rajagopalan and Rajendran, 2018, p. 439; Sabatino et al., 2021, p. 2058). However, a sensitivity analysis was performed for the heat transfer coefficient because it was fitted based on only one experiment and thus contains some uncertainty. The gas temperature profile within the column, especially at the beginning

of adsorption and TS desorption phases, depends on the chosen heat transfer coefficient, as shown in Figure 31. The heat transfer coefficient is changed +/- 80% between 6.2-55.5 W/(m^{2}K) that covers the entire range of values presented in the literature. The heat transfer coefficient defines the rate of heat transfer between the wall and the gas, and thus with a higher heat transfer coefficient, the gas reaches the temperature of the wall faster, and shorter adsorption and desorption times are needed. Therefore, the CO_2 productivity increases by 3% when h is increased by +80%, and correspondingly decreases by 14% when h is reduced by -80%. Although the heat transfer coefficient had high impact on CO_2 productivity, the impact on SER turned out to be small. The axial effective heat conductivity K_z did not have significant impact on either CO_2 productivity or SER in the parameter range of +/- 80%.

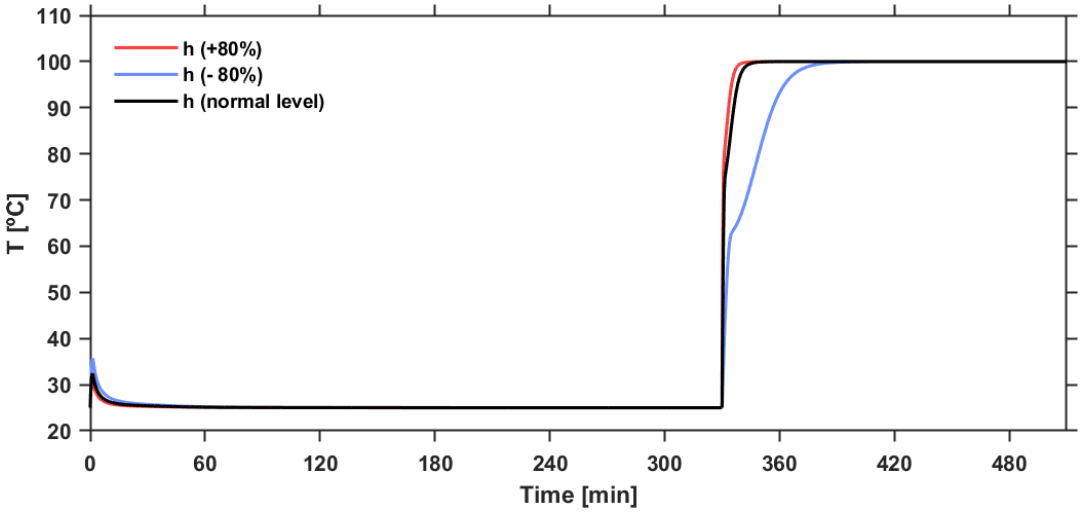

Figure 31. Mean gas temperature profiles in the adsorption column during one cycle simulated with different heat transfer coefficients.

The kinetic constants of forward CO_2 capture reactions in dry ($k_{f,1}$ = 0.41 bar^{-1}s^{-1}(mol/kg)$^{1-t1}$) and humid conditions ($k_{f,2}$ = 6.19 bar^{-2}s^{-1}(mol/kg)$^{1-t2}$) were estimated by fitting the dynamic model to experimental CO_2 concentration profiles. The fitted kinetic parameters are very close to the values reported by Elfving (2021, p. 93) in similar conditions. However, the CO_2 concentration profiles simulated with these fitted kinetic parameters did not completely match the experimental profile, and therefore the effects of kinetic parameters on CO_2 capture are evaluated in a more detailed sensitivity analysis. The kinetic parameters are changed +/- 80% between 0.08-0.73 bar^{-1}s^{-1}(mol/kg)$^{1-t1}$ and 1.24-11.13 bar^{-2}s^{-1}(mol/kg)$^{1-}$

^{t2} for reactions in dry and humid conditions, respectively. As these two kinetic parameters define the reaction rates of both dry and humid CO_2 capture reactions, the extents of dry and humid CO_2 capture reactions are changed when changing their kinetic parameters relative to each other. The humid CO_2 capture reaction is principally more favourable, as it requires less amines to capture the same amount of CO_2 according to reaction stoichiometry. If $k_{f,1}$ is reduced or $k_{f,2}$ is increased, the humid reaction becomes more dominant CO_2 capture mechanism, leading to an improved CO_2 adsorption rate while the achievable capacity remains the same, as shown in Figure 32. By promoting the humid reactions in either of these ways with +/- 80% changes to the kinetic parameters, the adsorption time is reduced by 38-43% using 99% cut-off criterion, resulting in 54-65% higher CO_2 productivities and slightly lower SER. On the other hand, if $k_{f,1}$ is increased or $k_{f,2}$ is reduced by 80%, it takes much longer for the CO_2 uptake profile to reach the equilibrium adsorption capacity or the defined cut-off point, and the CO_2 productivity may decrease up to 76% using the 99% cut-off criterion. The desorption phase is not affected so noticeably by the changing kinetic parameters as the adsorption phase.

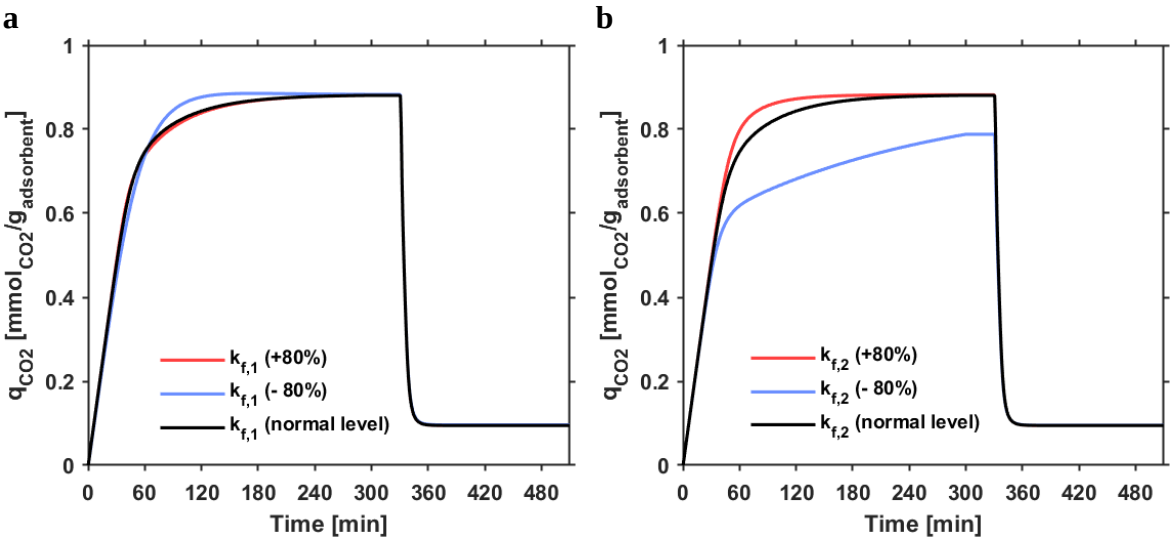

Figure 32. The CO_2 uptake profile during one cycle simulated with different forward kinetic constants for CO_2 capture reactions in a) dry conditions; b) humid conditions.

The kinetic constant of linear driving force model $k_{H2O,LDF}$ of 0.13 s^{-1} describing H_2O adsorption was fitted from experimental H_2O concentration profiles. The fitted constant is comparable with the value of 0.16 s^{-1} reported by Elfving (2021, p. 93) for the same

adsorbent, but it differs from the higher value used by Sabatino et al. (2021, p. 2058) of 1 s^{-1}. However, the effect of LDF-model kinetic constant on CO_2 productivity and SER was only up to around 3% even with larger ranges than +/- 80%.

Among the isotherm parameters of the 7-parameter model, the effect of maximum capacity of amine sites (q_m) being available for CO_2 capture reactions on CO_2 productivity and SER is one of the largest. In Figure 33, the effect of maximum amine capacity on CO_2 uptake is depicted by changing the maximum capacity by +/- 40% between 1.58-3.69 $mmol_{amine}/g_{adsorbent}$. With a 40% higher maximum capacity, the CO_2 uptake in the adsorption phase is increased by 63%, resulting in a 47% increase in working capacity from 0.76 $mmol_{CO2}/g_{adsorbent}$ to 1.12 $mmol_{CO2}/g_{adsorbent}$. Even though the cycle time is slightly prolonged with a higher q_m, the huge increase in working capacity ensures that the CO_2 productivity is increased while SER is decreased. Therefore, the CO_2 productivity increases by 33% and SER decreases by 25% when q_m is increased by +40%. The maximum capacity of amine sites can be increased in practice by raising the amine loading of the amine-functionalized adsorbent, and the improved CO_2 capture ability is the reason why adsorbent materials with high amine loadings are typically under development. However, the negative impacts on adsorption kinetics of too high amine loadings are not taken into account in the model.

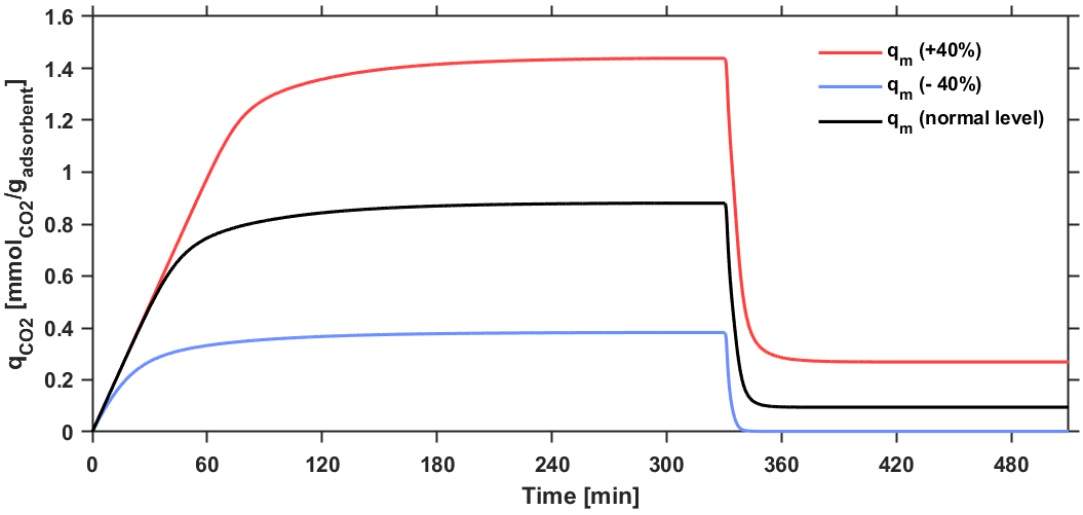

Figure 33. The CO_2 uptake profile during one cycle simulated with different maximum capacities of amine sites being available for CO_2 capture reactions.

The other isotherm parameters of the 7-parameter model are as well significantly affecting the CO_2 adsorption isotherm shape and the performance of the DAC process, but the effects of their changes in some +/- range are not as meaningful in the adsorbent design as the q_{m}. The achieved working capacity is higher for adsorbents that have higher reference adsorption affinity towards humid CO_2 capture reaction ($b_{0,2}$) or lower affinity towards dry reaction ($b_{0,1}$). Similarly, the working capacity is influenced by the exponential parameters of dry (t_1) and humid reactions (t_2). By promoting the humid CO_2 capture reaction, the working capacity and CO_2 productivity are increased, but as a negative side-effect the thermal energy requirement in regeneration is increased in forms of higher sensible and reaction heats of H_2O. The isosteric heats of adsorption for dry ($-\Delta H_1$) and humid reactions ($-\Delta H_2$) define the strengths of chemical bonds between the CO_2 molecules and the adsorbent material. Therefore, higher heats of adsorption increase the CO_2 adsorption capacity, but on the other hand also increase the energy requirement in regeneration. Despite of the higher energy requirement in this case, the CO_2 productivity and SER may improve because of higher working capacity.

Unlike the isotherm parameters of the 7-parameter model, the isotherm parameters of the GAB model do not greatly affect CO_2 productivity. These H_2O-related isotherm parameters are mainly affecting how much humidity from the feed gas is adsorbed to the adsorbent material and how high are the energy costs caused by regeneration of co-adsorbed H_2O. The monolayer adsorption capacity of H_2O ($q_{\mathrm{m,mono}}$) is probably the most important GAB isotherm model parameter as it defines the level of H_2O adsorption during the adsorption phase. In the Figure 34, the effect of $q_{\mathrm{m,mono}}$ on H_2O uptake is depicted by changing it +/- 40% between 1.55-3.61 $\mathrm{mmol_{H2O}/g_{adsorbent}}$. With a 40% higher $q_{\mathrm{m,mono}}$, the H_2O uptake in the adsorption phase is increased by 40%, resulting in a 3% higher CO_2 productivity. However, this comes with the cost of 16% higher SER due to the additional heat requirement of H_2O desorption. Other parameters of the GAB isotherm model (C_0, K_0, ΔH_{C}, ΔH_{K}) define the shape of the H_2O adsorption isotherm, but they are not covered in more detail in this work. The isosteric heat of H_2O adsorption ($-\Delta H_{\mathrm{H2O,0}}$) determines the strength of chemical bonds between the H_2O molecules and the adsorbent material, and therefore SER is 35% higher for materials that form stronger bonds with H_2O and have 80% higher $-\Delta H_{\mathrm{H2O,0}}$.

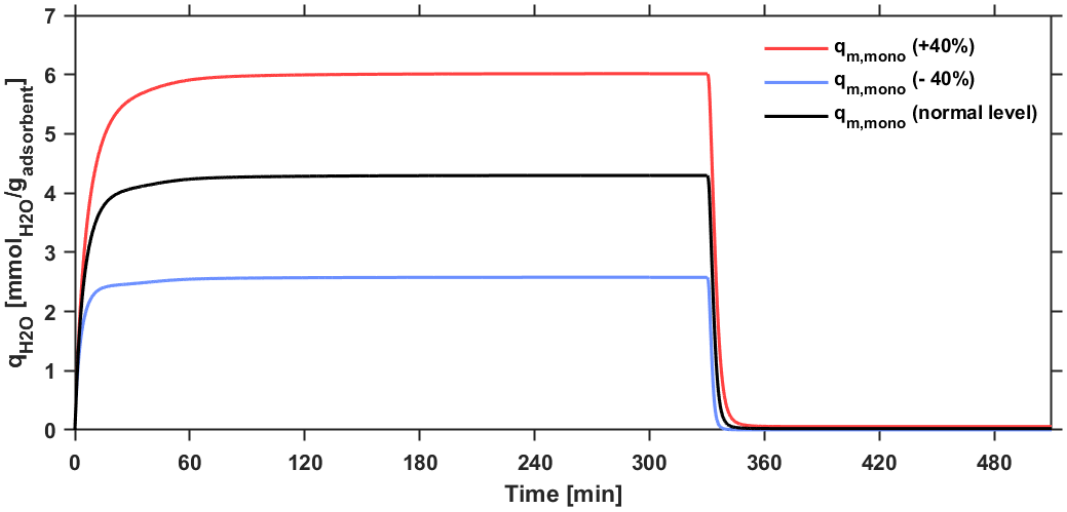

Figure 34. The H_2O uptake profile during one cycle simulated with different maximum monolayer adsorption capacities of H_2O.

Cyclic stability is one of the most important adsorbent material properties in terms of CO_2 productivity and operating costs of the DAC process, as it determines how many cycles the adsorbent can withstand before replacement. Based on the literature review in Section 3.2.2, a cyclic CO_2 and H_2O capacity drop coefficient (CCD) of 0.36 %/cycle was chosen as the base value for this analysis. Even higher cyclic capacity drops were reported by Jahandar Lashaki et al. (2019, pp. 3332–3341) for other adsorbents. The effect of CCD on adsorption and desorption capacities of CO_2 and H_2O is illustrated in Figure 35 by changing it +/- 80% between 0.07-0.65 %/cycle. It can instantly be seen that the CCD of 0.65 %/cycle is too high, because at that value, the adsorbent already loses over 14% of its working capacity during the first 20 cycles. With a CCD of 0.07 %/cycle, the 2% drop in working capacity during 20 cycles is much more tolerable, and at this rate, the adsorbent maintains half of its working capacity for 619 cycles. However, the adsorbent should last for thousands of cycles for the DAC process to be economically viable, and therefore adsorbents with even lower CCD should be developed (Jahandar Lashaki, Khiavi and Sayari, 2019). The H_2O capacities decrease at the same rate as the CO_2 capacities, as shown in Figure 35b, due to the same CCD coefficient used for both species. In the case of CO_2 in Figure 35a, the adsorption capacity is slightly higher than the desorption capacity. This is because there are momentarily conditions similar to TCSA regeneration in the column at the very beginning

of the adsorption phase leading to regeneration, when the temperature is still high, and the feed gas begins to flow into the column behaving like a purge gas. This desorbed CO_2 at the beginning of the adsorption phase is not counted in the amount of desorbed CO_2 of the regeneration phase.

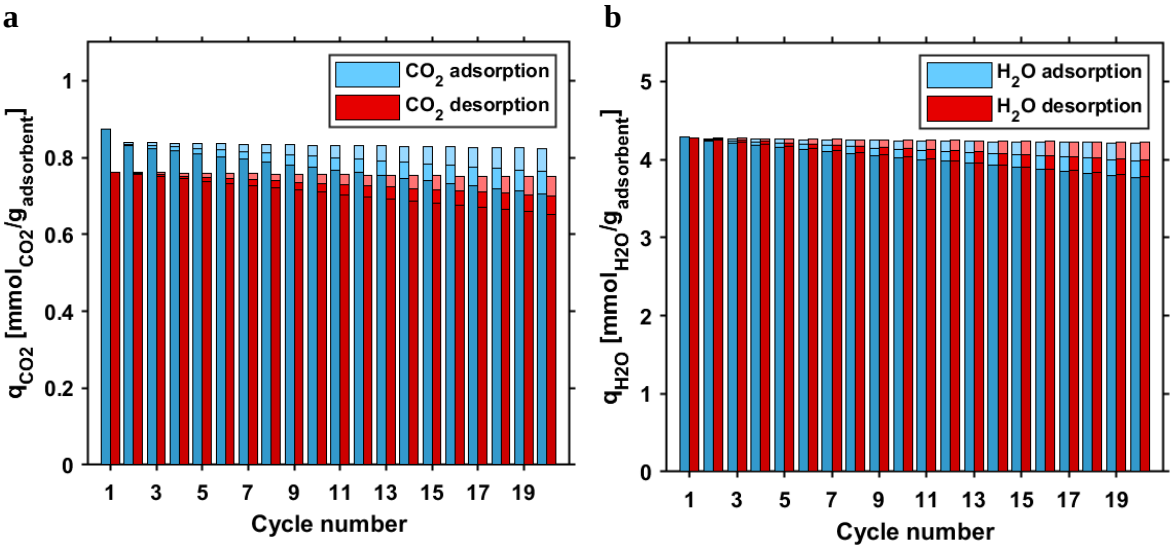

Figure 35. The adsorption and desorption capacities of a) CO_2 and b) H_2O in 20 repeated cycles with different cyclic capacity drop coefficients. A darker colour reflects an increase in the CCD coefficient by 80%, and a lighter colour an 80% reduction.

The effect of cyclic stability on CO_2 productivity and SER is analysed at the same +/- range as the adsorption and desorption capacities, as shown in Figure 36. The reduction in CO_2 productivity during the first 20 cycles is only 2% when the CCD is decreased by 80%, whereas a much higher reduction of 14% is occurring when the CCD is increased by 80%. Due to the constantly decreasing CO_2 adsorption ability of the adsorbent, SER is increased by 1% and 7% within the first 20 cycles with the 80% decrease and increase of CCD, respectively.

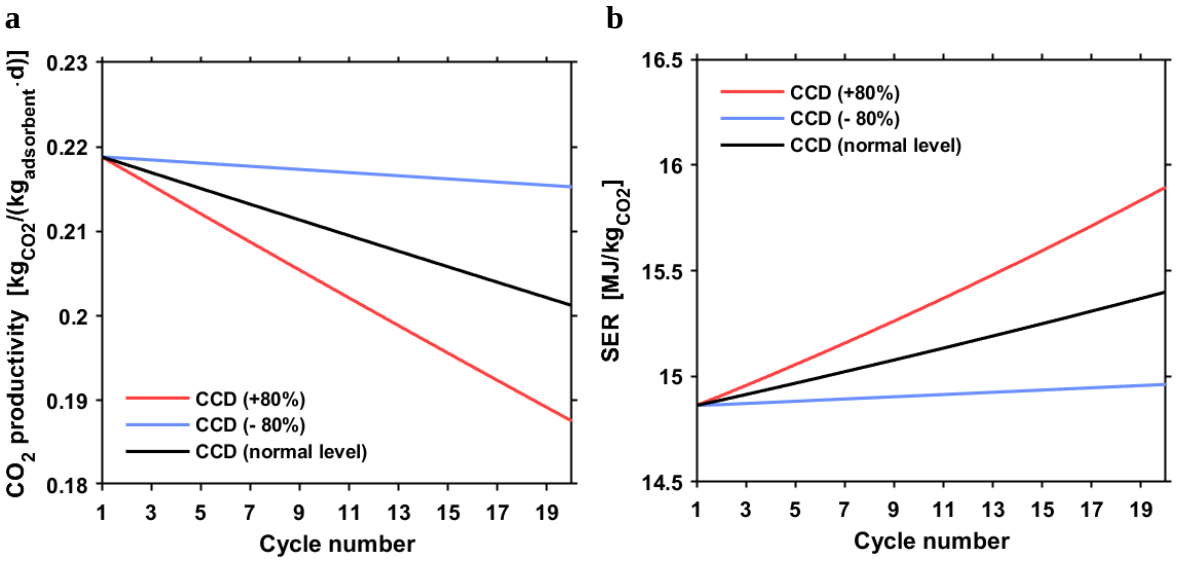

Figure 36. a) CO_2 productivity and b) SER simulated with different cyclic capacity drop coefficients in 20 consecutive cycles.

The other adsorbent material properties, such as particle density ρ_p, particle diameter d_p and specific heat capacity $c_{p,a}$, do not considerably affect the CO_2 productivity of the process, but they have a high impact on SER instead. Reducing the particle density from 720 kg/m^3 by even 20% leads to a huge increase in the pressure drop over the bed and thus to an increase in the electricity consumed by the air fans, as shown in Table 10. This is because the voidage of the bed decreases as the particle density decreases, and so there will be less space for gas to flow in the bed if the column dimensions and adsorbent mass are kept the same. Therefore, a high particle density of the adsorbent is favourable in terms of energy costs. Reducing the particle diameter from 0.60 mm also has the same effect of extremely increasing pressure drop and air fan related electricity consumption. Based on the Ergun equation used to calculate the pressure drop, the larger adsorbent particle diameter is favourable due to smaller pressure drop and energy costs. However, the effects of particle density and diameter on accessibility of the adsorption sites, and thus reaction kinetics, cannot be simulated with this model.

Table 10. Simulated pressure drop and air fan related SER for different particle densities and diameters.

		Pressure drop during adsorption [Pa]	SER of air fans [MJ/kg_{CO2}]
Particle density ρ_p [kg/m^3]			
576	(- 20%*)	1019	6.18
720	(Normal level)	132	0.80
1296	(+ 80%)	8	0.05
Particle diameter d_p [mm]			
0.12	(- 80%)	3059	18.80
0.60	(Normal level)	132	0.80
1.08	(+ 80%)	44	0.26

* For ρ_p only -20% is used instead of -40 and -80%, because the adsorbent particle density cannot be lower than the defined bulk density of 450 kg/m^3.

The specific heat capacity of the adsorbent has a large effect on the thermal energy consumption of the DAC process. According to Figure 28, the sensible heat of adsorbent may be up to 25% of the total SER in humid conditions and even up to 71% in dry conditions. The specific heat capacity of the adsorbent is changed +/- 80% between 316-2844 J/(kgK), while the values reported in the literature varies typically between 1500-2070 J/(kgK) for solid amine-functionalized adsorbents (Alesi and Kitchin, 2012, p. 6908; Wurzbacher et al., 2016, p. 1334; Sonnleitner, Schöny and Hofbauer, 2018, p. 391). The higher the specific heat capacity of the adsorbent, the greater the amount of thermal energy required to heat the bed and the longer it takes for the gas to reach the target adsorption or desorption temperature, as shown in Figure 37. The 80% higher specific heat capacity extends the desorption time by 19% and increases the SER by 19% using the 99% cut-off criterion. Respectively, the 80% lower specific heat capacity shortens the desorption time by 11% improving slightly the CO_2 productivity and reducing the SER by 19%. Therefore, a low specific heat capacity of the adsorbent is favourable in terms of SER and CO_2 productivity.

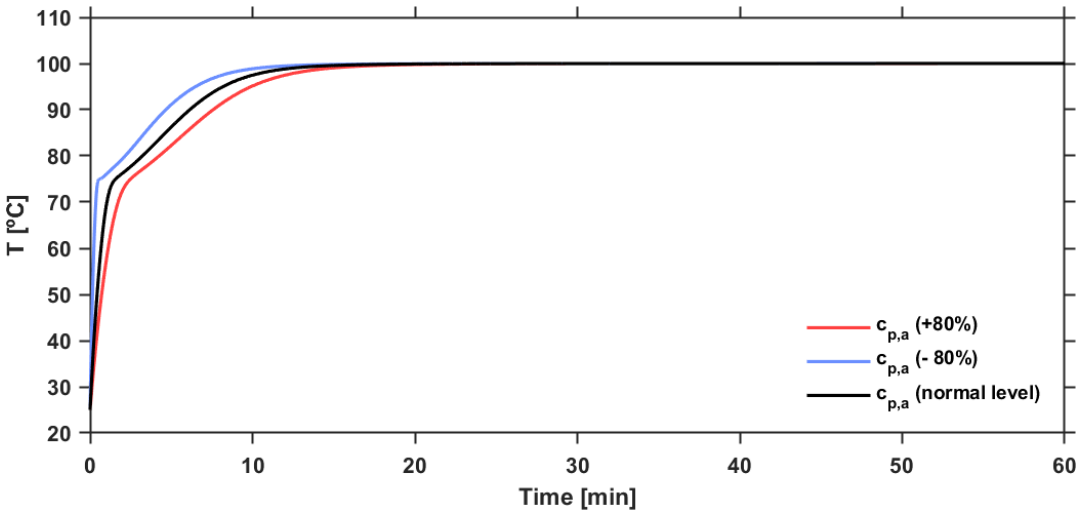

Figure 37. Mean gas temperature profiles in the adsorption column during TS desorption phase simulated with different specific heat capacities of adsorbent.

5. Conclusions

Direct air capture has shown high potential for climate change mitigation by removing CO_2 from the atmosphere and then either permanently storing it into geological storages to generate negative emissions or utilizing it as a feedstock in various applications. Storing can offset CO_2 emissions that are difficult to abate with conventional techniques. The cyclic LT DAC technology based on solid adsorbents has proven to be a particularly promising method for CO_2 capture. Among solid adsorbents, solid-supported amine-functionalized adsorbents have shown excellent CO_2 adsorption capacity and selectivity even from the low atmospheric CO_2 concentrations, making them a key research topic in the field of DAC.

However, the costs of DAC are still too high for large-scale deployment, being up to 850 €/t_{CO2} according to estimates. The high cost mainly comes from the high specific energy requirement of the process and the technical challenges of the adsorbents, such as stability problems. Despite of this, the novel LT DAC technology is estimated to have lots of potential for cost reduction. Improving the performance of the adsorbents is likely to be the most important factor in cost reduction. The main objective of this thesis was to evaluate how the cost-effectiveness of the DAC process could be improved, especially through novel adsorbent material development, but also through process parameter optimization.

In this thesis, the CO_2 adsorption performance of the novel amine-functionalized adsorbent was experimentally studied with a laboratory-scale fixed-bed adsorption/desorption device under different conditions relevant to DAC. With a closed TVSA cycle, CO_2 adsorption capacities of 0.43-0.47 $mmol_{CO2}/g_{adsorbent}$ were measured in dry conditions, while in humid conditions the adsorption capacities almost doubled from that, reaching 0.71-0.77 $mmol_{CO2}/g_{adsorbent}$. This proves that the co-adsorption of H_2O can significantly promote the CO_2 adsorption capacity of amine-functionalized adsorbents. However, these experimentally obtained CO_2 adsorption capacities did not outperform the capacities of the most promising amine-based adsorbents reported in the literature, which may reach up to 2-3 $mmol_{CO2}/g_{adsorbent}$. The regeneration temperature was also found to highly affect the working

capacity of the closed TVSA cycle. At 100 °C, almost all adsorbed CO_2 was desorbed, of which 60-65% had already been desorbed at 60 °C. In addition, differences in desorption performance were noticed between the regeneration methods. For example, by using N_2 purge gas in regeneration instead of vacuuming, a faster regeneration of the adsorbent bed was achieved. However, a more diluted CO_2 stream was obtained in this case, which may restrict the utilization or storage possibilities of the produced CO_2.

In the modelling part of this thesis, the cyclic DAC process was modelled by using the existing kinetic and dynamic CO_2 adsorption models proposed in the literature and making some improvements to them. The kinetic model was used to represent the adsorption and desorption of CO_2 and H_2O on the amine-functionalized adsorbent, considering the enhancing effect of humidity on the CO_2 adsorption capacity. The kinetic model was then used in the dynamic model together with mass and heat balance equations to describe the adsorption dynamics in a fixed-bed adsorption column. A detailed calculation of SER was added to the model, as well as mechanisms for optimizing the durations of the cycle phases and taking account of cyclic stability. The resulting model was used to simulate the performance of the adsorbent in the DAC process, especially the CO_2 productivity and SER, under different operating conditions and with changed adsorbent parameters.

The effect of operating conditions on CO_2 productivity and SER were simulated using model parameters consistent with the conditions of the conducted closed TVSA experiments. It was noticed that the operating conditions, such as humidity and regeneration temperature, significantly affected the performance of the adsorbent. 84-86% higher simulated working capacities were reached using feed air with 2 vol-% humidity compared to dry air, which is consistent with experiments. However, the higher working capacity under humid conditions also led to 91-183% longer cycle times, resulting in 3-35% lower CO_2 productivity. The SER was found to be lowest in the case of dry air due to the high regeneration energy requirement of humid conditions, which is caused by the high sensible and reaction heats of H_2O. Thus, according to these simulation results, using dry feed air was better option in the studied cases in terms of CO_2 productivity and SER. However, the performance could be further improved by developing the kinetic properties of the adsorbent in such a way that the higher working

capacity of the humid conditions could be combined with better productivity. Reducing the regeneration temperature from 100 °C to 60 °C, on the other hand, affected adversely on the working capacity, CO_2 productivity and SER, and thus cannot be considered applicable for a closed TVSA cycle. Increasing the regeneration temperature significantly is not reasonable either, as it would increase the thermal degradation of the amines.

The cycle time optimization and more specifically the choice of cut-off criterion also significantly affected the performance. By cutting off the adsorption and desorption phases before the equilibrium state was reached, the cycle could be greatly enhanced. With 99% cut-off criterion 20-21% higher working capacities and 8-13% lower SER were attained compared to 90% criterion, but on the other hand it led to 56-131% longer cycle times and thus 22-48% lower CO_2 productivity. The optimal solution would be to use different cut-off criteria for adsorption and desorption phases, so that high CO_2 productivity and low SER could be combined.

A sensitivity analysis of the adsorbent-related parameters was performed, in which the effects of different parameters on CO_2 capture performance were evaluated by changing them one at a time. The results showed that the kinetic parameters and the isotherm parameters of the 7-parameter model had a huge impact on CO_2 productivity, while SER was mostly affected by the GAB-model parameters and the adsorbent material properties. By changing the reaction mechanism between CO_2 and amines so that the humid reaction became more dominant, for example by enhancing the reaction kinetics of the adsorbent, the CO_2 adsorption rate and/or capacity were significantly improved, increasing the CO_2 productivity. On the other hand, the negative side-effect of the co-adsorbed humidity was the increased thermal energy requirement in regeneration caused by increased sensible and reaction heats of H_2O. This trade-off between CO_2 productivity and energy consumption has been recognized in the literature as well. However, SER can decrease even if the energy consumption increases if the working capacity increases sufficiently. Therefore, by increasing the maximum capacity of the amine sites in the adsorbent, the CO_2 productivity and SER were substantially improved because of the higher working capacity achieved. The cyclic stability was found to be crucial for the cyclic performance of the adsorbent as it had

a huge impact on both CO_2 productivity and SER. The higher was the cyclic drop in CO_2 capacity, the lower was the performance after a certain number of cycles. A reasonable cyclic capacity drop for the DAC process to be competitive was found to be clearly below 0.07 %/cycle.

In general, the modelled results can be considered quite accurate, because sufficiently good equivalency was achieved between the experimental and simulated concentration, temperature and capacity profiles in the model validation. Even higher accuracy might be reached by refitting the isotherm parameters to better match the possibly changed adsorbent. However, the model included some noteworthy simplifications, such as assumption of uniform wall temperature, velocity approximation, and idealized heat and mass transfer neglecting the concentration, temperature and pressure variations in the radial direction. Due to these simplifications, the model can only be used for modelling laboratory-scale fixed-bed DAC devices. The further development of the model could be beneficial so that it would also be suitable for modelling devices on a larger scale that are closer to real life applications. The experimental results also contained some uncertainty, particularly the desorption capacities of the closed TVSA cycle, which were measured using the %-scale meter that could better detect the high concentration peaks but was inaccurate at low concentrations between the peaks. This could perhaps be avoided by changing the experimental set up. The experimental accuracy could also be improved by repeating the experiments several times, always with a fresh sample, eliminating the effects of sample degradation and non-recurring errors.

As the results indicated, the performance of the amine-functionalized adsorbent in the LT DAC process can be significantly changed by switching the operating conditions or designing adsorbents with different properties. The CO_2 productivity and SER varied in the results between 0.01-0.50 $kg_{CO2}/(kg_{adsorbent} \cdot d)$ and 8.8-116 MJ/kg_{CO2}, respectively. The best achieved SER of 8.8 MJ/kg_{CO2}, for example, fell in the middle of the estimates of 3.6-13.1 MJ/kg_{CO2} reported in the literature for LT DAC systems. Since the thermal energy requirement, which often forms the greatest part of the SER, can be supplied by waste heat or other low-cost energy sources, the impact of CO_2 productivity on DAC costs is likely to

be greater. Therefore, the CO_2 productivity should be emphasized more in the development of novel adsorbent materials. However, the results were based on the effects of only one operating condition, adsorbent property, or cut-off criterion at a time. Thus, the DAC process could be further significantly improved by optimizing all these parameters simultaneously, potentially yielding beneficial synergies. The findings of this thesis can be used as a help in the optimization and development process, and most importantly, in reducing the costs of DAC.

References

Abd, A.A. *et al.* (2020) ‘Carbon dioxide removal through physical adsorption using carbonaceous and non-carbonaceous adsorbents: A review’, *Journal of Environmental Chemical Engineering*, 8(5), p. 104142. doi:10.1016/j.jece.2020.104142.

Alesi, W.R. and Kitchin, J.R. (2012) ‘Evaluation of a primary amine-functionalized ion-exchange resin for CO_2 capture’, *Industrial and Engineering Chemistry Research*, 51(19), pp. 6907–6915. doi:10.1021/ie300452c.

Al-Ghouti, M.A. and Da’ana, D.A. (2020) ‘Guidelines for the use and interpretation of adsorption isotherm models: A review’, *Journal of Hazardous Materials*, 393, p. 122383. doi:10.1016/j.jhazmat.2020.122383.

Birnbaum, M. (2021) ‘The world’s biggest plant to capture CO_2 from the air just opened in Iceland’, *The Washington Post*, 8 September. Available at: https://www.washingtonpost.com/s/climate-solutions/2021/09/08/co2-capture-plan-iceland-climeworks (Accessed: 6 April 2022).

Bollini, P. *et al.* (2012a) ‘Dynamics of CO_2 adsorption on amine adsorbents. 1. impact of heat effects’, *Industrial and Engineering Chemistry Research*, 51(46), pp. 15145–15152. doi:10.1021/ie301790a.

Bollini, P. *et al.* (2012b) ‘Dynamics of CO_2 adsorption on amine adsorbents. 2. insights into adsorbent design’, *Industrial and Engineering Chemistry Research*, 51(46), pp. 15153–15162. doi:10.1021/ie3017913.

Bos, M.J. *et al.* (2018) ‘Evaluating Regeneration Options of Solid Amine Sorbent for CO_2 Removal’, *Industrial and Engineering Chemistry Research*, 57(32), pp. 11141–11153. doi:10.1021/acs.iecr.8b00768.

Broehm, M., Strefler, J. and Bauer, N. (2015) ‘Techno-Economic Review of Direct Air Capture Systems for Large Scale Mitigation of Atmospheric CO_2’, *SSRN Electronic Journal* [Preprint]. doi:10.2139/ssrn.2665702.

Carbon Engineering (2022) *Our Story*. Available at: https://carbonengineering.com/our-story/ (Accessed: 12 August 2022).

Carbon180 (2022) *The DAC MAPP*. Available at: https://carbon180.org/dac-mapp (Accessed: 29 March 2022).

Chaikittisilp, W. *et al.* (2011) ‘Poly(L-lysine) brush-mesoporous silica hybrid material as a biomolecule-based adsorbent for CO_2 capture from simulated flue gas and air’, *Chemistry - A European Journal*, 17(38), pp. 10556–10561. doi:10.1002/chem.201101480.

Chen, C. and Tavoni, M. (2013) ‘Direct air capture of CO_2 and climate stabilization: A model based assessment’, *Climatic Change*, 118(1), pp. 59–72. doi:10.1007/s10584-013-0714-7.

Chen, C.H. *et al.* (2018) 'The "Missing" Bicarbonate in CO_2 Chemisorption Reactions on Solid Amine Sorbents', *Journal of the American Chemical Society*, 140(28), pp. 8648–8651. doi:10.1021/jacs.8b04520.

Choi, S. *et al.* (2011) 'Application of Amine-Tethered Solid Sorbents for Direct CO_2 Capture from the Ambient Air', *Environ. Sci. Technol*, 45(6), pp. 2420–2427. doi:10.1021/es102797w.

Climate Advisers (2022) *Global Thermostat*. Available at: https://www.climateadvisers.org/blog/what-companies-are-working-on-carbon-removal-and-carbon-capture/global-thermostat/ (Accessed: 5 April 2022).

Climeworks (2022) *Orca: the first large-scale plant*. Available at: https://climeworks.com/roadmap (Accessed: 12 August 2022).

Deutz, S. and Bardow, A. (2021) 'Life-cycle assessment of an industrial direct air capture process based on temperature–vacuum swing adsorption', *Nature Energy 2021 6:2*, 6(2), pp. 203–213. doi:10.1038/s41560-020-00771-9.

Do, D.D. (1998) *Adsorption Analysis: Equilibria and Kinetics*. Imperial College Press (Series on Chemical Engineering). doi:10.1142/p111.

EASAC (2018) *Negative emission technologies: What role in meeting Paris Agreement targets?* Available at: https://easac.eu/fileadmin/PDF_s/reports_statements/Negative_Carbon/EASAC_Report_on_Negative_Emission_Technologies.pdf (Accessed: 19 August 2022).

Elfving, J. *et al.* (2017) 'Modelling of equilibrium working capacity of PSA, TSA and TVSA processes for CO_2 adsorption under direct air capture conditions', *Journal of CO2 Utilization*, 22, pp. 270–277. doi:10.1016/j.jcou.2017.10.010.

Elfving, J. (2021) *Direct capture of CO_2 from air using amine-functionalized resin - Effect of humidity in modelling and evaluation of process concepts*. Available at: https://lutpub.lut.fi/handle/10024/163524 (Accessed: 29 March 2022).

Elfving, J. *et al.* (2021) 'Experimental comparison of regeneration methods for CO_2 concentration from air using amine-based adsorbent', *Chemical Engineering Journal*, 404, p. 126337. doi:10.1016/j.cej.2020.126337.

Elfving, J., Bajamundi, C. and Kauppinen, J. (2017) 'Characterization and Performance of Direct Air Capture Sorbent', *Energy Procedia*, 114, pp. 6087–6101. doi:10.1016/j.egypro.2017.03.1746.

Elfving, J. and Sainio, T. (2021) 'Kinetic approach to modelling CO_2 adsorption from humid air using amine-functionalized resin: Equilibrium isotherms and column dynamics', *Chemical Engineering Science*, 246, p. 116885. doi:10.1016/j.ces.2021.116885.

Erans, M. *et al.* (2022) 'Direct air capture: process technology, techno-economic and socio-political challenges', *Energy & Environmental Science*, 15(4), pp. 1360–1405. doi:10.1039/D1EE03523A.

European Central Bank (2022) *Euro foreign exchange reference rates: US dollar (USD)*. Available at: https://www.ecb.europa.eu/stats/policy_and_exchange_rates/euro_reference_exchange_rates/html/eurofxref-graph-usd.en.html (Accessed: 6 April 2022).

Fan, Y. and Jia, X. (2022) 'Progress in Amine-Functionalized Silica for CO_2 Capture: Important Roles of Support and Amine Structure', *Energy and Fuels*, 36(3), pp. 1252–1270. doi:10.1021/acs.energyfuels.1c03788.

Fasihi, M., Efimova, O. and Breyer, C. (2019) 'Techno-economic assessment of CO_2 direct air capture plants', *Journal of Cleaner Production*, 224, pp. 957–980. doi:10.1016/j.jclepro.2019.03.086.

Fawzy, S. *et al.* (2020) 'Strategies for mitigation of climate change: a review', *Environmental Chemistry Letters*, 18(6), pp. 2069–2094. doi:10.1007/s10311-020-01059-w.

Fernando, J. (2022) *Capital Expenditure (CapEx), Investopedia*. Available at: https://www.investopedia.com/terms/c/capitalexpenditure.asp (Accessed: 8 April 2022).

Fujikawa, S., Selyanchyn, R. and Kunitake, T. (2021) 'A new strategy for membrane-based direct air capture', *Polymer Journal*, 53(1), pp. 111–119. doi:10.1038/s41428-020-00429-z.

Fuss, S. *et al.* (2018) 'Negative emissions - Part 2: Costs, potentials and side effects', *Environmental Research Letters*, 13(6), p. 063002. doi:10.1088/1748-9326/aabf9f.

Gambhir, A. and Tavoni, M. (2019) 'Direct Air Carbon Capture and Sequestration: How It Works and How It Could Contribute to Climate-Change Mitigation', *One Earth*, 1(4), pp. 405–409. doi:10.1016/j.oneear.2019.11.006.

Gebald, C., Repond, N. and Wurzbacher, J.A. (2017) 'Steam assisted vacuum desorption process for carbon dioxide capture'. Available at: https://patents.google.com/patent/US10279306B2/en (Accessed: 23 March 2022).

Gelles, T. *et al.* (2020) 'Recent advances in development of amine functionalized adsorbents for CO_2 capture', *Adsorption*, 26(1), pp. 5–50. doi:10.1007/s10450-019-00151-0.

Goeppert, A. *et al.* (2012) 'Air as the renewable carbon source of the future: An overview of CO_2 capture from the atmosphere', *Energy and Environmental Science*, 5(7), pp. 7833–7853. doi:10.1039/c2ee21586a.

Green, D.W. and Perry, R.H. (2008) *Perry's Chemical Engineers' Handbook*. 8th edn. doi:10.1036/0071422943.

Haghpanah, R. *et al.* (2013) 'Multiobjective optimization of a four-step adsorption process for postcombustion CO_2 capture via finite volume simulation', *Industrial and Engineering Chemistry Research*, 52(11), pp. 4249–4265. doi:10.1021/ie302658y.

Halliday, C. and Hatton, T.A. (2021) ‘Sorbents for the Capture of CO_2 and Other Acid Gases: A Review’, *Industrial and Engineering Chemistry Research*, 60(26), pp. 9313–9346. doi:10.1021/acs.iecr.1c00597.

Hoffman, J.S. *et al.* (2014) ‘Parametric study for an immobilized amine sorbent in a regenerative carbon dioxide capture process’, *Fuel Processing Technology*, 126. doi:10.1016/j.fuproc.2014.04.027.

Hou, C. long *et al.* (2017) ‘Integrated direct air capture and CO_2 utilization of gas fertilizer based on moisture swing adsorption’, *Journal of Zhejiang University: Science A*, 18(10), pp. 819–830. doi:10.1631/jzus.A1700351.

House, K.Z. *et al.* (2011) ‘Economic and energetic analysis of capturing CO_2 from ambient air’, *Proceedings of the National Academy of Sciences of the United States of America*, 108(51), pp. 20428–20433. doi:10.1073/pnas.10122531.

IEA (2020a) *CCUS in Clean Energy Transitions*. Paris. Available at: https://www.iea.org/reports/ccus-in-clean-energy-transitions (Accessed: 19 August 2022).

IEA (2020b) *Energy Technology Perspectives 2020*. Paris. Available at: https://www.iea.org/reports/energy-technology-perspectives-2020 (Accessed: 19 August 2022).

IEA (2021a) *Direct Air Capture*. Available at: https://www.iea.org/reports/direct-air-capture (Accessed: 17 February 2022).

IEA (2021b) *Net Zero by 2050. A Roadmap for the Global Energy Sector*. Paris. Available at: https://www.iea.org/reports/net-zero-by-2050 (Accessed: 19 August 2022).

IEA (2022) *Direct Air Capture: A key technology for net zero*. Paris. Available at: https://www.iea.org/reports/direct-air-capture-2022 (Accessed: 12 August 2022).

IEAGHG (2021) *Global Assessment of Direct Air Capture Costs*. Available at: www.ieaghg.org.

IPCC (2021) *Summary for Policymakers. In: Climate Change 2021: The Physical Science Basis. Contribution of Working Group I to the Sixth Assessment Report of the Intergovernmental Panel on Climate*. Available at: https://www.ipcc.ch/report/ar6/wg1/downloads/report/IPCC_AR6_WGI_SPM_final.pdf (Accessed: 19 August 2022).

Ishimoto, Y. *et al.* (2017) ‘Putting Costs of Direct Air Capture in Context’, *SSRN Electronic Journal* [Preprint]. doi:10.2139/ssrn.2982422.

Jahandar Lashaki, M., Khiavi, S. and Sayari, A. (2019) ‘Stability of amine-functionalized CO_2 adsorbents: a multifaceted puzzle’, *Chemical Society Reviews*, 48(12), pp. 3320–3405. doi:10.1039/C8CS00877A.

Karjunen, H., Tynjälä, T. and Hyppänen, T. (2017) ‘A method for assessing infrastructure for CO_2 utilization: A case study of Finland’, *Applied Energy*, 205, pp. 33–43. doi:10.1016/j.apenergy.2017.07.111.

Kaufman, L. and Rathi, A. (2021) ‘Inside America’s Race to Scale Carbon-Capture Technology’, *Bloomberg*, 9 April. Available at: https://www.bloomberg.com/news/features/2021-04-09/inside-america-s-race-to-scale-carbon-capture-technology (Accessed: 12 August 2022).

Kearns, J. *et al.* (2017) ‘Developing a Consistent Database for Regional Geologic CO_2 Storage Capacity Worldwide’, *Energy Procedia*, 114, pp. 4697–4709. doi:10.1016/j.egypro.2017.03.1603.

Kintisch, E. (2014) ‘Can Sucking CO_2 Out of the Atmosphere Really Work?’, *MIT Technology Review*, 7 October. Available at: https://www.technologyreview.com/2014/10/07/171023/can-sucking-co2-out-of-the-atmosphere-really-work/ (Accessed: 5 April 2022).

Kolle, J.M., Fayaz, M. and Sayari, A. (2021) ‘Understanding the Effect of Water on CO_2 Adsorption’, *Chemical Reviews*, 121(13), pp. 7280–7345. doi:10.1021/acs.chemrev.0c00762.

Kosky, P. *et al.* (2021) ‘Mechanical Engineering’, *Exploring Engineering*, pp. 317–340. doi:10.1016/B978-0-12-815073-3.00014-4.

Kulkarni, A.R. and Sholl, D.S. (2012) ‘Analysis of equilibrium-based TSA processes for direct capture of CO_2 from Air’, *Industrial and Engineering Chemistry Research*, 51(25), pp. 8631–8645. doi:10.1021/ie300691c.

Kwon, H.T. *et al.* (2019) ‘Aminopolymer-Impregnated Hierarchical Silica Structures: Unexpected Equivalent CO_2 Uptake under Simulated Air Capture and Flue Gas Capture Conditions’, *Chemistry of Materials*, (31), pp. 5229–5237. doi:10.1021/acs.chemmater.9b01474.

Lackner, K., Ziock, H.-J. and Grimes, P. (1999) ‘Carbon Dioxide Extraction From Air: Is It An Option?’, in *24th Annual Technical Conference on Coal Utilization and Fuel Systems*. Los Alamos.

Lackner, K.S. (2009) ‘Capture of carbon dioxide from ambient air’, *The European Physical Journal Special Topics*, 176(1), pp. 93–106. doi:10.1140/epjst/e2009-01150-3.

Larsen, J. *et al.* (2019) *Capturing Leadership: Policies for the US to Advance Direct Air Capture Technology*. Available at: https://rhg.com/research/capturing-leadership-policies-for-the-us-to-advance-direct-air-capture-technology/ (Accessed: 5 April 2022).

Li, K., Kress, J.D. and Mebane, D.S. (2016) ‘The Mechanism of CO_2 Adsorption under Dry and Humid Conditions in Mesoporous Silica-Supported Amine Sorbents’, *Journal of Physical Chemistry C*, 120(41), pp. 23683–23691. doi:10.1021/acs.jpcc.6b08808.

Li, W. *et al.* (2010) ‘Steam-Stripping for Regeneration of Supported Amine-Based CO_2 Adsorbents’, *ChemSusChem*, 3(8), pp. 899–903. doi:10.1002/cssc.201000131.

Liao, P.-Q. *et al.* (2016) ‘Putting an ultrahigh concentration of amine groups into a metal-organic framework for CO_2 capture at low pressures’, *Chemical Science*, 7(10), pp. 6528–6533. doi:10.1039/c6sc00836d.

Lindsey, R. (2020) *Climate Change: Atmospheric Carbon Dioxide*. Available at: https://www.climate.gov/news-features/understanding-climate/climate-change-atmospheric-carbon-dioxide (Accessed: 17 February 2022).

McDonald, T.M. *et al.* (2012) 'Capture of carbon dioxide from air and flue gas in the alkylamine-appended metal-organic framework mmen-Mg_2(dobpdc)', *Journal of the American Chemical Society*, 134(16), pp. 7056–7065. doi:10.1021/ja300034j.

McQueen, N. *et al.* (2021) 'A review of direct air capture (DAC): scaling up commercial technologies and innovating for the future', *Progress in Energy*, 3(3), p. 032001. doi:10.1088/2516-1083/abf1ce.

Nakao, S.-I. *et al.* (2019) *Advanced CO_2 Capture Technologies: Absorption, Adsorption, and Membrane Separation Methods*. Cham: Springer. doi:10.1007/978-3-030-18858-0.

National Academies of Sciences (2019) *Negative Emissions Technologies and Reliable Sequestration: A Research Agenda*. Washington: National Academies Press. doi:10.17226/25259.

Oschatz, M. and Antonietti, M. (2018) 'A search for selectivity to enable CO_2 capture with porous adsorbents', *Energy & Environmental Science*, 11(1), pp. 57–70. doi:10.1039/c7ee02110k.

Pettinari, C. and Tombesi, A. (2020) 'Metal-organic frameworks for carbon dioxide capture', *MRS Energy & Sustainability*, 7(35). doi:10.1557/mre.2020.30.

Quirijns, E.J. *et al.* (2005) 'Sorption isotherms, GAB parameters and isosteric heat of sorption', *Journal of the Science of Food and Agriculture*, 85(11), pp. 1805–1814. doi:10.1002/jsfa.2140.

Rajagopalan, A.K. and Rajendran, A. (2018) 'The effect of nitrogen adsorption on vacuum swing adsorption based post-combustion CO_2 capture', *International Journal of Greenhouse Gas Control*, 78, pp. 437–447. doi:10.1016/j.ijggc.2018.09.002.

Rastegar, S.O. and Gu, T. (2017) 'Empirical correlations for axial dispersion coefficient and Peclet number in fixed-bed columns', *Journal of Chromatography A*, 1490, pp. 133–137. doi:10.1016/j.chroma.2017.02.026.

Realmonte, G. *et al.* (2019) 'An inter-model assessment of the role of direct air capture in deep mitigation pathways', *Nature Communications 2019 10:1*, 10(1), pp. 1–12. doi:10.1038/s41467-019-10842-5.

Ritchie, H., Roser, M. and Rosado, P. (2020) *CO_2 and Greenhouse Gas Emissions*, *Our World in Data*. Available at: https://ourworldindata.org/greenhouse-gas-emissions (Accessed: 10 August 2022).

Ruthven, D.M. (1984) *Principles of Adsorption and Adsorption Processes*. John Wiley & Sons. doi:0-471-86606-7.

Sabatino, F. *et al.* (2021) 'A comparative energy and costs assessment and optimization for direct air capture technologies', *Joule*, 5(8), pp. 2047–2076. doi:10.1016/j.joule.2021.05.023.

Sandhu, N.K. *et al.* (2016) 'Steam Regeneration of Polyethylenimine-Impregnated Silica Sorbent for Postcombustion CO_2 Capture: A Multicyclic Study', *Industrial and Engineering Chemistry Research*, 55(7), pp. 2210–2220. doi:10.1021/acs.iecr.5b04741.

Sanz-Pérez, E.S. *et al.* (2016) 'Direct Capture of CO_2 from Ambient Air', *Chemical Reviews*, 116(19), pp. 11840–11876. doi:10.1021/acs.chemrev.6b00173.

Seader, J.D., Henley, E.J. and Roper, D.K. (2011) *Separation Process Principles*. 3rd edn. John Wiley & Sons.

Serna-Guerrero, R., Belmabkhout, Y. and Sayari, A. (2010) 'Influence of regeneration conditions on the cyclic performance of amine-grafted mesoporous silica for CO_2 capture: An experimental and statistical study', *Chemical Engineering Science*, 65(14), pp. 4166–4172. doi:10.1016/j.ces.2010.04.029.

Shafeeyan, M.S., Wan Daud, W.M.A. and Shamiri, A. (2014) 'A review of mathematical modeling of fixed-bed columns for carbon dioxide adsorption', *Chemical Engineering Research and Design*, 92(5), pp. 961–988. doi:10.1016/j.cherd.2013.08.018.

Shi, X. *et al.* (2020) 'Sorbents for the Direct Capture of CO_2 from Ambient Air', *Angewandte Chemie*, 132(18), pp. 7048–7072. doi:10.1002/ange.201906756.

Simon, A.J. *et al.* (2011) 'Systems analysis and cost estimates for large scale capture of carbon dioxide from air', *Energy Procedia*, 4, pp. 2893–2900. doi:10.1016/j.egypro.2011.02.196.

Sing, K.S.W. *et al.* (1985) 'Reporting Physisorption Data for Gas/Solid Systems with Special Reference to the Determination of Surface Area and Porosity', *Pure and Applied Chemistry*, 57(4), pp. 603–619. doi:10.1351/pac198557040603.

Sinha, A. *et al.* (2017) 'Systems Design and Economic Analysis of Direct Air Capture of CO_2 through Temperature Vacuum Swing Adsorption Using MIL-101(Cr)-PEI-800 and mmen-Mg_2(dobpdc) MOF Adsorbents', *Industrial and Engineering Chemistry Research*, 56(3), pp. 750–764. doi:10.1021/acs.iecr.6b03887.

Sircar, S. and Hufton, J.R. (2000) 'Why Does the Linear Driving Force Model for Adsorption Kinetics Work?', *Adsorption*, 6(2), pp. 137–147. doi:10.1023/A:1008965317983.

Sonnleitner, E., Schöny, G. and Hofbauer, H. (2018) 'Assessment of zeolite 13X and Lewatit® VP OC 1065 for application in a continuous temperature swing adsorption process for biogas upgrading', *Biomass Conversion and Biorefinery*, 8(2), pp. 379–395. doi:10.1007/s13399-017-0293-3.

Stampi-Bombelli, V., van der Spek, M. and Mazzotti, M. (2020) 'Analysis of direct capture of CO_2 from ambient air via steam-assisted temperature–vacuum swing adsorption', *Adsorption*, 26(7), pp. 1183–1197. doi:-10.1007/s10450-020-00249-w.

Sujan, A.R. *et al.* (2019) 'Direct CO_2 Capture from Air using Poly(ethylenimine)-Loaded Polymer/Silica Fiber Sorbents', *ACS Sustainable Chemistry and Engineering*, 7(5), pp. 5264–5273. doi:10.1021/acssuschemeng.8b06203.

Tollefson, J. (2018) ‘Sucking carbon dioxide from air is cheaper than scientists thought’, *Nature*, 558(7709), p. 173. doi:10.1038/d41586-018-05357-w.

UNEP (2021) *Emissions Gap Report 2021*. Available at: https://www.unep.org/resources/emissions-gap-report-2021 (Accessed: 23 August 2022).

UNFCCC (2015) *Paris Agreement*. Available at: https://unfccc.int/sites/default/files/english_paris_agreement.pdf (Accessed: 23 August 2022).

Ünveren, E.E. *et al.* (2017) ‘Solid amine sorbents for CO_2 capture by chemical adsorption: A review’, *Petroleum*, 3(1), pp. 37–50. doi:10.1016/j.petlm.2016.11.001.

Vázquez, F.V. *et al.* (2018) ‘Power-to-X technology using renewable electricity and carbon dioxide from ambient air: SOLETAIR proof-of-concept and improved process concept’, *Journal of CO2 Utilization*, 28, pp. 235–246. doi:10.1016/j.jcou.2018.09.026.

Wang, J. *et al.* (2015) ‘Application of polyethylenimine-impregnated solid adsorbents for direct capture of low-concentration CO_2’, *AIChE Journal*, 61(3), pp. 972–980. doi:10.1002/aic.14679.

Wijesiri, R.P. *et al.* (2019) ‘Desorption Process for Capturing CO_2 from Air with Supported Amine Sorbent’, *Industrial and Engineering Chemistry Research*, 58(34), pp. 15606–15618. doi:10.1021/acs.iecr.9b03140.

Wurzbacher, J.A. *et al.* (2016) ‘Heat and mass transfer of temperature–vacuum swing desorption for CO_2 capture from air’, *Chemical Engineering Journal*, 283, pp. 1329–1338. doi:10.1016/j.cej.2015.08.035.

Wurzbacher, J.A., Gebald, C. and Steinfeld, A. (2011) ‘Separation of CO_2 from air by temperature-vacuum swing adsorption using diamine -functionalized silica gel’, *Energy & Environmental Science*, 4(9), pp. 3584–3592. doi:10.1039/C1EE01681D.

Yang, M. *et al.* (2019) ‘Recent Advances in CO_2 Adsorption from Air: a Review’, *Current Pollution Reports*, 5(4), pp. 272–293. doi:10.1007/s40726-019-00128-1.

Yu, Q. and Brilman, W. (2020) ‘A Radial Flow Contactor for Ambient Air CO_2 Capture’, *Applied Sciences*, 10(3), p. 1080. doi:10.3390/app10031080.

Zhang, W. *et al.* (2014) ‘Capturing CO_2 from ambient air using a polyethyleneimine–silica adsorbent in fluidized beds’, *Chemical Engineering Science*, 116, pp. 306–316. doi:10.1016/j.ces.2014.05.018.

Zhu, X. *et al.* (2021) ‘Design of steam-assisted temperature vacuum-swing adsorption processes for efficient CO_2 capture from ambient air’, *Renewable and Sustainable Energy Reviews*, 137, p. 110651. doi:10.1016/j.rser.2020.110651.

Zolfaghari, Z. *et al.* (2022) ‘Direct air capture from demonstration to commercialization stage: A bibliometric analysis’, *International Journal of Energy Research*, 46(1), pp. 383–396. doi:10.1002/er.7203.

Appendix 1. DAC plants in operation and under development.

Company	Country	Sector	CO_2 storage or use	Start-up year	CO2 capture capacity [t_{CO2}/year]	Reference
Global Thermostat	United States	R&D	Not known	2010	500	[1] [4]
Global Thermostat	United States	R&D	Not known	2013	1000	[1] [4]
Climeworks	Germany	R&D	Use	2015	1	[1]
Carbon Engineering	Canada	Power-to-X	Use	2015	Up to 365	[1]
Climeworks	Switzerland	Power-to-X	Use	2016	50	[1] [4]
Climeworks	Switzerland	Greenhouse fertilization	Use	2017	900	[1] [2]
Climeworks	Iceland	Mineralization of CO_2	Storage	2017	50	[1] [2]
Climeworks	Switzerland	Beverage carbonation	Use	2018	600	[1] [2]
Climeworks	Switzerland	Power-to-X	Use	2018	3	[1] [4]
Climeworks	Italy	Power-to-X	Use	2018	150	[1] [4]
Global Thermostat	United States	R&D	Not known	2018 (shut down 2019)	<4000	[4] [5]
Climeworks	Germany	Power-to-X	Use	2019	3	[1]
Climeworks	Netherlands	Power-to-X	Use	2019	3	[1] [4]
Climeworks	Germany	Power-to-X	Use	2019	3	[1]
Climeworks	Germany	Power-to-X	Use	2019	50	[1]
Zheijiang University	China	Greenhouse fertilization	Use	2019	10	[4]
Climeworks	Germany	Power-to-X	Use	2020	50	[1] [4]
Climeworks	Germany	Power-to-X	Use	2020	3	[1] [4]
Climeworks	Germany	Power-to-X	Use	2020	1	[1] [4]
Climeworks	Iceland	Mineralization of CO_2	Storage	2021	4000	[1] [2]
Climeworks	Iceland	Mineralization of CO_2	Storage	Under construction	36000	[2]
Carbon Engineering	United States	CO_2 removal	Storage	Under engineering	1000000	[3]
Carbon Engineering	United Kingdom	CO_2 removal	Storage	Under engineering	500000	[3]

References: [1]: (IEA, 2022, p. 19), [2]: (Climeworks, 2022), [3]: (Carbon Engineering, 2022), [4]: (Carbon180, 2022), [5]: (Kaufman and Rathi, 2021)

Appendix 2. Model parameters used in the dynamic CO_2 adsorption model validation and experiment-based calculations of CO_2 productivity and SER.

Symbol	Parameter	Value & unit	Source
Simulation parameters:			
n	Number of nodes	50	Assumption.
Heat transfer parameters:			
K_z	Axial effective heat conductivity	Variable	Calculated by correlation.
Process conditions:			
T_w	Column wall temperature	~25 °C [1,2], 100-103 °C [3]	Set equal to the measured bed temperature.
P_{ext}	External/ambient pressure	1.013 bar	Set equal to the standard atmospheric pressure.
P_1	Pressure in the column before vacuuming	~1 bar	Set equal to P2 before vacuuming.
P_2	Vacuum pressure at given time point	25-1000 mbar	Calculated from the simulated partial pressures of the species.
P_{vac}	Target vacuum pressure	25 mbar	Measured from the outlet.
Inlet gas properties:			
T_{feed}	Feed gas temperature	~25 °C [1,2], 98 °C [3]	Set equal to the measured bed temperature. [1,2] In the TS desorption phase set equal to the measured bed temperature without an adsorbent sample. [3]
P_{feed}	Feed gas pressure	1.05 bar	Measured before the column.
$\dot{V}_{feed}$	Feed gas flow rate	500 ml/min [1], 0/1000 ml/min [2,3]	From experimental setpoints.
$y_{CO2,feed}$	Feed volume fraction of CO_2	363-370 ppm	Measured from the outlet.
$y_{H2O,feed}$	Feed volume fraction of H_2O	1.925-1.927 vol-%	Measured from the outlet.
v_i	Interstitial velocity	0-0.35 m/s	Calculated from the flow rate and voidage. [1] Approximated with a mechanism based on the difference between total pressure and vacuum pressure in the desorption phase of the closed inlet model. [2,3]
v_s	Superficial velocity	0-0.13 m/s	Calculated from the interstitial velocity and voidage.
Gas properties:			
ν	Kinematic viscosity of gas mixture	$1.5 \cdot 10^{-5}$ m^2/s	From (Elfving, 2021, p. 64).
ρ_g	Gas density	0.016-1.18 kg/m^3	Calculated from the volume fractions and densities of individual species.
$c_{p,CO2}$	Specific heat capacity of CO_2	844 J/(kg K)	Calculated by NIST correlation.
$c_{p,H2O}$	Specific heat capacity of H_2O in liquid phase	4183 J/(kg K)	Calculated by NIST correlation.
$c_{p,H2O,v}$	Specific heat capacity of H_2O in vapour phase	1864 J/(kg K)	Calculated by NIST correlation.
$c_{p,N2}$	Specific heat capacity of N_2	1040 J/(kg K)	Calculated by NIST correlation.
$c_{p,g}$	Specific heat capacity of gas mixture	Variable	Calculated from the mass fractions and specific heat capacities of individual species.
$\dot{n}_{CO2}$	Molar flow rate of desorbed CO_2	Variable	Calculated from the uptake and sample mass.
$\dot{n}_{H2O}$	Molar flow rate of desorbed H_2O	Variable	Calculated from the uptake and sample mass.

[1] during adsorption phase, [2] during pre-vacuuming/purge phase, [3] during TS desorption phase.

Appendix 2. (continued)

Symbol	Parameter	Value & unit	Source
Adsorbent properties:			
ρ_B	Adsorbent bulk density	450 kg/m^3	Measured by Elfving (2021, p. 59).
ε	Adsorbent bed voidage	0.375	From safety data sheet of the adsorbent.
ρ_p	Adsorbent particle density	720 kg/m^3	Calculated from the bulk density and bed voidage.
d_p	Adsorbent particle diameter	$6 \cdot 10^{-4}$ m	Measured by Elfving et al. (2017)
$c_{p,a}$	Specific heat capacity of adsorbent	1580 J/(kg K)	From (Sonnleitner, Schöny and Hofbauer, 2018, p. 391)
m_a	Mass of adsorbent in bed	0.47 g	Measured mass of the sample from which the pre-adsorbed substances have been subtracted.
Geometry of the bed:			
R_{bed}	Adsorbent bed radius	0.0045 m	Measured the inner radius of the column.
L_{bed}	Adsorbent bed length	0.016 m	Calculated from the adsorbent mass, bulk density and bed radius.

[1] during adsorption phase, [2] during pre-vacuuming/purge phase, [3] during TS desorption phase.

Appendix 3. Model parameters used in the sensitivity analysis that differ from the previously presented parameters.

Symbol	Parameter	Value & unit	Source
T_{w}	Column wall temperature	25 °C [1,2], 100 °C [3]	Rounded from the measured bed temperatures.
T_{feed}	Feed gas temperature	25 °C [1,2]	Rounded from the measured bed temperatures. [1,2] No feed gas in the TS desorption phase of the closed TVSA cycle. [3]
P_{feed}	Feed gas pressure	1.013 bar	Set equal to the standard atmospheric pressure.
$y_{\mathrm{CO2,feed}}$	Feed volume fraction of CO_2	400 ppm	Rounded from the measurements. Typical for DAC literature.
$y_{\mathrm{H2O,feed}}$	Feed volume fraction of H_2O	2 vol-%	Rounded from the measurements.
m_{a}	Mass of adsorbent in bed	0.5 g	Rounded from the measured masses of the ~0.5 g samples.

[1] during adsorption phase, [2] during pre-vacuuming phase, [3] during TS desorption phase.

Appendix 4. Experimental and simulated profiles from the closed TVSA experiment and closed-inlet model a) for temperature in the adsorption phase; b) for temperature in the desorption phase; c) for CO_2 concentration in the adsorption phase; d) for H_2O concentration in the adsorption phase.

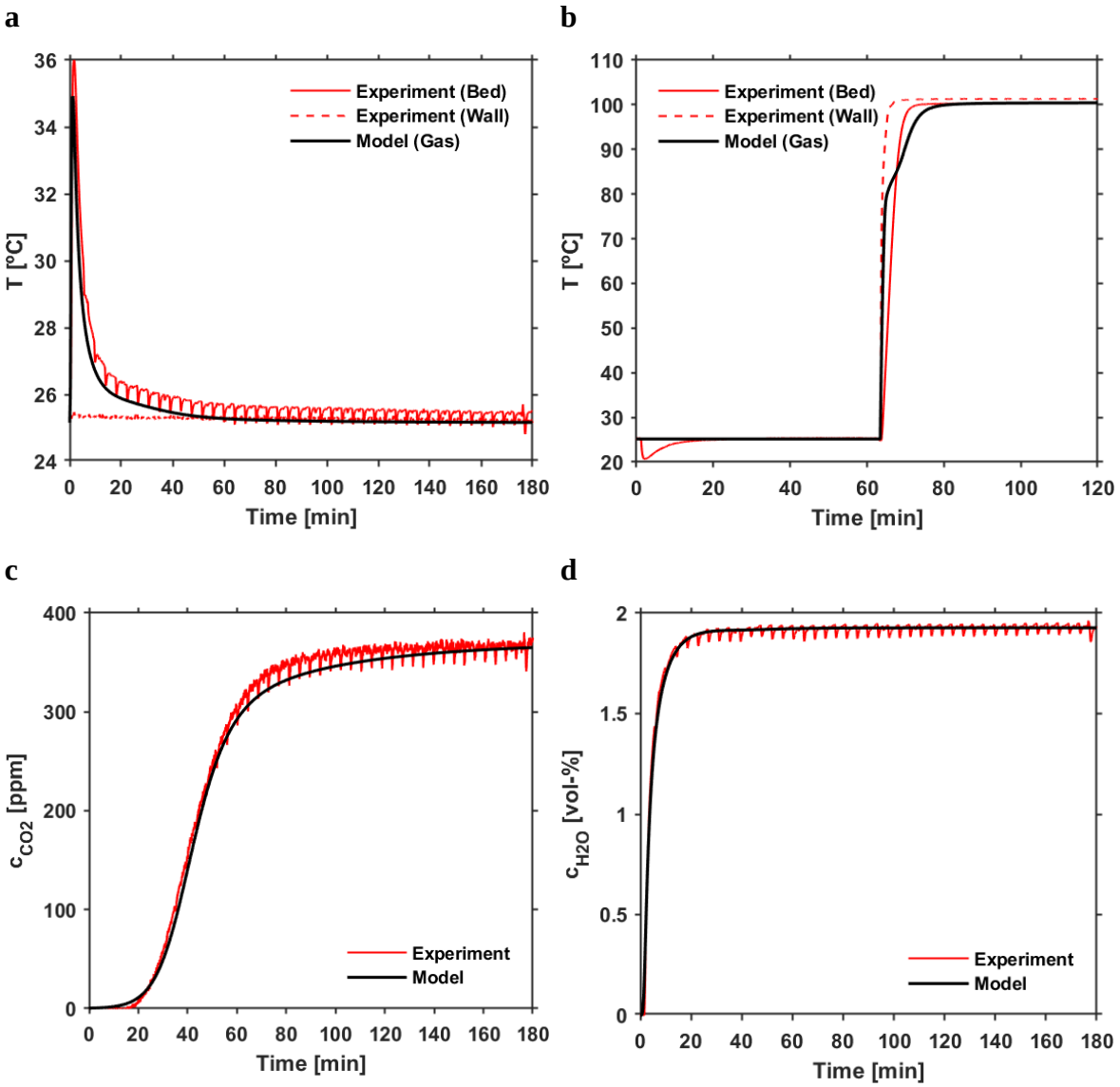

Appendix 5. Experimental and simulated adsorption/desorption capacity profiles from the TCSA experiments and open-inlet model a) for CO_2 in the adsorption phase; b) for H_2O in the adsorption phase; c) for CO_2 in the desorption phase; d) for H_2O in the desorption phase.

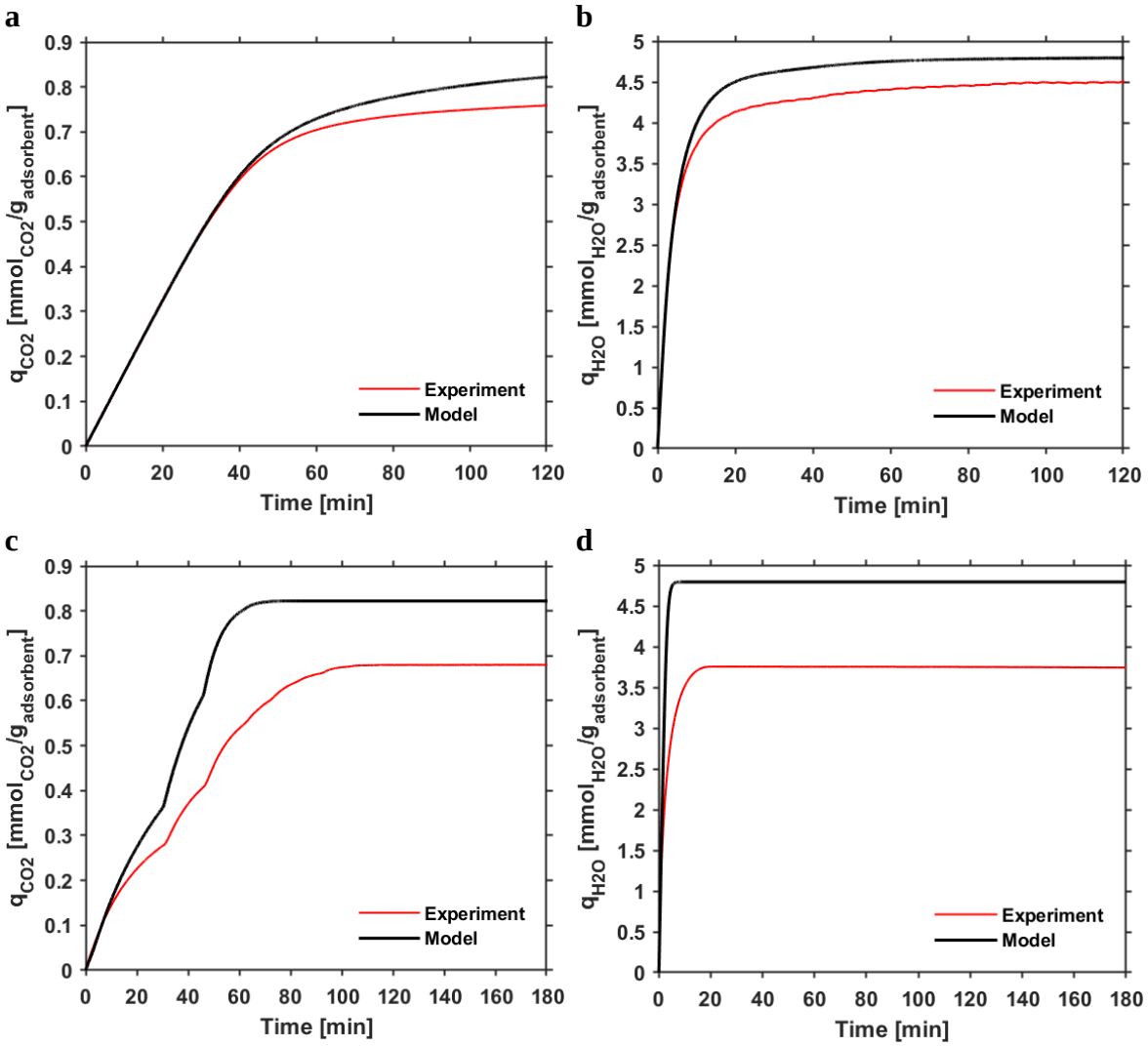

Appendix 6. Experimental and simulated adsorption/desorption capacity profiles from the closed TVSA experiments and closed-inlet model a) for CO_2 in the adsorption phase; b) for H_2O in the adsorption phase; c) for CO_2 in the desorption phase; d) for H_2O in the desorption phase.

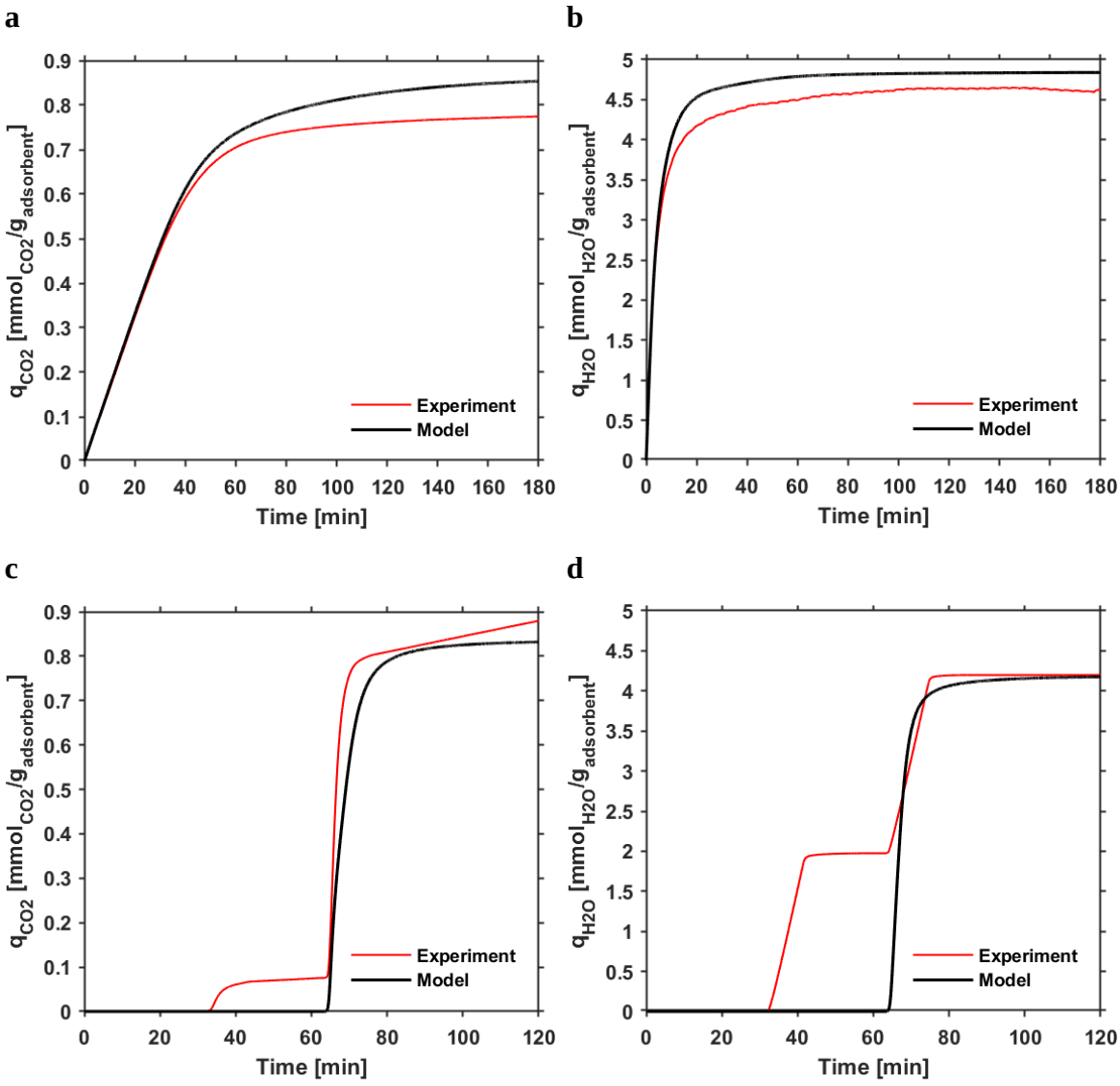

Appendix 7. The impacts of certain +/- changes in the adsorbent-related parameters on CO_2 productivity and SER.

	CO_2 productivity [$kg_{CO2}/(kg_{adsorbent}\cdot d)$] (Base value = 0.219)				SER [MJ/kg_{CO2}] (Base value = 14.86)			
	-80%	-40%	+40%	+80%	-80%	-40%	+40%	+80%
Heat transfer parameters:								
h	0.188	0.211	0.223	0.226	15.23	14.99	14.78	14.72
K_z	0.219	0.219	0.219	0.219	14.86	14.86	14.86	14.86
Kinetic parameters:								
$k_{f,1}$	0.362	0.227	0.217	0.216	14.60	14.84	14.87	14.87
$k_{f,2}$	0.053	0.144	0.282	0.337	17.60	15.32	14.66	14.55
$k_{H2O,LDF}$	0.225	0.220	0.218	0.218	14.46	14.79	14.89	14.91
7-parameter model isotherm parameters:								
q_m	0.010	0.114	0.290	0.340	115.90	26.65	11.19	9.28
$b_{0,1}$	0.270	0.234	0.213	0.214	13.28	14.15	15.43	15.90
$b_{0,2}$	0.456	0.289	0.189	0.172	18.41	16.13	14.02	13.43
$-\Delta H_1$	0.021	0.095	0.256	0.261	92.42	27.59	13.58	13.84
$-\Delta H_2$	0.172	0.202	0.225	0.220	14.33	14.98	15.05	15.71
t_1	0.341	0.280	0.171	0.139	13.11	13.60	16.93	19.30
t_2	0.154	0.175	0.298	0.504	17.46	16.13	13.81	12.95
GAB-model isotherm parameters:								
$q_{m,mono}$	0.209	0.211	0.225	0.228	9.24	12.33	17.17	19.48
C_0	0.209	0.212	0.224	0.227	11.58	14.24	15.05	15.10
K_0	0.209	0.211	0.219	-	8.81	11.38	23.85	-
ΔH_C	0.209	0.210	0.229	0.229	10.11	12.71	15.70	15.87
ΔH_K	0.219	0.219	0.219	0.219	14.86	14.86	14.86	14.86
$-\Delta H_{H2O,0}$	0.237	0.223	0.216	0.214	9.36	12.22	17.49	20.11
Adsorbent material properties:								
ρ_p	-	0.217*	0.220	0.220	-	20.14*	14.25	14.20
d_p	0.220	0.220	0.218	0.216	32.88	16.21	14.49	14.35
$c_{p,a}$	0.222	0.220	0.217	0.216	12.00	13.42	16.30	17.74
CCD**	-	-	-	-	-	-	-	-

* -20% is used instead of -40 and -80%; ** The effect of cyclic capacity drop is evaluated in a different way.